ABSTRACT

Title of Dissertation: EFFECTS OF FERROELECTRIC PROPERTIES ON MECHANICAL BEHAVIOR OF CLASS II MULTILAYER CERAMIC CAPACITORS

Nga Man Jennifa Li, Doctor of Philosophy, 2019

Dissertation Directed By: Professor Patrick McCluskey
Dr. Diganta Das
Department of Mechanical Engineering

Class II Multilayer Ceramic Capacitors (MLCCs) are one of the most widely adopted types of passive components in modern electronic systems due to their high volumetric efficiency. Mechanical failures are dominant in MLCCs due to the brittle nature of the ceramic dielectric. Over the years, there have been many studies

on the effect of design parameters, assembly parameters on crack susceptibility of these parts.

Barium Titanate ($BaTiO_3$) based ceramic is used as the dielectric in Class II MLCCs. This material is responsible for capacitance aging and temperature dependent properties in these units. Changes in mechanical properties due to electrical and mechanical loading or loading history is widely reported in the literature for bulk $BaTiO_3$ and other ferroelectric materials. However, these effects have yet to be reported for Class II MLCCs components in the literature.

With the indentation technique becoming more popular in research and development, more studies have adopted the technique for assessing mechanical properties of MLCCs and other electronic components. However, indentation measured properties are dependent on test parameters. In the case of ferroelectric materials, the properties also depend on texture of the specimen and other electromechanical coupling effects. In this study, baseline measurements of mechanical properties under various test parameters as well as treatment history of MLCCs are established using the Oliver-Pharr method.

Two mechanisms are evaluated for the potential change in flexural strength for MLCCs with DC voltage history. The first one is the fracture toughness anisotropy caused by domain switching. The second one is the change in stress distribution in the MLCC body with the increase in effective dielectric texture (crystallinity) due to poling under a bending load.

Finally, flexural strength is measured for commercial MLCCs with different volumetric ratio of effective dielectric, and an empirical relationship is developed to relate the change in flexural strength to the applied poling voltage and the volumetric ratio of the tested units.

EFFECTS OF FERROELECTRIC PROPERTIES ON MECHANICAL BEHAVIOR OF CLASS II MULTILAYER CERAMIC CAPACITORS

by

Nga Man Jennifa Li

Dissertation Submitted to the Faculty of Graduate School of the
University of Maryland, College Park in partial fulfillment
of the requirements for the degree of
Doctor of Philosophy
2019

Advisory Committee:
Professor Patrick McCluskey, Chair
Dr. Diganta Das, Co-chair
Professor Hugh Bruck
Professor Aris Christou
Professor Peter Sandborn
Professor Sung Lee

Acknowledgements

I would like to thank my advisor, Professor McCluskey for his continuous support and guidance during my studies at the University of Maryland. I would also like to thank my co-advisor Dr. Diganta Das, for his patience and invaluable advices. Over the years, I have had exposure to diverse research projects, and opportunities from which I have grown to become an independent researcher today. This would not have been possible without the unconditional help from both of my advisors, and I am filled with gratitude for them. I would also like to thank my advisory committee members for their time and suggestions for improvements of my work.

I would like to thank all faculty and staff at the Mechanical Engineering department for creating a great learning and working environment. I especially want to thank Professor Han, for letting me run my experiment with his lab facilities. I also would like to thank HyunSeop, Jack, Ryan, Sukrut, Arthur for their warm welcome in their lab. I would like to thank Professor. Dasgupta and Dr. Thamire, being their Teaching Assistant allowed me to work closely with them and their knowledge and hard work is truly an inspiration. I especially acknowledge the help from Dr. Chiou, Dr. Rao, and Dr. Liou at the AIM lab for the EBSD analysis. I would also like to thank Dr. Bob Utter for always being helpful and supportive both as a lab manager and as a friend.

I would like to thank all my friends here at UMD. Chandra, Ali, Hannes, you have set a great example for me as a PhD student. Maira, Chaobo, Roozbeh, Alex, you

have made office so much fun. Abishek, Sneha and Qian, thank you so much for the amazing homemade dinners and the CATAN nights. I would also like to thank all the students in Prof. McCluskey's group: Maxim, Zhaoxi, Yonatan, Erick, Kunal, Sriram, Andy, Alex, Gilad, it has been a pleasure to have all of you in the group.

I would like to thank Subramani. You are the best person I have met besides my mother. I am so lucky to have you in my life. I would also like to thank Subramani's family for their care and support.

I would like to thank Boomer. The emotional support and love that you have offered is priceless.

Finally, I would like to thank my family for their unlimited patience, unconditional love, and most importantly, for believing in me.

Table of Contents

List of Figures

List of Tables

1. Multilayer Ceramic Capacitors and their Failure Mechanisms

Multilayer Ceramic Capacitors (MLCCs) are one of the most widely adopted passive components in modern electronic systems and reliability of these units have been extensively evaluated. In Section 1.1, MLCCs are introduced in the aspects of their typical construction, dominance in the capacitor market, and their classifications. In Section 1.2, reported failure mechanisms for MLCCs are reviewed.

1.1 Introduction to Multilayer Ceramic Capacitors

MLCCs are capacitors made of layers of metal electrodes and ceramic dielectrics with an interleaved construction as shown in Figure 1 [1]. They are the most widely adopted passive components in modern electronics. Global capacitor market share in percentage by capacitor type from 2003 to 2019 is shown in Figure 2**.** Over the years, the global market share of MLCC has been on a steady increase. In 2019, ceramic capacitors account for up to 65% of the global capacitor market value [2]. MLCCs are used in electronic systems across different industries. The heavy reliance of MLCCs in modern electronics can be highlighted by the following examples: each GoPro camera contains 320 MLCCs, an iPhone X contains 1000 MLCCs and there are about 10,000 MLCCs in a Tesla electric vehicle [3].

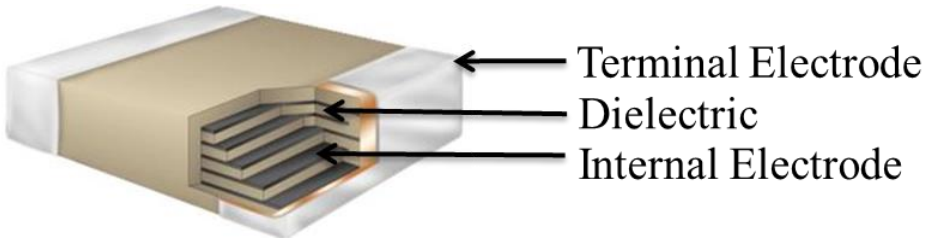

Figure 1. Structure of a Multilayer Ceramic Capacitor [1]

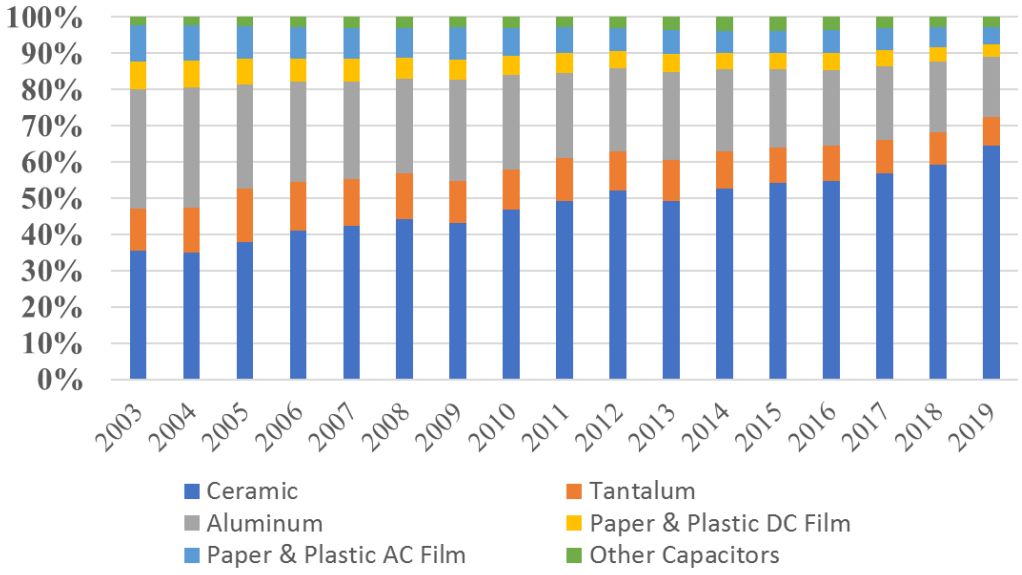

Figure 2. Global Capacitor Market Share (%) by Capacitor Type 2013-2019 [2]

MLCCs are divided into sub-classes based on the characteristics of the dielectric, specifically aging characteristics and temperature stability. However, there is some lack of clarity regarding MLCC classes from different manufacturers due to two standards that are in effect [4][5]. Some characteristics of dielectric materials belong to the designated classes by both standards are summarized in Table 1. The IEC and EIA standards both give a similar description to class I dielectrics, dielectrics in this class has a relatively low dielectric constant, low dissipation factor, and has a relatively low dependence on temperature and voltage compared

to other classes. The main difference which causes the confusion in the industry is the classification for Barium Titanate ($BaTiO_3$) based ceramics that exhibit an aging effect over time. While the IEC standard groups common dielectrics with aging effect as Class II, EIA standard further divide these dielectrics based on their temperature characteristics into Class II and Class III. For this reason, the classes to which Y5V and Z5U MLCCs belong vary depending on the part manufacturers. To avoid confusion, the classification used by the IEC standard is followed in this study. Therefore, Class II MLCCs in this study refers to MLCCs with dielectrics that exhibit ferroelectric properties. Aging effects and temperature instability of Class II MLCCs stems from their inherent ferroelectric properties, which will be discussed in detail in the later sections. All Class II MLCCs are made of high weight percentage of $BaTiO_3$, for example, 90-98% for X7R, 80-94% for Z5U [6].

Table 1. Classification of Common Ceramic Dielectric from IEC and EIA Standard [4][5]

IEC Class	**Description**	**Materials**	**Common temperature characteristics**
Class I	• Low Dielectric Constant (K) • (5 to a few hundred) • Low Dissipation Factor(<<0.01) • Most stable with temperature and voltage	TiO_2 or $CaTiO_3$ with additive materials	C0G (NP0)
Class II	• High K (1000 to 20,000) • Higher Dissipation Factor • Ages with time • Less stable than Class I	$BaTiO_3$ with additives	X7R, Y5V, Z5U

Typical aging characteristics for dielectrics from different classes are illustrated in Figure 3. Class I dielectric does not exhibit aging effects. Class II dielectrics undergo aging with a logarithmic loss in capacitance. Typical aging rates of Class II MLCCs differ based on their temperature characteristics. For the most common class II dielectrics, Y5V typically exhibits the highest aging rate, followed by Z5U and X7R [6].

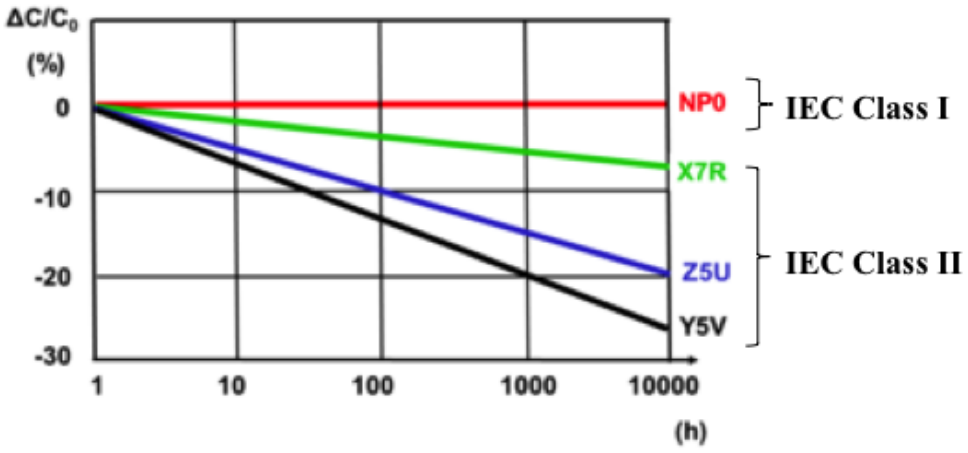

Figure 3. Typical Aging Characteristics of Dielectric Sub-Classes [6][8]

According to an article published in 2019, Class II MLCCs constitutes about 75% of the MLCC market [9]. They are typically used for bypass, decoupling, filtering in different end-markets depending on their sizes. For example, 0201 (0.02”×0.01”) and 0402 (0.04”×0.02”) are largely used in wireless handsets. While units of bigger sizes such as 0603(0.06”×0.02”), 0805 (0.08”×0.05”), 1206(0.12”×0.06”) or larger are widely used in automotive, industrial, consumer electronics, or even defense applications. The market demand for Class II MLCCs with the mentioned configurations have doubled in value from the year 2016 to 2018 [9].

1.2 Failure Mechanisms in MLCCs

Failure mechanisms in MLCCs have been extensively studied in the literature. Out of all reported mechanisms, the most dominant ones are mechanical failures such as flex cracking, fracture due to the brittle nature of the dielectric body. Defects that are potentially introduced into the ceramic at any phases of the MLCCs' life cycle can also make the units more prone to such failures. Other failure mechanisms caused by prolonged exposure to high voltage and humidity have also been reported and studied in the literature. In this section, various failure mechanisms and significant findings on these failure mechanisms are reviewed.

1.2.1 Mechanical Failures

MLCCs are susceptible to mechanical failures because of the brittle nature of the ceramic dielectric. The most common failure mechanisms are fracture due to mechanical stresses such as pick and place, board flexures or due to thermomechanical stresses such as reflow or temperature swings in their applications.

For mechanical failures, most of the studies looked into the effect of design or manufacturing parameters of MLCCs. For example, physical sizes of MLCCs [10][15][17], use of standard and flexible termination in MLCC designs [19] and the dielectric type being used [12][13], and number of electrodes [13]. Some researchers put focus on assembly parameters such as type of solder

[14][15][17][18], solder fillet height [15] and pad size [16], PCB materials and thickness [18] and effect of different pre-stress conditions such as isothermal aging [10] and thermal humidity bias [19]. These studies were conducted mostly by experiment or finite element analysis.

Some of the main findings from these studies include: MLCCs assembled with Pb-free solder are more crack resistant compared to that with SnPb solders [14], C0G MLCCs are found to be more resistant to flex cracking than X7R MLCCs [14], and MLCCs with bigger size are more susceptible to flex-cracking [10][15][17], capacitors with a higher solder fillet height are more susceptible to thermal shock cracks [15] and capacitors with a thicker PCB results in flex cracking at lower deflections than thinner boards of the same materials [18].

MLCCs are even more susceptible to fracture in situations where defects are being introduced at different points of their life cycles. Voids, micro-cracks and delamination can be introduced into MLCCs from material processing in the early manufacturing stage. After the parts are manufactured, they are subjected to mechanical stresses that can introduce cracks, for example, during pick and place or soldering. When MLCCs are being assembled and operated, they are exposed to mechanical and thermal-mechanical stresses that can also induce defects.

1.2.2 Electrical Failures

Prolonged exposure to high voltage causes dielectric degradation in MLCCs, and such failure are accelerated by high temperature. Using a highly accelerated stress

test matrix with voltage from 150V to 250V, and temperature from 155ºC to 175°C, Liu et al. [28][29] identified three leakage current patterns corresponding to avalanche breakdown, slow degradation, and thermal runaway under the high voltage high temperature stress conditions. Defects such as voids, delamination and cracks were found to be the cause for avalanche breakdown in the early failed units. However, it should be noted that such early failures may not take place at a regular voltage stress level. When the early failed population is removed, the mean time to failure was extrapolated to be more than 10^5 years at room temperature and rated voltage using the Arrhenius Relationships.

Electrical failures are known to be accelerated by temperature-humidity bias (THB) in MLCCs. It has been widely reported that electrical failure in MLCCs involve a microscopic path between internal electrodes, e.g. voids or cracks, penetration of moisture of contaminants into the path, and migration of electrode materials along the path by an electrochemical process [20][21][22][23]. As a result, leakage current of a capacitor increases and causes a capacitor to fail. It was found in another study [24] that moisture condensation in a pre-existing crack in ceramics can take place through a capillary effect, and therefore, a high humidity environment is not necessary for such failures to take place. Since defects in ceramic bodies are known to play a major role in electrical failures, several screening methods involving THB [25], or high temperature and voltage [26] are developed to eliminate defective units that can lead to field failures.

Another water induced electrical degradation of $BaTiO_3$ ceramics is discovered by Chen [30]. It was reported that when electricity and humidity are present,

electrolysis of water occurs and resistance of $BaTiO_3$ can decrease by orders of magnitudes, which causes the dielectric loss to surge and result in electrical failure.

An irreversible time dependent degradation phenomenon in $BaTiO_3$ MLCCs under 2600 hours of autoclave conditions (high temperature, humidity and pressure) has been discovered by Donohoe [31][32].

2 Properties of Ferroelectric Materials and Ferroelectric Dielectric for Class II MLCCs

Ferroelectric materials are often identified by effects specific to their applications. In MLCCs, it is often characterized by capacitance aging over time, or its instability with temperature. By definition, ferroelectric materials are defined as materials that exhibit spontaneous polarization that is reversible by an external electric field. This material property originates from a unique crystal symmetry of the material. In Section 2.1, the classification of materials based on their crystal symmetries are introduced. Depending on crystal symmetries, materials can exhibit all or none of piezoelectric, pyroelectric and ferroelectric properties.

In Section 2.2, the origin of ferroelectric properties is discussed using the perovskite structure of $BaTiO_3$- dielectric for Class II MLCCs. Owing to their unique characteristics, material properties of ferroelectrics are dependent on multiple environmental factors as well as time. In Section 2.3, the effect of temperature, voltage history (poling), and aging on ferroelectrics are selected for discussion for the interest of MLCC application.

2.1 Crystallographic Point Groups for Ferroelectric Materials

A crystal is characterized by a periodic repetition of the atomic lattice structure in all directions of space. Unit cell is the smallest repetitive part of a crystal, and symmetry of the unit cell define properties of the material. Symmetry properties of unit cells are categorized into 32 crystal classes, also known as crystallographic point groups [34][35].

Under the 32 classes, 11 classes are centrosymmetric and 21 classes are non-centrosymmetric. All of the crystalline materials come under the 21 non centrosymmetric classes (with the exception of group 432) exhibit the phenomenon of piezoelectricity, which means that mechanical stress will generate a charge separation on the faces of the crystal (direct piezoelectric effect) and will undergo mechanical strain when subjected to an electric field (converse piezoelectric effect). One of the 21 classes, though classified as the non-centrosymmetric class, possesses other combined symmetry elements, resulting in no piezoelectric effects. Therefore, there are only 20 classes of non-centrosymmetric crystals with piezoelectricity.

A sub-set 10 under these 20 classes come with a unique axis of symmetry. These crystals are said to be polar. Polar crystals are piezoelectric and also exhibit pyroelectricity, which means that a charge separation will appear on their surfaces when their temperature is changed. Polar structures effectively have a dielectric polarization "built in" to the unit cell of the crystal structure, known as spontaneous polarization. The application of stress or a change in temperature causes a change in the dipole moment and it is this change that causes the separation of charge on the surfaces of the crystal. The direction and magnitude of the spontaneous polarization in a polar dielectric can be changed by the application of an electric field, but on removal of the field it will return to its zero-field value.

A sub-set of the set of polar dielectrics exists for which the application of a field of sufficient magnitude will cause the spontaneous polarization to switch to

a different, stable direction. Upon removal of the field the polarization will not spontaneously return to its original direction and magnitude. These crystals are called *ferroelectric*. Therefore, ferroelectrics possess piezoelectric, pyroelectric, and ferroelectric properties.

There are 4 sub-categories of ferroelectric ceramics each with their representative crystal structure. The most important group is the Oxygen Octahedra, also known as Perovskites, have an ABO_3 crystal structure. The most common ferroelectrics used today such as $BaTiO_3$, PZT come under this group of ferroelectrics. The relationships between the sets of piezoelectric, pyroelectric, ferroelectrics and perovskites are as shown in the Venn diagram in [36][37][38].

Ferroelectric materials are widely adopted in the electronics industry for many of their properties. They include ferroelectric hysteresis used in non-volatile memories, high piezoelectric effects used in sensors, actuators, high pyroelectric coefficients used in infra-red detectors [38]. For capacitors application, ferroelectric materials are selected because of their high permittivity. Apart from capacitor applications, $BaTiO_3$ based material are also used in some prototype piezo devices including loud-speakers, biocompatible nanogenerators, self-powered fluid velocity sensors [39].

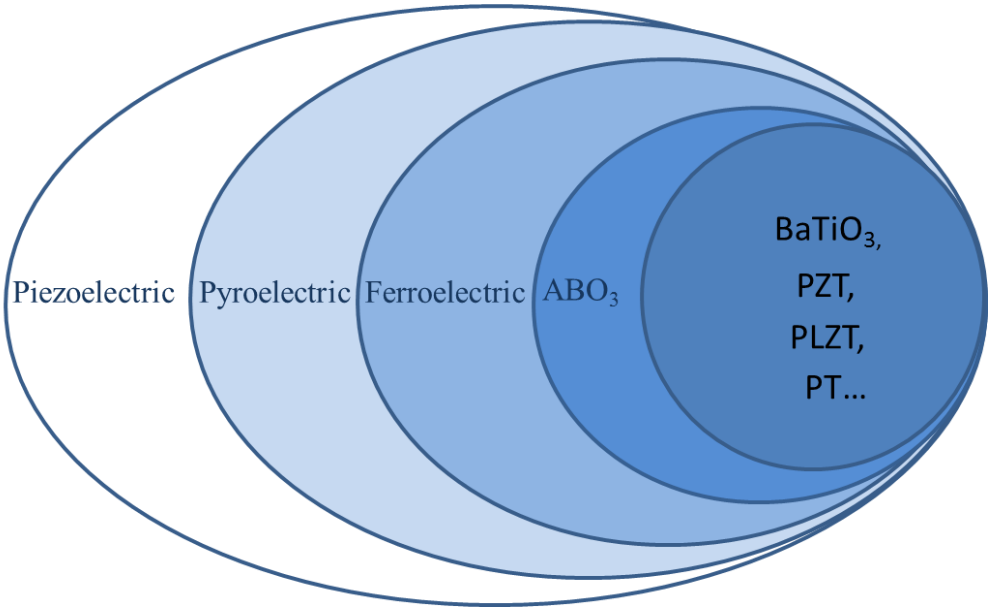

Figure 4.Venn Diagram of Piezoelectrics, Pyroelectrics and Ferroelectrics

2.2 Ferroelectric Dielectric Used in Class II MLCCs

Ferroelectric materials are characterized by the presence of reversible spontaneous polarization. Spontaneous in this context represents a non-zero polarization in the material in the absence of an applied electric field, while reversible refers to the possibility of the direction of the spontaneous polarization being reversed by an applied field [37]. $BaTiO_3$ is one of the most widely adopted ferroelectric material, constitutes 80-98% in class II MLCC dielectrics [6]. It has a perovskite crystal structure with a Ti atom at the center, Ba atoms at the corners and O atoms at the face centers. $BaTiO_3$ possesses both paraelectricity and ferroelectricity depending on their phases. Paraelectrics belong to the centrosymmetric crystal classes. While paraelectrics can also exhibit polarization with exposure to an electric field, ferroelectric materials do not lose ionic polarization when an electric field is

removed as oppose to paraelectrics [46]. The crystal structure has four phases which changes with temperature. Above the Curie temperature (~120°C), all atoms in a crystal remain at their equilibrium position. As the temperature is lowered, it goes through successive phase transitions to three different ferroelectric phases as shown in Figure 5 [38][40]. Below 120°C, center Ti atom displace from the center in <001> , <011> and <111> directions in the temperature ranges of 4°C to 120°C, -90°C to 4°C and below -90°C respectively. In these temperature ranges, crystal structures take the shape of tetragonal, orthorhombic, rhombohedral respectively. Ferroelectricity in these phases was originated from the elongations of the crystals in different directions. The interest in our study primarily lies in the ferroelectric phase of the material which corresponds to normal operating temperature of MLCCs. This displacement of the center Ti atom results in a net dipole moment in the c-axis of the crystal structure which contribute to ferroelectricity the material from 4°C to 120°C. Spontaneous polarization does not contribute to a net polarization in a polycrystalline material at a "stress free" state as the localized spontaneous polarizations cancel out in the macroscopic scale and the net polarization of the material remains zero.

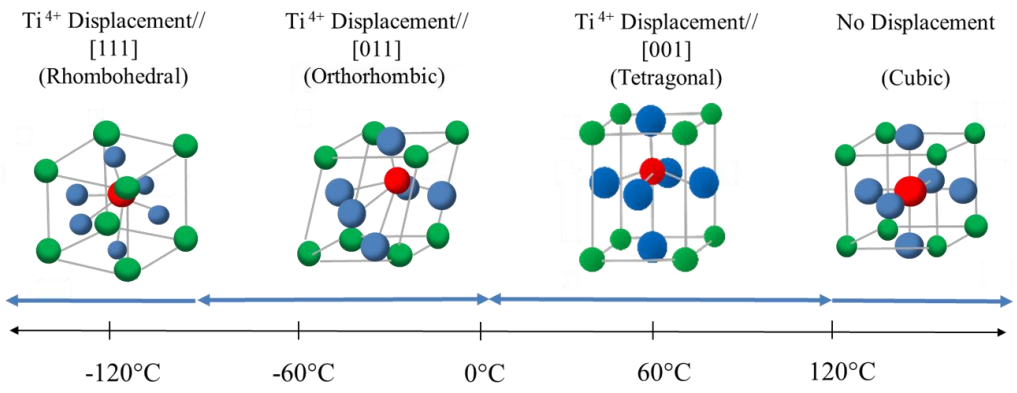

Figure 5. Phase Change of $BaTiO_3$ with Temperature

The localized spontaneous polarizations, known as domains, constitute the electromechanical coupling intrinsic properties of ferroelectric materials so that polarization and strain of the materials are coupled with mechanical and electrical stimuli. In another words, ferroelectric domains can be re-oriented under electric or mechanical stresses, under effects that are often termed ferroelectric and ferroelastic effect respectively.

The response of ferroelectric $BaTiO_3$ crystals under different stress fields are illustrated in Figure 6. When a material is not polarized and stress-free, the crystallites and domains have a random distribution theoretically, as shown in 4(a). When an electric field is applied across the material, crystallites and domains line up with the direction of electric field as shown in 4(b). When a tensile stress is applied across the material, crystallites and domains align in the stress direction as shown in 4(c) and compressive stress aligns domain in the perpendicular direction of the stress as shown in 4(d).

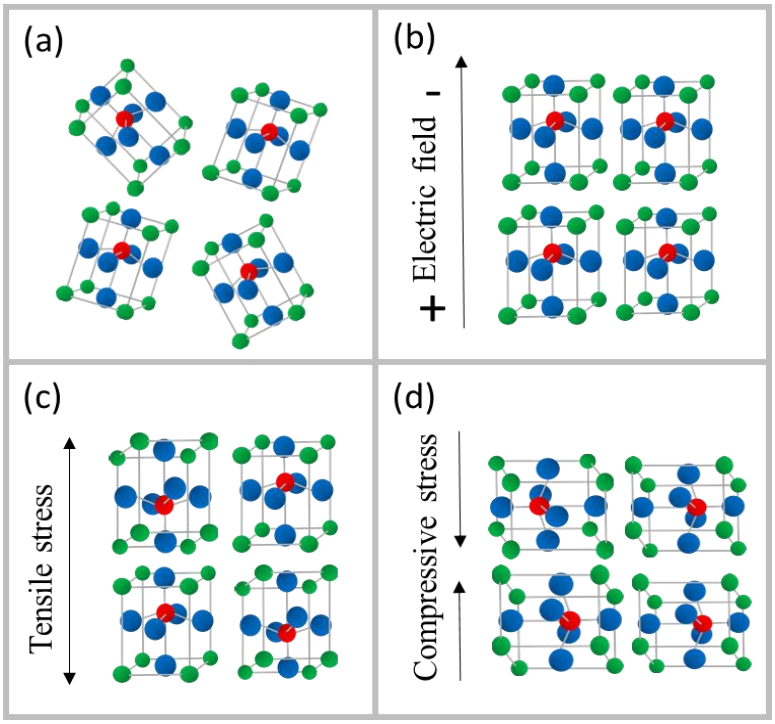

Figure 6. Illustration of $BaTiO_3$ Crystallites (a) Under no polarization or mechanical stress (b) Under an Electric Field (c) Under tensile stress (d) Compressive stress

2.3 Stress and Time Dependent Material Properties of Ferroelectric Materials

Material properties of ferroelectric materials depend on mechanical stresses and electrical stresses due to stress induced crystallographic re-orientation. Material properties can also depend on temperature because of phase change across certain temperatures. In this section, time (aging) and voltage history (poling) on material properties of ferroelectrics are reviewed with a focus on mechanical properties for the interest of MLCC reliability.

2.3.1 Effect of Voltage History (Poling) on Material Properties

Poling is the application of a high electric field that orients most of the dipoles in the direction of the field. It is a standard procedure for enabling or maximizing piezoelectric behavior in ferroelectrics, which is crucial in applications such as sensors, actuators, non-volatile memories. This is achieved by aligning randomly oriented domains in a ferroelectric or piezoelectric materials with an electric field. After the removal of the poling field, remnant polarization remains in the material and the material is known is "poled" or polarized, which exhibit higher level of piezoelectricity than "unpoled" ones. A graphical illustration of domain reorientation due to poling is shown in Figure 7.

A typical ferroelectric hysteresis loop is shown in Figure 8. When the applied electric field is small, the increase in polarization follows a linear relationship with the applied field due to field-induced polarization (OA). Upon the removal of the small field, the polarization decreases linearly back to the origin because the field was not large enough to cause domain switching. At a higher electric field, polarization increases non-linearly because of domains switching towards the direction of the applied field (AB). At a high electric field, polarization reaches a saturated value P_p (BC). As the field is gradually reduced, polarization reduces. Extrapolating back from the saturated polarization is the spontaneous polarization P_s, Remnant polarization P_r is less than P_s when field is zero because some back-switching happens for some domains. A coercive field (E_c) in the opposite direction can being the polarization back to zero [37].

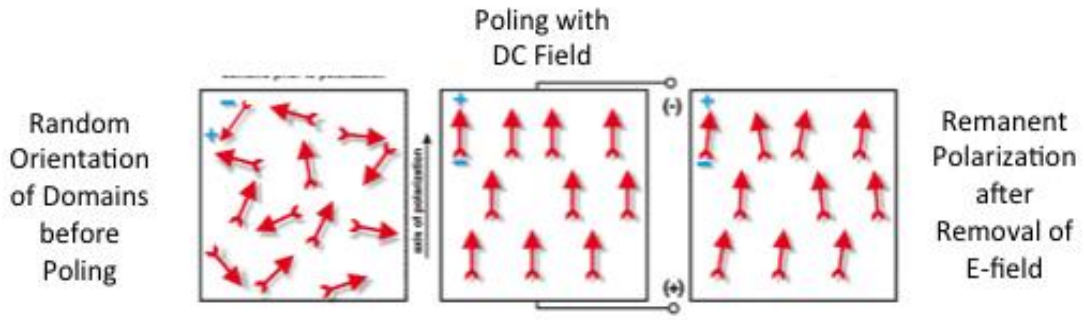

Figure 7. Alignment of Domains with Poling

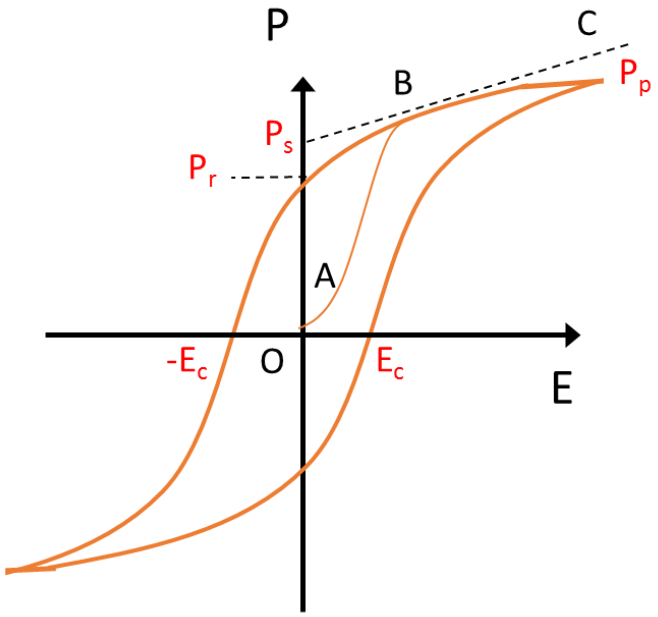

Figure 8. Typical Ferroelectric Hysteresis Loop

A higher level of piezoelectricity can produce a higher electric response under mechanical stresses, or a higher mechanical strain under an electric field, which is also known as a higher piezoelectric sensitivity.

A lot of researches have been carried out to evaluate the effect of poling and the resultant piezoelectric effects in these materials. For example, chemical modification (doping) of the material [75], mechanical stress during poling [76][100], and most dominantly temperature during poling process [109]. In practicality, poling often involves heating above Curie Temperature to maximize the degree of poling. In this study, only the effect of remnant polarization due to poling at room temperature is evaluated for the interest of MLCCs.

Apart from the increase in piezoelectric constants, poling is reported to have reforming effects on dielectric constants and elastic constants in ferroelectric materials followed by a gradual aging effect similar to after cooling from Curie Temperature [112]. Compared to aging, the effects of poling on mechanical properties are widely reported. Some of the reported effects of poling in the (DC voltage history) on tensile and bending strength in the literature are summarized in Table 2, and effects of poling on fracture toughness are included in Table 3.

Tanimoto et al. [65] evaluated the tensile strength of poled and unpoled samples of PZT. It was found that tensile strength of the specimen increases when for specimens poled in the thickness direction, and decreases for specimens that are poled in the length direction.

In a system of zirconia ceramics disperse with $BaTiO_3$ particles, Seo et al. [69][70] observed an increase in bending strengths after the specimen was poled in the thickness direction, and a decrease after the specimen is poled in the length direction. It was also found that the bending strength of the poled specimen returns to the original values after it is heat reformed above T_c of $BaTiO_3$. The increase is

attributed to the internal stress built up in the material matrix for a poled sample. However, the origins of the proposed internal stress was not elaborated. Indentation was also performed to evaluate to compare fracture toughness for poled and unpoled samples, and it was found that fracture toughness has increased in the poling direction and reduced in the length direction of the specimen. Therefore, the increase in flexural strength is also attributed to the crack detour in the poling direction.

Efe et al. [71] evaluate the effect of poling on bending strengths of a solid solution of sodium bismuth titanate (NBT) and $BaTiO_3$, and PZT using a 3-point bending set up. When both of these materials are poled in the thickness direction, the bending strengths increase compared to when they are not poled. However, the poling conditions are not specified in this study. Like the other studies, it was also found that bending strength reduces as these materials were poled in the length direction.

As the effective dielectric in MLCCs can only be polarized in the thickness direction, only the effects of polarization in the thickness direction are included in Table 2.

Table 2. Effect of Polarization in Thickness Direction on Tensile and Bending Strength of Ferroelectrics

Mechanical Properties	Test Method	Material	Poling Condition	Before (MPa)	After (MPa)
Tensile Strength	Tensile Test	PZT [65]	N/A	49.4MPa	51.3MPa
Bending Strength	3 Point Bending	$BaTiO_3$/8YSZ (10 mol% and 5 mol%) [69]	Room temperature 8kV/mm for 30 min	220MPa/ 270MPa	244MPa/ 300MPa
		$BaTiO_3$/8YSZ [70]	Room temperature 6kV/mm for 30 min	182MPa	209MPa
		PZT[71]	N/A	143MPa	150MPa
		NBT-5.5BT[71]	N/A	160MPa	165MPa

Table 3. Effects of Poling on Fracture Toughness of Ferroelectrics

Mechanical Property	Test Method	Material	Poling Condition	Before ($MPam^{0.5}$)	After ($MPam^{0.5}$)	Direction
Fracture Toughness	Indentation	$BaTiO_3$ [72]	80°C 1.25kV/mm for 10 min	0.6	0.79	∥
				0.62	0.59	⊥
		Al_2O_3-$BaTiO_3$ [72]	120°C 3.75kV/mm for 10 min	4.48	5.1	∥
				4.48	3.7	⊥
		PZT [73]	Not Specified	1.18	1.99	∥
				1.18	0.74	⊥
		NBT-5.5BT [71]	Not Specified	1.8	2	∥
				1.8	1.6	⊥

The last column in Table 3 indicates the relative position of the measured fracture toughness to the poling direction, with // indicating parallel and ⊥ indicating perpendicular to the poling direction respectively. In all the reported measurements, fracture toughness is found to be anisotropic in poled ferroelectric samples.

Fracture toughness (K_{IC}) are found to be anisotropic for poled ferroelectric samples. The results vary with composition and processing parameters of materials, but it is widely established that K_{IC} parallel to poling direction increase with a larger degree, and K_{IC} perpendicular to the poling direction increase or decrease with a smaller degree.

2.3.2 Time Dependent Material Properties (Aging)

Capacitance aging is the most well-known effect for Class II MLCCs due to ferroelectric properties of $BaTiO_3$. Class II MLCC undergo a logarithmic aging of capacitance over time and recommendations are made by manufacturers to reform the capacitors at 150ºC for a 15 to 30 minutes to reform the capacitance values.

The phenomenon of capacitance loss can be explained with the change in polarization in the effective dielectric over aging. Electric Susceptibility (χ_e) is defined as the degree of polarization (P) of a dielectric material in response to an applied electric field (E), where ε_o denotes the permittivity of free space.

$$\chi_e = \frac{P}{\varepsilon_o E}$$

Capacitance of a capacitor can be represented as the product of relative permittivity (ε_r) and effective area of electrodes (A), divided by separation between electrodes.

$$C = \frac{\varepsilon_r A}{d}$$

Since ε_r is related to χ_e, the reduction in degree of polarization of an aged Class II MLCC suffers a loss in dielectric constant (ε_r) and capacitance.

$$\varepsilon_r = 1 + \chi_e$$

Unlike other reliability studies where “aging” is used in a broader perspective to describe the effect(s) under a prolong exposure to a certain environment, the term

"aging" in ferroelectric materials is used in a more restrictive manner. Aging for ferroelectrics typically refer to the process that produces variations of dielectric, piezoelectric, ferroelectric properties over time and in the absence of an external field [47]. There are extensive studies on the aging of ferroelectrics since the 1950s and a few mechanisms have been proposed for the origin of aging. They include domain nucleation and splitting [48][49][50][51][52], reorientation of defect dipoles, [44][45][58], space charge formation [53] and ionic drift [55][56].

180° domains and 90° domain walls describe walls between neighboring domains that are pointing at opposite directions and perpendicular directions representing higher and lower energy states respectively. It has been widely reported that a large number of 90° domain walls exist in well-aged samples [48][49]. Domain splitting and nucleation describes the gradual change in domain's configuration to achieve a more stable state [48][52].

Reorientation of defect dipoles, also known as the volume/bulk effect refers to the unintentional and intentional defects present in the system, that stabilize in preferred lattice sites over time, creating an internal bias that constrains the switching of the polarization along specific directions [44][45][58].

Space charge formation and ionic drift refers to the diffusion of charged defects, ions, vacancies and ions into certain regions and cause pinning of the domain wall positions. When the space charge forms at domain walls, it is known as the domain effect [44][45], when these ions, defects diffuse into dissimilar phases such as secondary phases, pores and electrodes, it is known as the grain boundary effect [44][45]. These regions with space charge accumulation represents source of

internal bias field that hinders the reversal of polarizations under electric field [53][53][55][56].

All of these mechanisms are known to contribute to domain wall immobilization which inhibits the reversal of spontaneous polarizations by an electric field. As of now, the main cause of aging process remains a debate.

A simplified illustration of domain configuration at different phases of aging is illustrated in Figure 9 [57]. At above Curie temperature, there are no spontaneous polarization or domains in the material due to the cubic, paraelectric phase of the crystal structure. When the temperature is brought below the Curie Tempature, crystal structure transits from a cubic, paraelectric phase into a tetragonal, ferroelectric phase in which spontaneously polarization is formed resulting in domains within grains as shown in the top left picture. When the material is fresh cooling down from Curie Temperature, domain structures are not in a stable state, which is typically characterized by 180° domain walls between neighboring domains pointing at opposite directions. Having no clamping or pinning effects that develop over aging, these domains can be aligned or reversed with a relatively low electric field. After a period of time, domains that were randomly oriented will gradually be re-arranged to a form with lower energy state, which is characterized by 90° domain walls between domains which are perpendicular to each other. These neighboring perpendicular domain exerts a clamping effect on the domain walls. In addition, space charge accumulated at grain boundaries also have a pinning effect on domains. With a combination of these aging mechanisms, reversal or alignment

of domains are inhibited and a relatively higher electric field is required to cause the same degree of polarization.

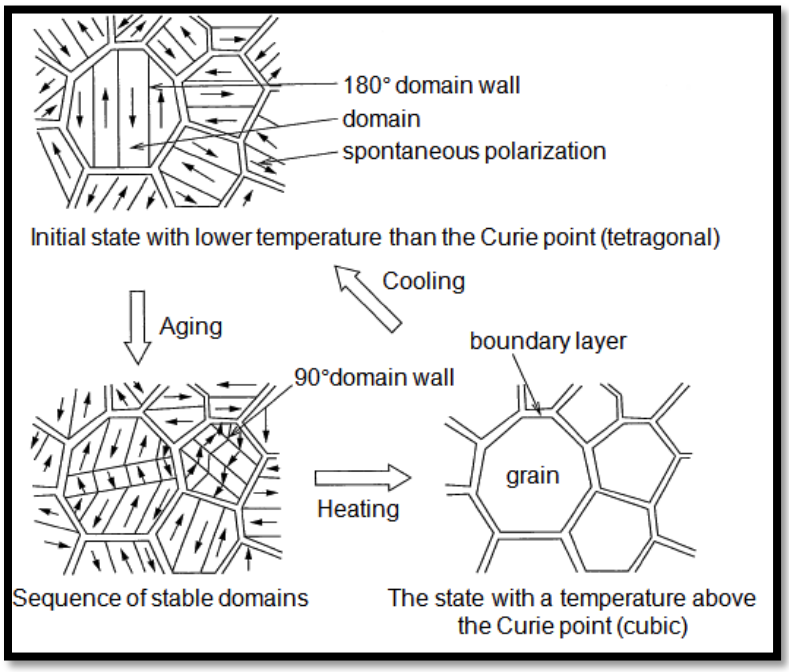

Figure 9. Immobilization of Domain Walls over Aging of Ferroelectrics [57]

Apart from the abundant work on different theories of aging, the following aspects of dielectric aging in ferroelectrics has been studied. For example, the effect of temperature and additives on the loss in permittivity or capacitance over time and the study of domain structure evolution over time. Temperature is reported to increase aging rate for 8% $CaTiO_3$ doped $BaTiO_3$ and pure $BaTiO_3$ [59][49], and a doping level of 4wt% $CaTiO_3$ results in a minimum aging rate in $CaTiO_3$ doped $BaTiO_3$.

Compared to the effect of poling treatment, the effect of aging/ heat reforming on mechanical properties of ferroelectrics are not as widely reported.

Mason has shown that over an aging period of 1 month at room temperature, there was a ~5% increase in elastic modulus for $BaTiO_3$ samples [59]. Mason did not give any physical explanation to this finding. Plessner later explained the effect by the decrease in contribution to elasticity in the bulk material due to the more stable positions of the domain walls after aging [62].

Zhang et al. [60] compared the failure stress of poled (as-received) PZT specimen, and poled PZT specimen that has been aged on the shelf for 4 years using ball-on-ring (BOR) mechanical testing, and it was observed that the aged specimen had a lower average strength.

2.4 Summary of Literature Review and Research Gaps

MLCCs are susceptible to mechanical failures. In the literature, the effect of design parameters, manufacture parameters, assembly parameters and environmental stresses on such failures are widely reported.

Material properties of ferroelectric materials are dependent on electrical, and mechanical loading history due to their inherent electromechanical coupling characteristics. Flexural strengths, fracture toughness are reported to change after poling for ferroelectrics. Class II MLCCs, with their dielectric made of a ferroelectric material-$BaTiO_3$, demonstrates well-known characteristics such as capacitance aging, and temperature instability owing to their ferroelectric properties. Yet, the effect of electrical, and mechanical loading history on mechanical behavior of these units are yet to be reported in the literature.

From the local perspective, effective dielectric layers in MLCCs are under mechanical residual stress, or a combination of electrical loading history and mechanical residual stress depending on whether the unit is unpoled or poled. Therefore, the study of a ferroelectric ceramic material under such complex loading condition/ history in an actual application (MLCC) can reflect the material's response in their natural "stress state" rather than controlled test parameters in the literature.

From the global perspective, unlike other bulk ferroelectric materials tested in the literature, MLCC has a unique architecture in which only the effective dielectric can be poled by the sandwiching positive and negative electrodes. Therefore, the change in global mechanical properties of an MLCC as a whole, such as flexural strength or bending strength, can be different from the reported trends in the literature.

As aging/heat reforming and poling (DC voltage history) are common life cycle stresses for MLCC units, the mechanical behavior of MLCC units at a local level, and a global level under such loading histories should be evaluated to have a comprehensive understanding on how the intrinsic ferroelectric properties could affect robustness of these units.

3 Mechanical Properties Characterization of Commercial Class II MLCCs by Indentation

Traditionally, board flex tests are used for evaluating crack susceptibility and reliability of MLCCs [10][14][15][16][18][19]. In a board flex test, MLCCs are mounted on a PCB which is subjected to a 3 point/4 point bending load. During the test, electrical parameters such as Capacitance and Dissipation Factor are monitored. Failures of the tested MLCCs are indicated by excessive parametric drift or cracking of the devices. A board flex test set up with the use of 3 point bending as described in AEC-Q200-005A [76] is shown in Figure 10.

One of the advantages of using board flex tests to study mechanical failures for MLCCs is that there is no specific size and dimension requirements like other mechanical properties characterization techniques. In addition, when combined with other assembly parameters such as solder type and solder fillet height, the test results can resemble field failures due to board flexures. With proper strain gauge installation, some studies have managed to test multiple MLCCs mounted on a PCB at the same time [19].

However, board flex test has its limitations. Output of the test is a distribution of MLCC failures instead of quantitative mechanical properties. In addition, failure in this test can be highly dependent on, or even solely because of assembly parameters, as electrical parameter drift can be caused by interconnect failures of the board alone. Therefore, while board flex test is a good option for comparing different assembly or board design parameters on MLCC failures during board flexures, there is a need for an alternative test when a more precise characterization of

mechanical properties of MLCCs is necessary. For example, material properties for input in finite element analysis, or when the effects of processing parameters on mechanical properties are being compared.

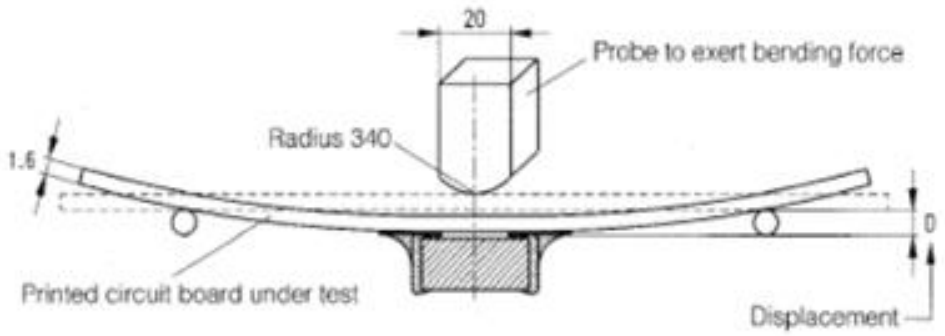

Figure 10. Board Flex Test Set Up in AEC-Q200-005A

In the recent decade, indentation is gaining popularity in research and development and more studies are using this technology for mechanical properties measurement of MLCCs [77][78][79][80] and other small electronic components [82]. The reported mechanical properties serve as a new source of data for academia or the industry to carry out thermo-mechanical reliability evaluation for small electronic components, or for new design justification.

The Oliver-Pharr method used for deriving mechanical properties from indentation data, due to its ease of execution, is used overwhelmingly in the industry and in the academia regardless of its limitations. In the indentation field of research, different effects due to measuring conditions and residual stresses on indentation measured properties have been extensively studied [83][84][85][86][89][90][91][96].

However, these effects are not given enough consideration when indentation is used as an application.

In this section, the effects of measuring load, measuring location, and indenter tip geometry on measured mechanical properties by indentation are evaluated on commercial MLCCs. By understanding the limitations and implications of the indentation measured properties, the use of indentation for mechanical properties characterization of MLCCs, and other electronic components can be facilitated.

Another limitation of the method is that it applies only to monolithic and isotropic materials [98], and this property of a specimen may not be known in reality (Polycrystalline $BaTiO_3$ can go from isotropic to close to transversely isotropic depending on its texture). Together with the complexity that come with electromechanical coupling effect inherent in ferroelectric/ piezoelectric materials, a numerical solution for mechanical properties is rendered extremely complex with abundant assumptions.

Therefore, the objective of this study is to establish baseline measurements using the Oliver-Pharr method under different test parameters, as well as MLCC treatment parameters of interest, so that the effects of the parameters under evaluation can be characterized.

3.1 Working Principal of Indentation

During an indentation, a load is applied to the unit under test using an indenter tip. The measurement process, which involves loading and unloading of the indenter tip into and out of the unit, results in a loading versus displacement curve as shown

in Figure 11. From the loading vs displacement relationship, mechanical properties such as elastic modulus and hardness are derived using the Oliver-Pharr method [93] as described below. Elastic modulus and Poisson ratio of the diamond tip (E_i and v_i), and the sample (E_s and v_s) are related to the Reduced Modulus (E_r) that is deduced from the loading versus displacement curve with the following relationships.

$$\frac{1}{E_r} = \frac{1 - {v_i}^2}{E_i} + \frac{1 - {v_s}^2}{E_s}$$

$$E_r = \frac{\sqrt{\pi}}{2} \frac{S}{\sqrt{A(h_c)}}$$

Stiffness of sample (S) is defined as the slope of the initial unloading curve.

$$S = \left. \frac{dP}{dh} \right| h_{max}$$

h_c can be further derived from the load versus displacement curve with the following equations, where P_{max} is the maximum load and h_{max} is the maximum penetration depth during an indentation as shown in Figure 12.

$$h_c = h_{max} - \varepsilon \frac{P_{max}}{S}$$

Using geometrical relationships for an indenter tips, $A(h_c)$ is equal to $24.56{h_c}^2$, and $24.504{h_c}^2$ respectively.

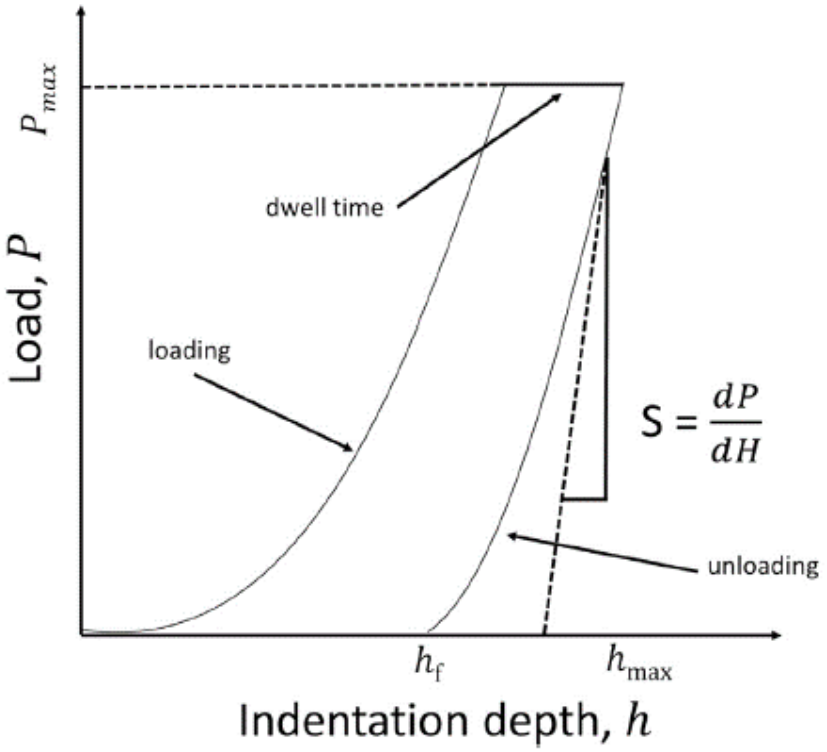

Figure 11. Key Elements from a Typical Loading-Displacement Curve of an Indentation

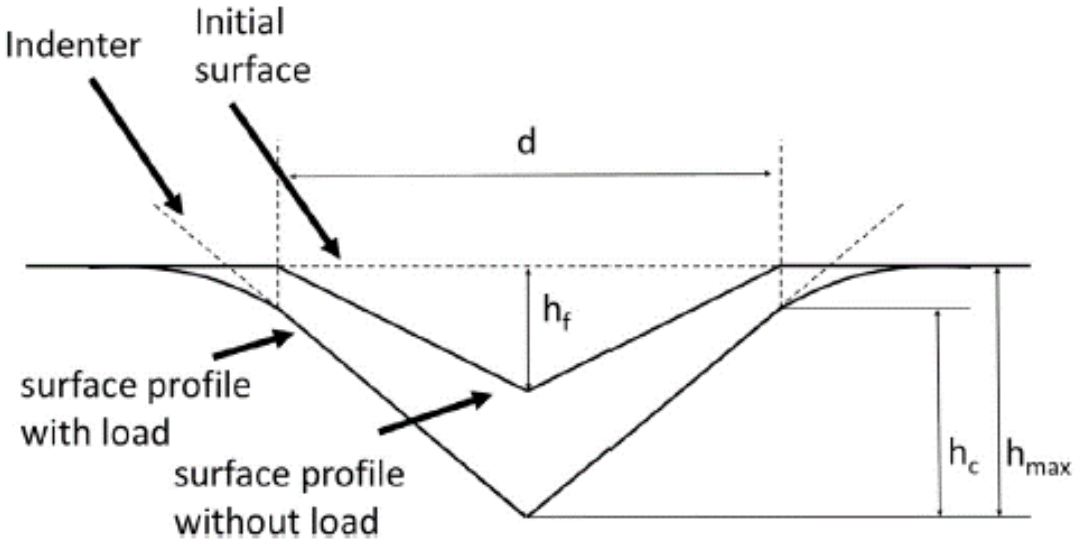

Figure 12. Geometrical Profile of an Indented Surface during and after Indentation

Hardness of the test unit can be derived from the following relationship

$$H = \frac{P_{max}}{A(h_c)}$$

3.2 Review of Mechanical Properties of Ceramic Dielectric Measured by Indentation

In this section, mechanical properties characterized for ceramic dielectric by indentation and derived using the Oliver-Pharr method are reviewed.

Chen [77] uses indentation as one of the mechanical properties characterization technique for MLCC with X7R dielectrics and reported an elastic modulus of 200 GPa. Wereszczak et al. [79] measured elastic modulus, hardness and fracture toughness of MLCCs with X7R dielectric from three different manufacturers. However, the load being used and the location of the indentations being made were not specified in these two studies. Kim [78] evaluated elastic modulus, hardness and fracture toughness at two different planes of MLCCs. He concluded that both elastic modulus and hardness are isotropic, and modulus at the area with and without termination coverage is not significantly different. While different loads of 100 mN to 300 mN are used for indentation, the effect of load is not addressed in this study. Ryu et al. [80] evaluated mechanical properties of $BaTiO_3$ with different dopants and sintering processes. In this study, a 5 mN load was used to measure elastic modulus and hardness of the test specimens. Shin et al. [81] evaluated hardness and residual stresses of 'bare MLCCs' of bare MLCCs without terminals.

In this study, it was found that the measured hardness decreases after a certain distance from the internal electrodes on 3 different planes, which reflects the effect of internal electrodes on the measured hardness. However, since the MLCCs under test were not fully manufactured, it does not reflect the effect of end terminations on the measured values of commercial MLCCs. Summary of the mentioned studies are included in Table 4. In most of these studies, hardness and elastic modulus were reported as average values with percentage errors that are independent of test parameters and other factors. In the indentation field of research, the effect of measurement load, residual stresses, or indenter tip geometry on measured values of other materials have been reported. Therefore, to facilitate the use of the technology in the electronics industry, it is important to account for these effects on the indentation characterized mechanical properties derived with the Oliver-Pharr method.

Table 4. Indentation Measured Elastic Modulus and Hardness for Ceramic Dielectric

Test Units	**Load (mN)**	**Tip**	**Elastic Modulus (GPa)**	**Hardness (GPa)**	**Reference**
MLCC(X7R)	N/A	N/A	200	/	[77]
MLCC(X7R)	100-300	Berkovich	175-183	11.5-12	[78]
MLCC(X7R)	"Low Loads"	Berkovich	192-203	11.3	[79]
$BaTiO_3$ with additives	5	Berkovich	156.5-173.6	12-14.1	[80]
MLCC(Y5V)	250	Vickers	/	6.8-11	[81]

3.3 Effect of Test Parameters: Experimental Procedure and Results

In the first part of the study, the effect of measuring parameters, including measuring load, location, and indenter tip geometry are evaluated. Commercial MLCCs with X7R dielectric from 2 manufacturers of sizes 1206 and 1210 respectively are used in this study. All samples are ground and polished with 0.05 μm diamond suspension to an optical finish. In this study, a Keysight G200 system was used for measuring elastic modulus and hardness on the samples. To evaluate the effect of measuring load, and location, two MLCCs from each manufacturer is used. One of the MLCCs from each manufacturer was indented using a 150mN measuring load, and the other was indented using a 300mN load as shown in Table

5 with a Berkovich indenter tip. For each of the MLCCs, 20 indentations are made from the terminal to the middle of the capacitor on both sides of the MLCCs as shown in Figure 13.

Table 5. Test Matrix for Location and Load Dependency Study

	150mN	**300mN**
MLCC-A	1	1
MLCC-B	1	1

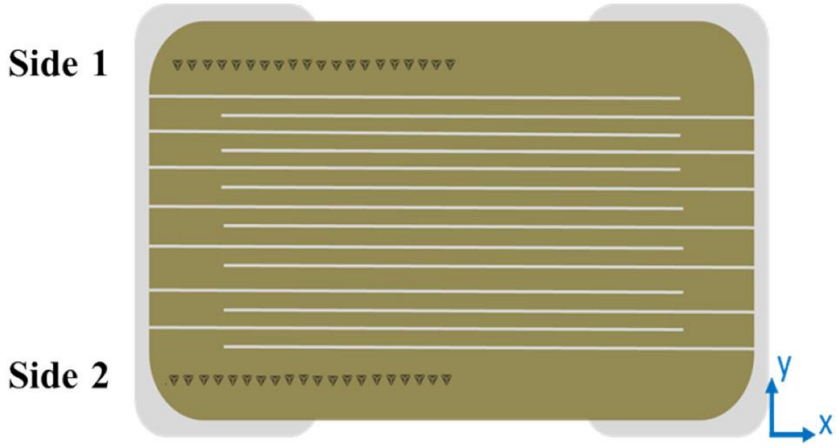

Figure 13. Illustration of Indentations Made on Cross-Sectioned MLCC Units

To evaluate the effect of different tip geometry, indentations are repeated at 150 mN using a Vickers tip on both sides of an MLCC, so that the effect is compared for both MLCC-As and Bs as shown in Table 6. To overcome part to part variations,

indentations are performed for 2 MLCC units from each group for the study of tip geometry.

Table 6. Test Matrix for Indenter Tip Geometry Dependency Study

	Berkovich	**Vickers**
MLCC-A	2	2
MLCC-B	2	2

3.3.1 Effect of Measuring Load

In this part of the study, peak loads of 150 mN and 300 mN were used. 20 indentations were performed from the terminal to the middle of the capacitor on the sides of the MLCCs as shown in Figure 13, and indentations are made with Berkovich indenter tip for studying the effect of measuring load. For MLCCs from manufacturer A (MLCC-As), it was found that the measured elastic modulus is strongly dependent on load, with a mean of 223.5 GPa and 191.8 GPa for 150 mN and 300 mN respectively as shown in Figure 14. For Manufacturer B (MLCC-Bs), load dependence is also observed, with a mean of 198 GPa and 181.2 GPa for 150 mN and for 300 mN respectively as shown in Figure 15. While hardness is load dependent for both samples, the dependence is less significant for both samples as shown in Figure 16 and Figure 17.

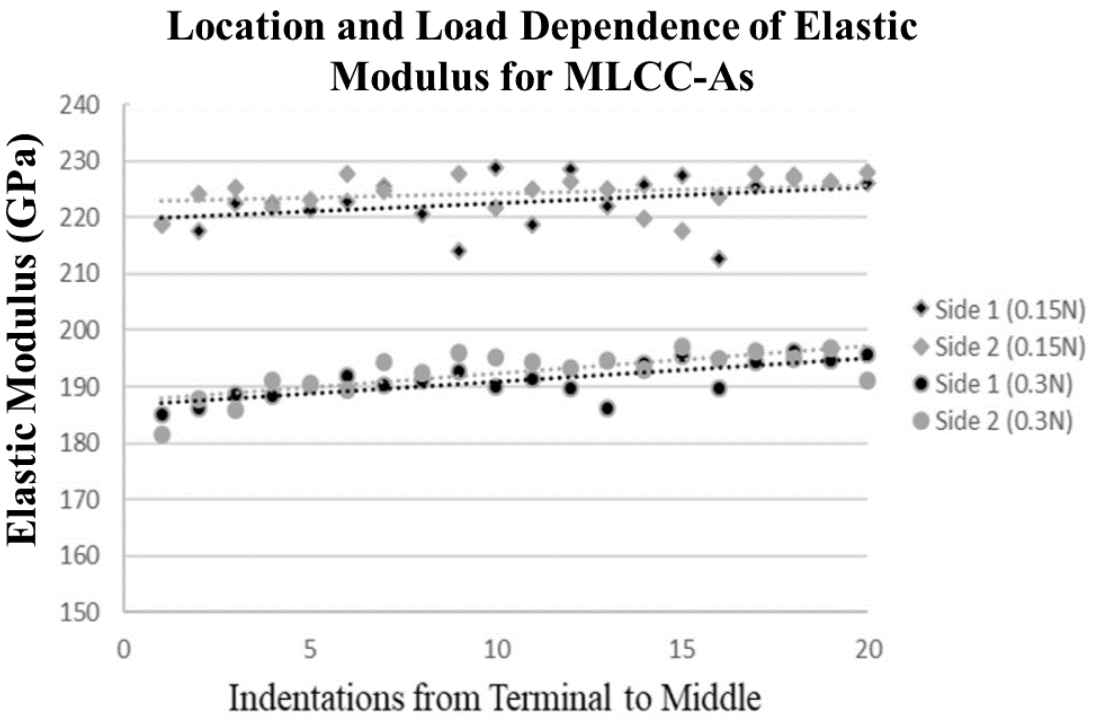

Figure 14. Location and Load Dependence of Elastic Modulus for MLCC-As

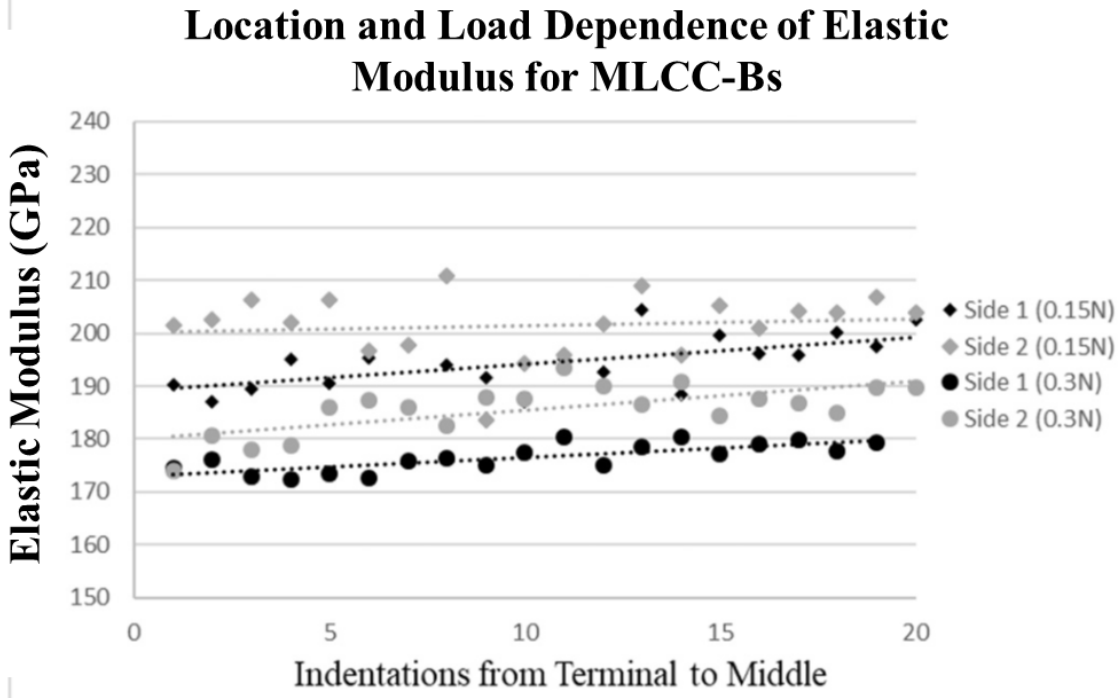

Figure 15. Location and Load Dependence of Elastic Modulus for MLCC-Bs

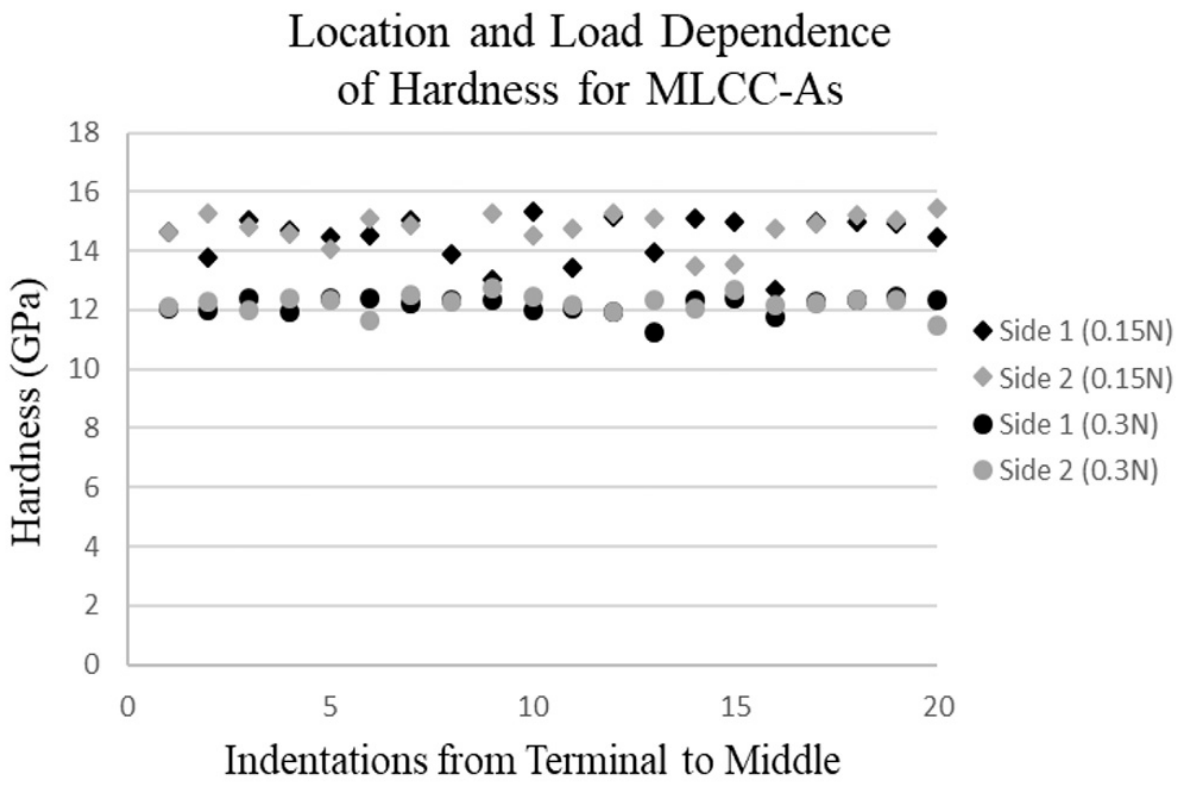

Figure 16. Location and Load Dependence of Hardness for MLCC-As

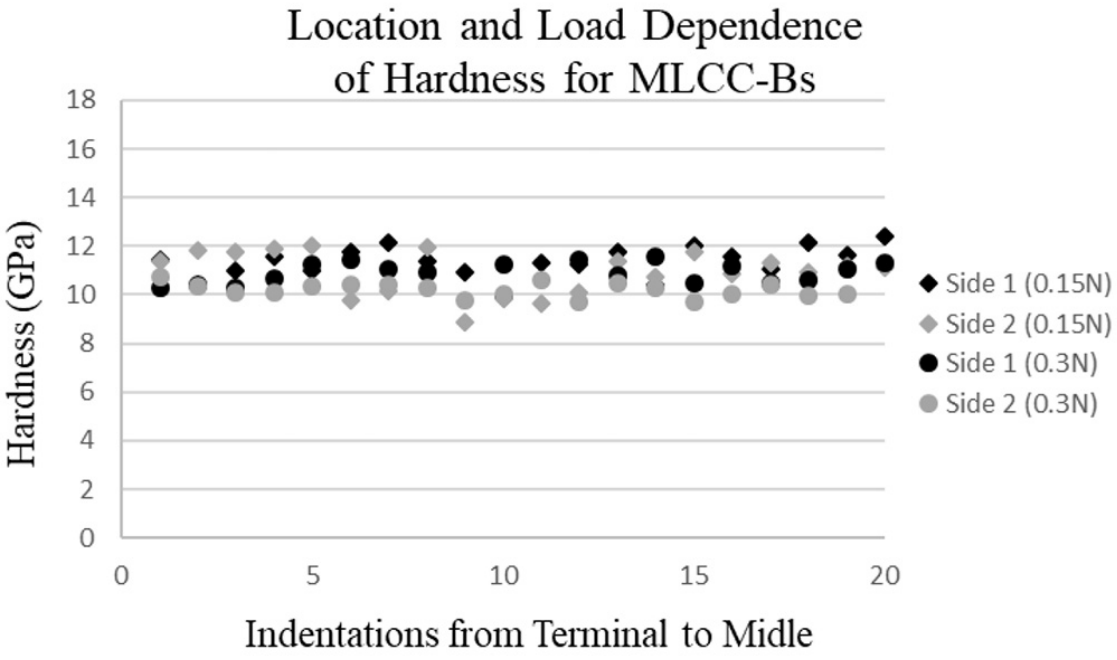

Figure 17. Location and Load Dependence of Hardness for MLCC-Bs

3.3.2 Effect of Location

For both MLCC-As and Bs, an increase in elastic modulus is observed as indentations move from one side of the capacitor towards the middle as shown in Figure 14 and Figure 15. Location dependence of hardness is not significant for both MLCC-As and Bs compared to elastic modulus. The average values from indentation 1 to 5 of the MLCC on each side (total 10), and the ones from indentations 15 to 20 are compared and tabulated in *Table 7*.

Table 7. Comparison of Averaged Mechanical Properties from Indents 1-5 and Indents 15-20

	Elastic Modulus Average for Indents 1-5	**Elastic Modulus Average for Indents 15-20**	**Hardness Average for Indents 1-5**	**Hardness Average for Indents 15-20**
MLCC-As (150mN)	221.59± 2.35	225.07± 4.28	14.6± 0.41	14.74± 0.73
MLCC-As (300mN)	187.56± 2.8	194.5± 2.19	12.19± 0.19	12.17± 0.29
MLCC-Bs (150mN)	197.11± 7.03	201.16± 3.51	11.43±0.48	11.45±0.5
MLCC-Bs (300mN)	177.03± 4.15	183.24± 4.81	10.46±0.34	10.5±0.44

3.3.3 Effect of Indenter Tip Geometry

To evaluate the effect of different indenter tip geometry, the same measurements are performed at 150 mN with a Vickers tip and the results are compared with the measurements made with the Berkovich tip. It is found that both elastic modulus and hardness measured with a Berkovich tip have a higher value than the ones measured with a Vickers tip for both MLCC samples as shown in Figure 18. The difference in values are more significant for MLCC-As than for MLCC-Bs.

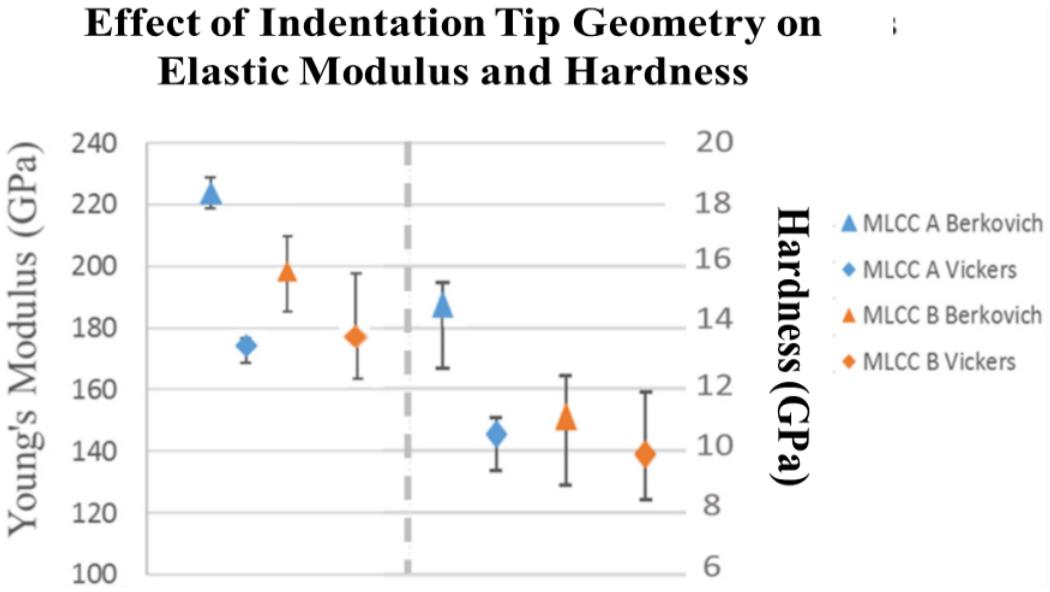

Figure 18. Effect of Indentation Tip Geometry on Elastic Modulus and Hardness

3.4 Discussion

The observed effects of load dependence, location dependence and indenter geometry dependence of mechanical properties derived from the Oliver-Pharr

method are discussed in this section. Other implications from the large set of indentation measured mechanical properties data are also discussed.

3.4.1 Load Dependence (Indentation Size Effect)

It is widely reported that measured hardness and elastic modulus increases with a reducing load, known as Indenter Size Effect (ISE). It represents a complex relationship between measurement load and measured hardness depending on the material. The phenomenon can be associated with different causes such as work hardening, roughness, pile-up, sink-in, and indenter shape [85][86]. It is generally agreed that ISE observed in indentation tests is a rather complex phenomenon and cannot be explained based on one mechanism [87]. For ceramic materials, ISE is typically explained with material responses at low loads which lead to over-estimated properties, such as significant effect of elastic recoveries [88] at low loads. Added to properties of different materials, more efforts in the literature focus on modeling the observed effect rather than concluding a dominant mechanism responsible for ISE. Gong [89] has published the decrease in measured Vickers hardness with increasing load from 5 N to 45 N for 12 ceramic materials. A Proportional Specimen Resistance (PSR) model [90] or modified version [89] is commonly used to model ISE. In this model, the applied test load, P, and the diagonal length of the indentation, d, is found to follow the relationship below. The coefficient k values specific to indenter tip geometry is given in Table 8.

$$P = a_1 d + a_2 d^2$$

$$\frac{P}{d} = a_1 + a_2 d$$

$$a_2 = \frac{H_T}{k}$$

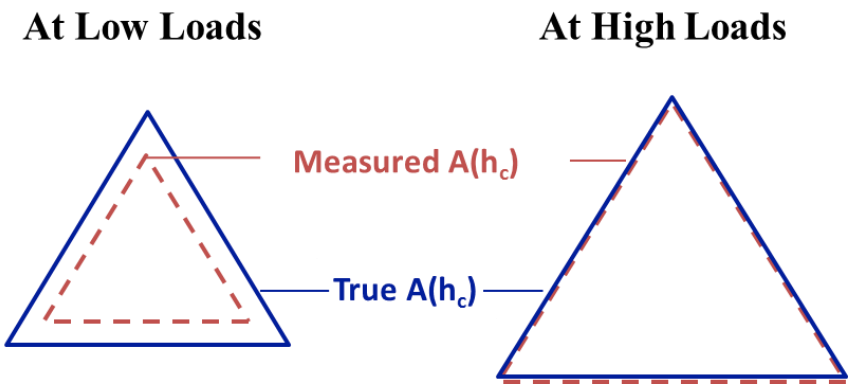

Figure 19. Over-estimation of Elastic Modulus and Hardness due to Smaller Measured Contact Area at Low Loads

Table 8. Indenter Tip Coefficient k for PSR Model

Indenter Tip	**k** (for P in Newton, d in meter)
Vickers	1.854
Berkovich	1.732
Knoop	14.229

In this relationship, ISE is represented by the a_1 term while the load independent hardness (H_T) is represented by the a_2 term. 20 indentations at 150mN, 300mN, and 400mN respectively were on MLCC-Bs were compared to evaluate the fitness of PSR on the samples under a small load range (150 mN to 400 mN). d of each indentation is measured as shown in Figure 20. The average values of P/d vs d are

plotted as shown in Figure 21 and are found to be linear as proposed in the ISE model. This represents that this relationship can sufficiently model ISE on MLCC-Bs over the measurement load range. H_T is then found to be roughly 8.7 GPa by the multiplication of the curve fitted parameter a_2 and indenter tip coefficient k. Directly measured load dependent hardness and the calculated independent hardness is shown in Figure 21.

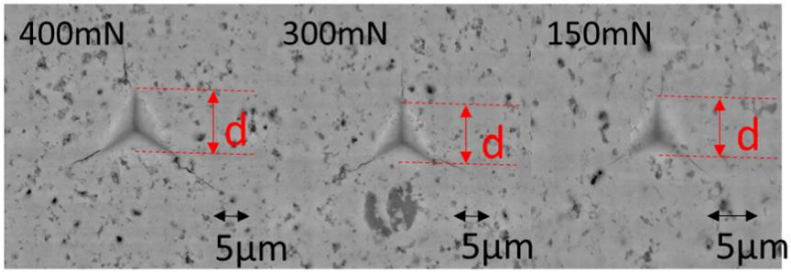

Figure 20. Berkovich Indents at 400 mN, 300 mN and 150 mN (left to right).

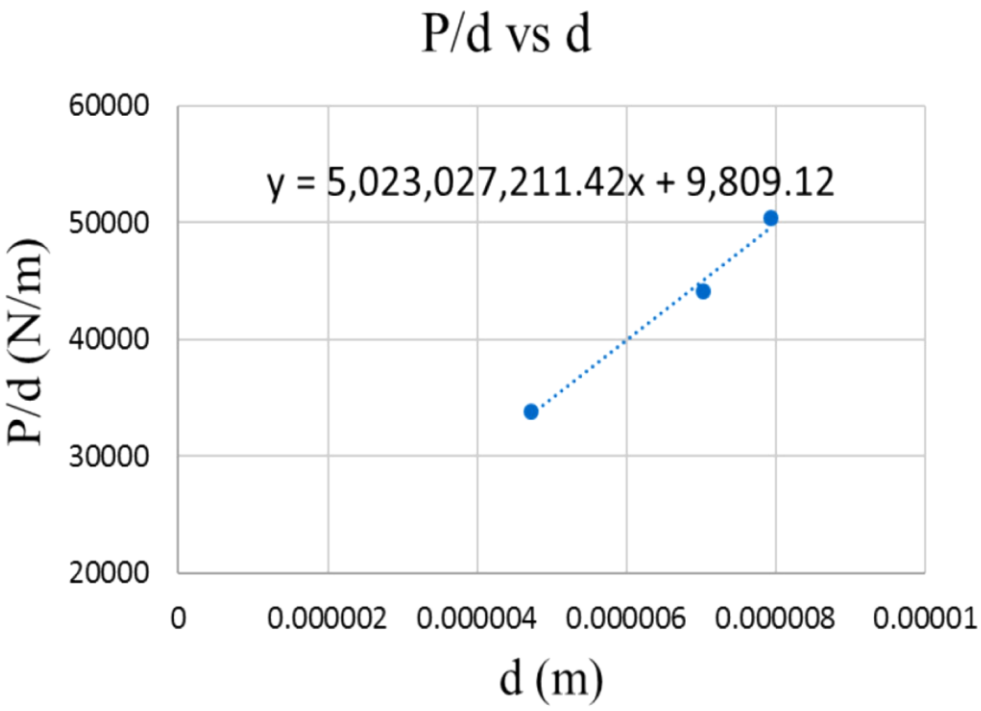

Figure 21. P/d vs d for MLCC-Bs (150mN, 300mN, 400mN)

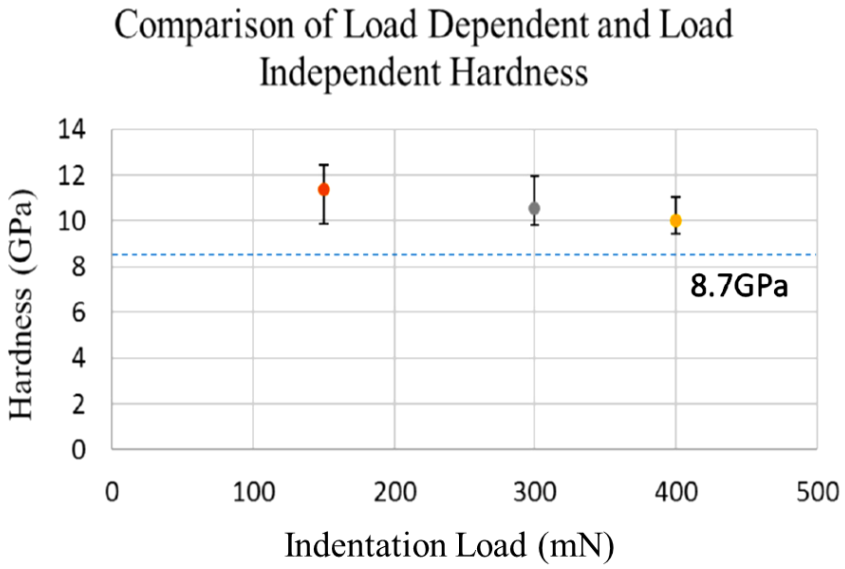

Figure 22. Measured Load Dependent Hardness and Calculated Load Independent Hardness

While the effect of load on measured elastic modulus is not as well established, the same load dependent phenomenon is reported for some materials in the literature [84]. Using the relationship between the initial slope of the unloading curve, and contact depth h_c as described in Section 3.1, a load independent elastic modulus can be derived from indentations made with different loads. A load independent elastic modulus of 172 GPa is calculated using the measurement results from the three different loads as shown in Fig. 12.

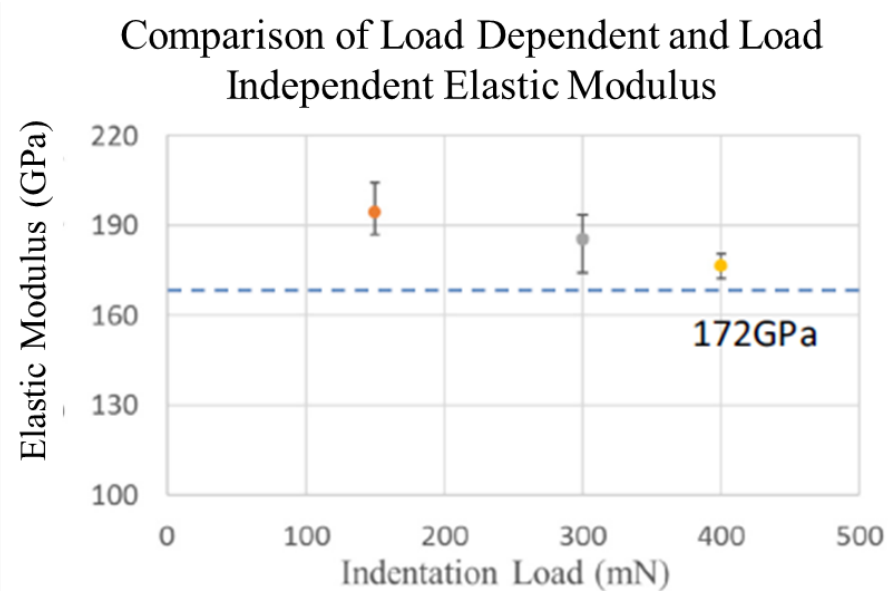

Figure 23. Measured Load Dependent Elastic Modulus and Calculated Load Independent Elastic Modulus

3.4.2 Location Dependence (Residual Stress Effect)

An un-poled, ceramic dielectric raw material should exhibit homogenous mechanical properties. Different processes involved in the manufacturing of MLCCs, however, can introduce residual stresses at various locations in an MLCC that are reflected in its location dependent mechanical properties. This can be

explained by residual stress introduced to the capacitor body due to the processing conditions of MLCCs. Prume [95] has measured residual stresses along the longer side of MLCCs with X-ray Diffraction. He observed a transition from tensile stress at the terminal to compressive stress in the middle of MLCCs with two different physical sizes (1206, 1210). The increase in hardness and elastic modulus with compressive stress and decrease with tensile stress has been reported for a variety of materials when indentation data were analyzed by standard methods [91], [96]. Chen et al. [97] used finite element analysis to evaluate the effect of residual stress on hardness and stiffness and concluded that tensile residual stress assist plastic deformation, and compressive residual stress reduce plastic deformation in a specimen, which explains the change in contact depth and the transition of measured elastic modulus in this study. This location dependence of the measured properties reflects the residual stress transition along the length direction reported for commercial MLCCs.

3.4.3 Indenter Tip Geometry Dependence and Other Observations

There are only a handful of studies that report the effect of indenter tip geometry on measured mechanical properties in the literature. In one of the more comprehensive studies that cover a variety of materials by Sakharova et al. [99] it is concluded that hardness measured by Berkovich tip is higher than Vickers to an observable degree when the ratio of residual indentation depth after unloading (h_f) to indentation depth at the maximum load (h_{max}), h_f/h_{max} is smaller than 0.65. This is attributed to the different plastic strain distribution induced by different tip

geometries for such ratios. However, the materials being covered in this study are not specified. In our study, h_f/h_{max} is found to be 0.87 ± 0.03 for both MLCC-As and Bs. Therefore, it is believed that the study in [99] did not cover ceramic dielectric materials, as the distinction between measurements from both indenter tips is significant well above the suggested threshold. Mechanical properties of ceramic dielectrics in MLCCs are known to differ based on dielectric formulation and processing conditions. Apart from the investigated factors, more scattered data is observed for MLCC-Bs compared to MLCC-As which can be attributed to their higher porosity as shown in Figure 24. Difference in measurements on both sides of MLCC-Bs also suggests an unsymmetrical residual stress on both sides of the capacitor body being introduced due to manufacturing processes. This indicates that the indentation technique also shows potential as an alternative to compare part variations that can be adopted in part selection or screening procedures of MLCCs and other electronic components.

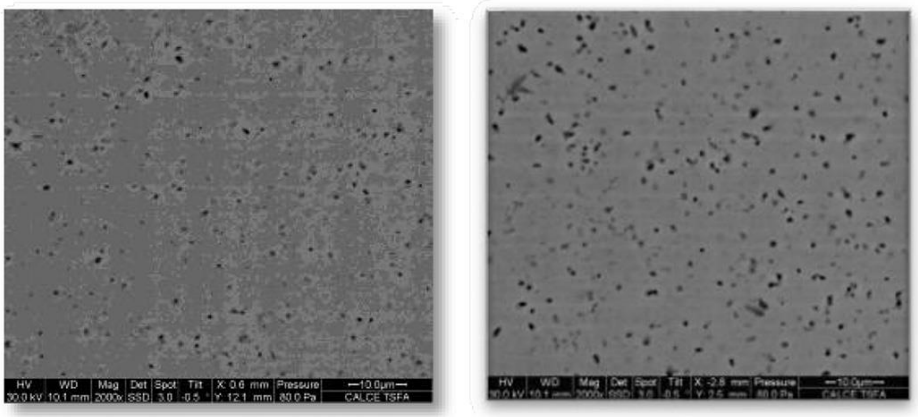

Figure 24. Porosity of MLCCs-A (left) and B (right) dielectric at 2000×

3.5 Effect of MLCC Treatment: Experimental Procedure and Results

In the second part of the study, the effect of voltage history and aging on indentation measured mechanical properties are evaluated. To study the effect of voltage history, the same MLCC units from the two manufacturers were used. The MLCC samples were reformed at 150°C for 30 minutes to minimize any effect of aging or electrical tests performed by the part manufacturer prior to packaging. Some units were then exposed to DC voltage applications (poling) at various voltage levels below or equal to their rated voltage as shown in Figure 25.

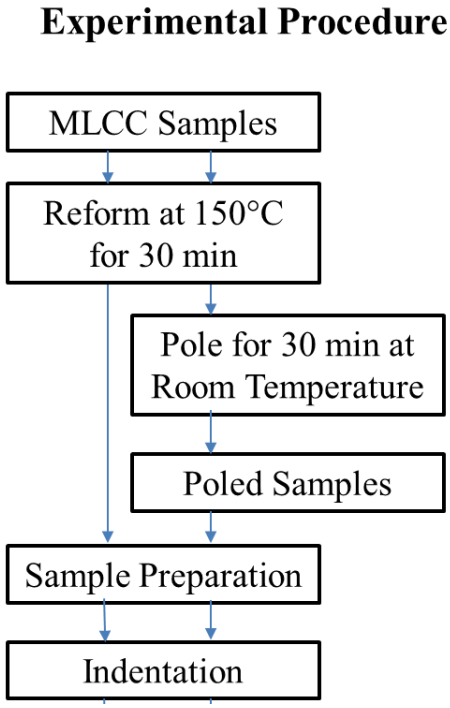

Figure 25. Experimental Procedure for Evaluation on Effect of Voltage History on Indentation Measured Mechanical Properties

Baseline measurements were performed on 4 MLCCs for each manufacturer. 2 samples are used for each poling condition to account for part variability as shown in Table 9, and 20 indents were made in between the electrodes as shown in Figure 26 for each sample with Vickers indenter. Since the inter-electrode spacing for MLCC-As and Bs are not the same (about 10μm and 20μm respectively), measuring load at 100mN and 150mN are used respectively to minimize the variance of measured values and interference with the electrodes. The indents made with 100mN for MLCC-As and 150mN for MLCC-Bs in between the electrodes are shown in Figure 27. After poling, samples were potted in epoxy for sample preparation. Since an exposure to temperature above the Curie temperature can de-polarize the samples, potting compound systems with a minimal exothermal reaction over curing was selected.

Table 9. Test Matrix for Poling History Dependency

	Baseline	**Each Poling Condition**
MLCC-A	4	2
MLCC-B	4	2

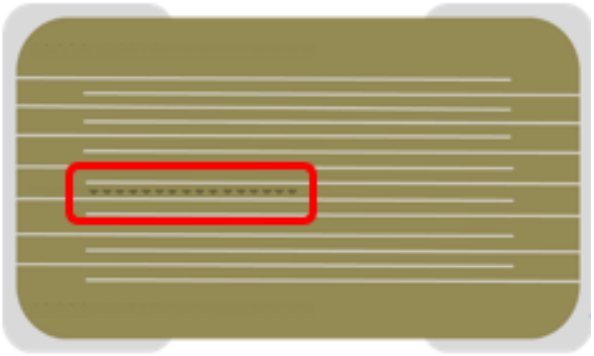

Figure 26. Indentations for Evaluation of Poling Effects

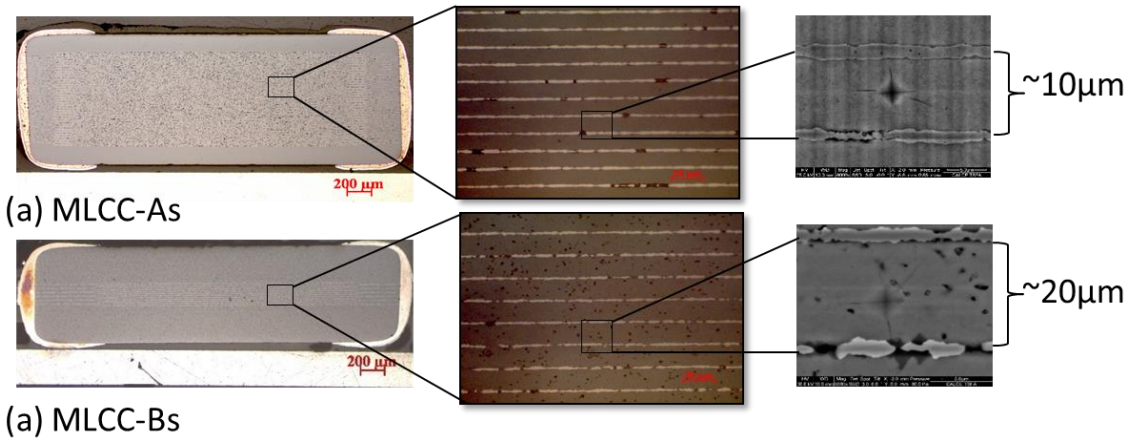

Figure 27. Indents Made in between Electrodes on (a) MLCC-As, (b) MLCC-Bs

Aged MLCCs in original packaging (tape and reel) were acquired to evaluate the effect of aging/reforming in this study. The MLCCs are of 1210 size and from 2001 from its date code, which is about 17 years old at the time the experiment was run assuming a normal storage environment. A series of destructive and non-destructive evaluation below has been carried out to ensure authenticity of these parts. They include the validation of part number, verification of part and packaging material (e.g. tape and reel) dimensions, verification of electrode material, verification of electrical parameters on reformed parts, and the inspection for

anomalies or defects on part body. Results of the evaluation show no evidence of counterfeiting in these parts.

The experimental procedure for evaluating the effect of aging/ heat reforming is shown in Figure 28. 4 MLCCs were reformed at 150°C for 30 minutes, and 4 aged MLCCs from the original package were cross-sectioned and polished according to the sample preparation steps discussed above. 20 indentations are made with 150mN on one side of the MLCC as shown in Figure 13 with Vickers' indenter tip. Indents are made within 24 hours after poling to minimize the aging effect for the reformed samples.

Table 10. Test Matrix for Aging/Heat Reforming Dependency

	Baseline
Aged MLCCs	4
Reformed MLCCs	4

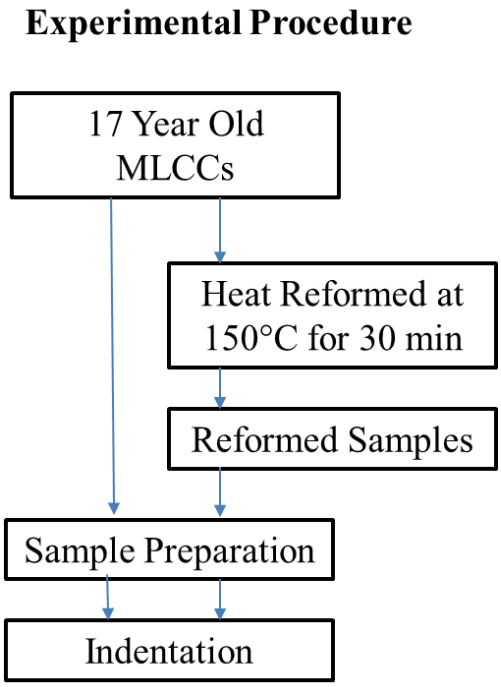

Figure 28. Experimental Procedure for Evaluation on Effect of Aging/ Heat Reforming on Indentation Measured Mechanical Properties

3.5.1 Effect of Voltage History

The effect of poling voltage on indentation measured elastic modulus for MLCC-As and MLCC-Bs are shown in Figure 29 and Figure 30 respectively. Elastic modulus in these figures are normalized to the average value of the unpoled units.

Variation of indentation measured elastic moduli follow a decreasing trend with the increase in poling voltage (field), the decrease appeared to stabilize for units poled at 1500V/mm. At rated voltage, average elastic modulus went through a 24% and 22% loss compared to the unpoled value for MLCC-As and Bs respectively.

The effect of poling voltage on indentation measured hardness for MLCC-As and MLCC-Bs are shown in Figure 31 and Figure 32. Similar to the trend for elastic modulus, hardness also follows a decreasing trend, with larger variances.

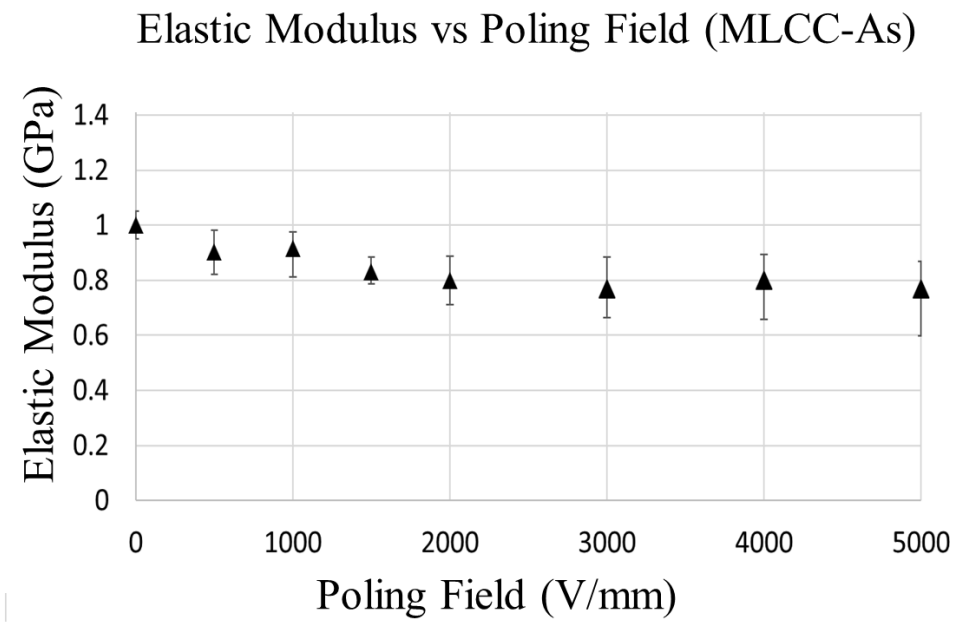

Figure 29. Effect of Poling Field of Indentation Measured Elastic Modulus for MLCC-As

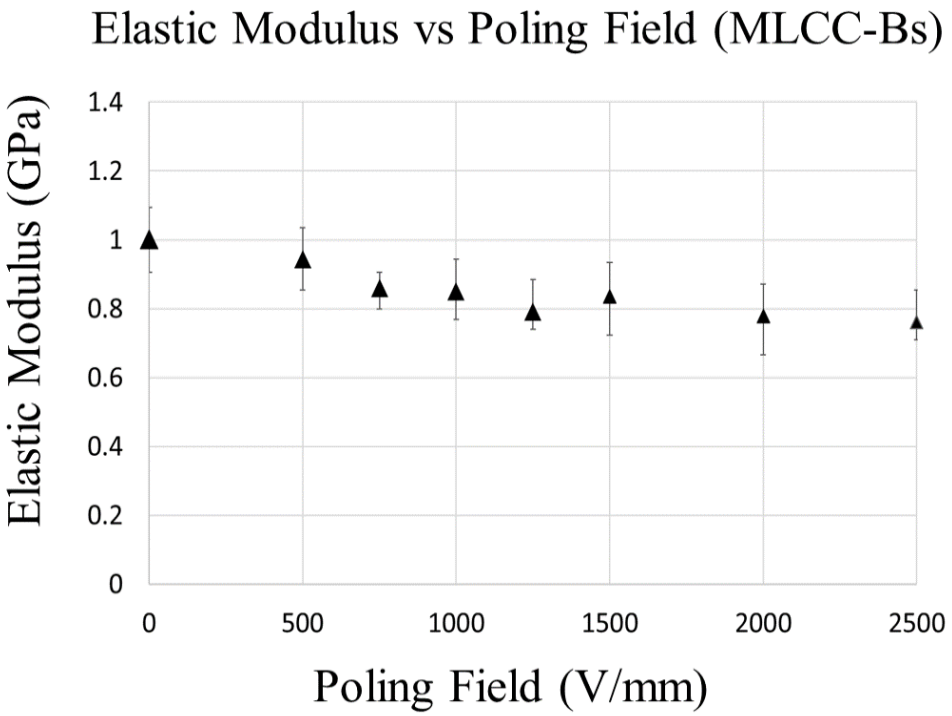

Figure 30. Effect of Poling Field on Indentation Measured Hardness for MLCC-Bs

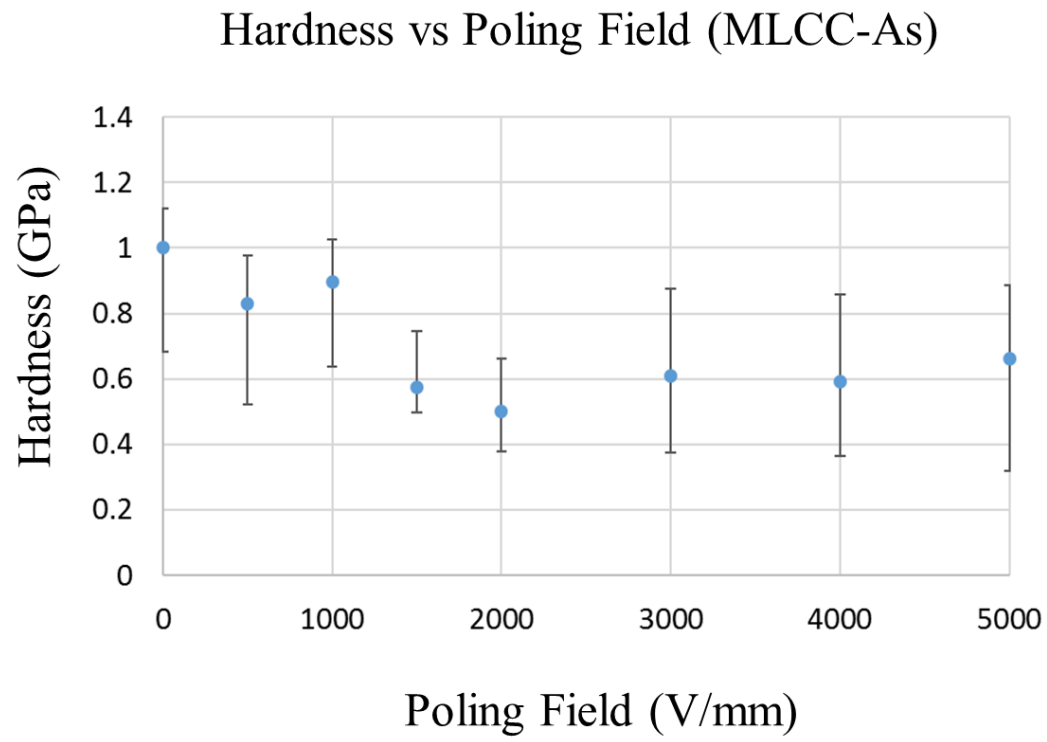

Figure 31. Effect of Poling on Indentation Measured Hardness for MLCC-As

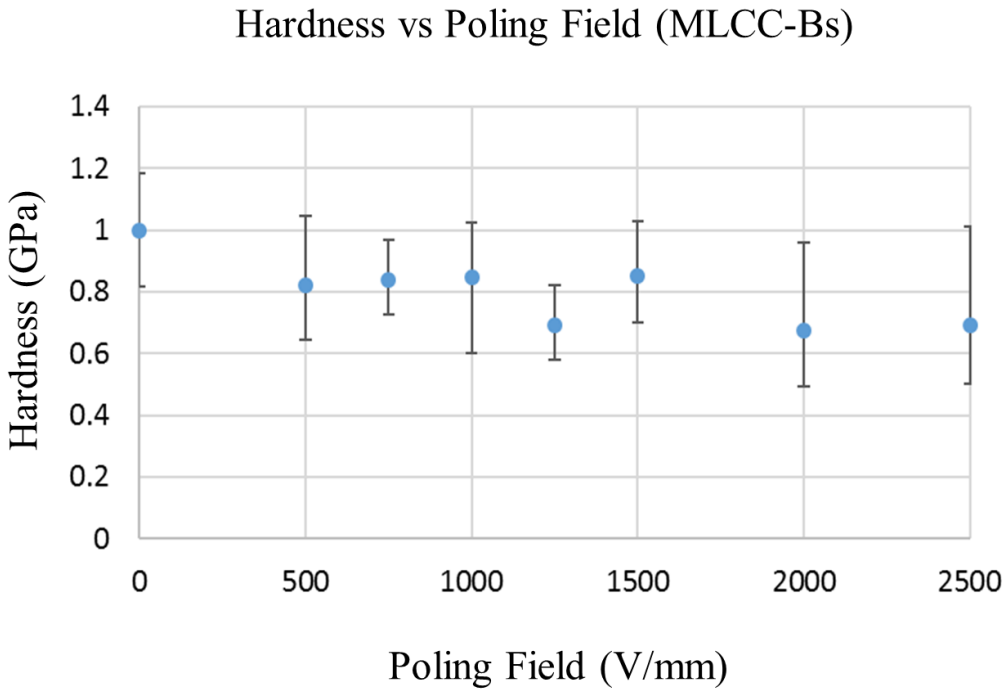

Figure 32. Effect of Poling on Indentation Measured Hardness for MLCC-Bs

3.5.2 Effects of Aging/ Heat Reforming

Indentations are made on the 4 aged MLCCs, and the 4 reformed MLCCs. Elastic moduli and hardness measured from the terminal to the middle of an MLCC is plotted in Figure 33 and Figure 34 respectively. The elastic moduli and hardness from aged and reformed MLCCs are represented by red circles and blue cross respectively.

From the result, the measured elastic moduli of the 2 groups are significantly overlapped with the 17 year old MLCCs have average values of 168.6, 170.5, 175.5 and 176.6 GPa and the ones for the reformed MLCCs have average values of 172.3,

175.8, 177.1 and 178.8 GPa respectively. For hardness, the average values from aged MLCCs are 9.47, 9.71, 9.78, 10.05 GPa, while the reformed ones are 9.68, 9.69, 9.7, 9.95 GPa. The results indicate a negligible effect of aging/heat reforming on indentation measured elastic modulus and hardness.

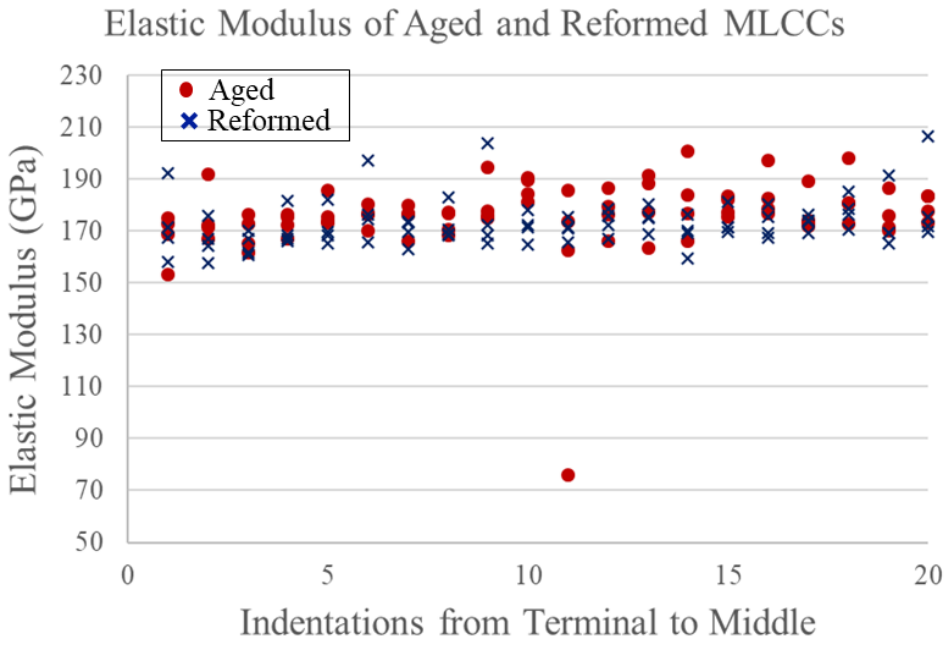

Figure 33. Effect of Aging/Reforming on Elastic Modulus of MLCCs

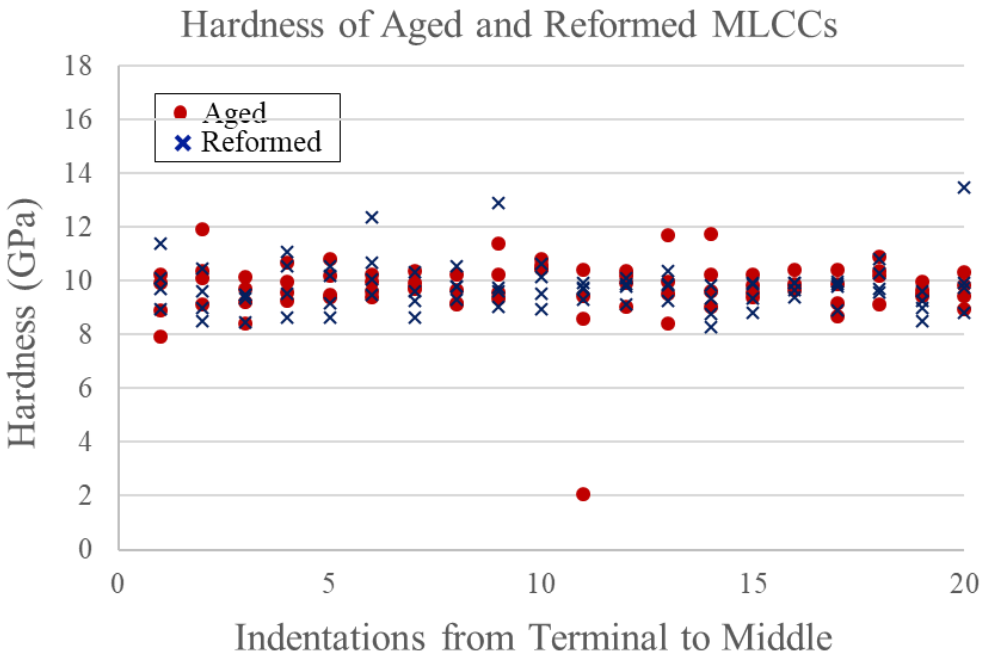

Figure 34. Effect of Aging/Reforming on Hardness of MLCCs

3.6 Discussion

The increase in poling voltage results in a decreasing trend in the measured elastic modulus and hardness of the tested MLCCs using the Oliver-Pharr method.

Indentation characterized properties of piezoelectric materials have been shown to be dependent on polarization state of the material and the applied voltage to the specimen during the test. The change is often reasoned by the change in stress distribution under the indenter due to electromechanical coupling for poled and unpoled materials [92], or domain switching in response to the loading and unloading steps during an indentation [94]. However, it is unclear which effect is more dominant for the observed dependence. A potential explanation for the observed decrease in elastic modulus and hardness can be loading induced domain

re-orientation. With loading, in-plane compressive stress forces the domains to line up in the thickness direction of the capacitor. For an unpoled material, more domains are in random orientations. Therefore, more energy is dissipated in domain switching for unpoled materials, resulting in a smaller depth, thus rendering a higher hardness and modulus.

Indentation measured elastic modulus and hardness for a 17 year old MLCC closely resembles to the values of the ones that are reformed, indicating the aging effects of 17 years in original packaging does not cause any significant change in mechanical properties measured by the indentation technique.

3.7 Conclusion

The application of indentation in evaluating mechanical properties of electronic components has become more commonplace in the recent decade. Oliver-Pharr method is the most common method in deriving mechanical properties from indentation data. In this section, we evaluated the effect of test parameters (measurement load, choice of indenter tip, and location) and MLCC treatment (voltage history and aging/heat reforming) on the measured elastic modulus and hardness in commercial MLCCs using the Oliver-Pharr method. The results in this section can serve as a baseline of indentation measured properties under different test parameters and with MLCCs under different treatment.

For the effect of test parameters, we found that elastic modulus and hardness decreases with increasing load due to the Indenter Size Effect (ISE). PSR model and linear fitting was used for obtaining load independent values from

measurements obtained from 3 different loads. For the effect of location, it was observed that elastic modulus increases from the terminal ends to the middle of the tested MLCCs, representing a transition in residual stress from tensile to compressive from the terminal to the middle of an MLCC induced by manufacturing processes. For the effect of indenter tip geometry, hardness and elastic modulus measured with Berkovich indenter tips yield higher value than that by Vickers tips for the tested MLCC units with a h_f/h_{max} of 0.87 ± 0.03, which may suggest that the tip geometry effect has a wider h_f/h_{max} ratio coverage than reported (< 0.65) in the literature.

For voltage history, both measured elastic modulus and hardness show a decreasing trend with an increase in poling voltage. This effect is potentially caused by the change in indentation depth accompanied by domain switching.

For the effect of MLCC treatment, the measured properties before and after heat reforming of the 17 year-old MLCCs do not show noticeable difference, indicating the aging at normal storage condition for 17 years do not constitute observable changes in mechanical properties measured by the indentation technique.

As a summary, although indentation is a convenient method for assessing mechanical properties for small devices, the measured properties vary with test parameters. Caution should be taken when one attempt to compare indentation measured properties. Oliver-Pharr method is not meant for deriving properties for materials that are not isotropic, nor does it offer an undemanding solution in deciphering the complex electromechanical coupling effect for ferroelectric/piezoelectric materials. However, the method is used regardless of its

applicability in the industry due to its wide adoption and sometimes, it is found to be the default method in commercial indentation systems. With the baseline measurements established in this study, the effect of voltage history and heat reforming/aging on MLCCs, or other ferroelectric/ piezoelectric devices can be addressed.

4 Evaluation of Potential Mechanisms for Increased Flexural Strength in Commercial MLCCs

From literature review, flexural strength or bending strength of a ferroelectric material are reported to increase after electrical poling/ voltage application. As the dielectric of MLCC is made of $BaTiO_3$, the same phenomenon should be expected. This effect implies a more robust MLCC under flexural stresses after exposure to a DC voltage stress for a certain period of time.

In this section, two mechanisms are proposed to potential flexural strength increase in commercial MLCCs. In Section 4.1, the effect of switch toughening induced fracture toughness is discussed and proven by using Vickers' indentation. In Section 4.2, the effect of voltage history on crystallographic/ domain orientations is evaluated using EBSD on a commercial MLCC unit. With the evidence of change in crystallographic orientations after poling, stress analysis (FEA) on MLCC body is carried out under using a 3 point bending set up with elastic properties as a function of dielectric texture as an input. From the result of these two studies, the two mechanisms can potentially contribute to increase in flexural strength of commercial MLCCs by increasing the strength of the effective dielectric layers, and reducing stresses acting on the MLCC body.

4.1 Switch Toughening Induced Fracture Toughness Anisotropy

Domain switching at crack tips are reported to inhibit crack growth. This effect is known as switch toughening. This effect results in fracture toughness anisotropy in poled ferroelectrics because of the preferred orientations of domains in the

specimen. In this section, switch toughening mechanism resulting from a series of ferroelectric and ferroelastic effects is discussed. It is one of the potential mechanisms for the increase in flexural strength in poled ferroelectric materials because it inhibits the growth of cracks in the thickness direction. This effect is usually evaluated by Vickers' indentation in the literature. In this study, the same method is used to confirm whether fracture toughness anisotropy exist for poled commercial MLCC units, and if the effect strengthens for higher poling voltages.

4.1.1 Switch Toughening

For a ferroelectric material, material properties are highly dependent on domain orientations. One of the most demonstrated effect in the literature is switch toughening. The strength of the switch toughening depends on the relative position between crack tip and domain orientations around the crack tip. In this section, the effect of switch toughening in an unpoled and a poled ferroelectric material are discussed Domain orientations are illustrated as blue rectangles in Figure 35 and Figure 36, and cracks in perpendicular directions are considered.

For an unpoled ferroelectric material at a "stress free" state, ferroelectric domains should be randomly distributed across the material is shown in Figure 35. When a crack propagates through the material, tensile stress acts perpendicular to the crack propagating direction as shown in Figure 35 (a).The tensile stress at the crack tip causes the domains to switch along the tensile stress direction by the ferroelastic effect as illustrated in Figure 35 (b)[102][103]. This domain switching process consumes available elastic energy and increases the activation energy barrier for

the formation of new crack surfaces, resulting in the toughening effect [104][105]. For an unpoled ferroelectric, the domain orientations with respect to any crack direction should be the same due to the initial random distribution of domain orientations. Therefore, for a crack that is propagation in a different direction, the amount of switch toughening effect should be equivalent and results in a similar crack length as shown in Figure 35 (c) and (d). Therefore, fracture toughness is isotropic due to the same amount of toughening effect for cracks propagating in all directions.

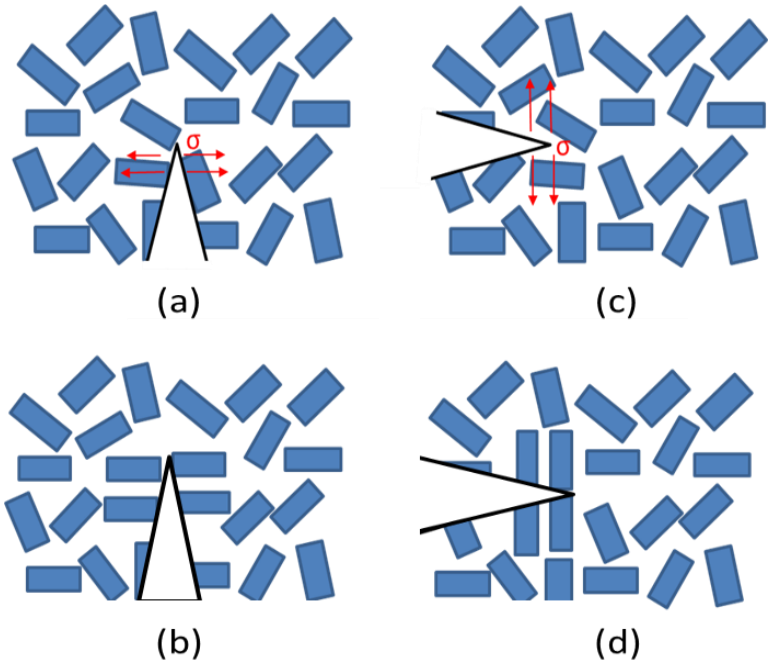

Figure 35. Switch Toughening Effect in Unpoled Ferroelectric Material

A poled ferroelectric material is illustrated in Figure 36, the perfectly aligned domains is used for demonstration purpose. In reality, the domains in a polycrystalline material cannot be 100% aligned primarily due to inter-granular constraints to domain wall motions [106]. In Figure 36 (a), a crack propagates in

the poling direction. Due to the tensile stress acting on the crack tip perpendicular to crack propagating direction, domains that are initially parallel to the propagating direction are switched to the perpendicular direction. As more domains are in the "preferred" orientation for switching in this case, the consumption of elastic energy for domain switching in the crack tip vicinity is higher and results in a more significant crack growth inhibition compared to in the case of an unpoled material as shown in Figure 36 (b). For a crack that propagates perpendicular to the poling direction as shown in Figure 36 (c), tensile stress acts on the crack tip vicinity like the previous cases. However, since the domain orientations are already parallel to the tensile stress direction, stress-induced ferroelastic domain switching does not take place in this case. For this reason, new crack surface can be generated with the available local elastic energy and continue to grow as shown in Figure 36 (d). This explains the reason for fracture toughness anisotropy existence in poled ferroelectrics but not unpoled ones.

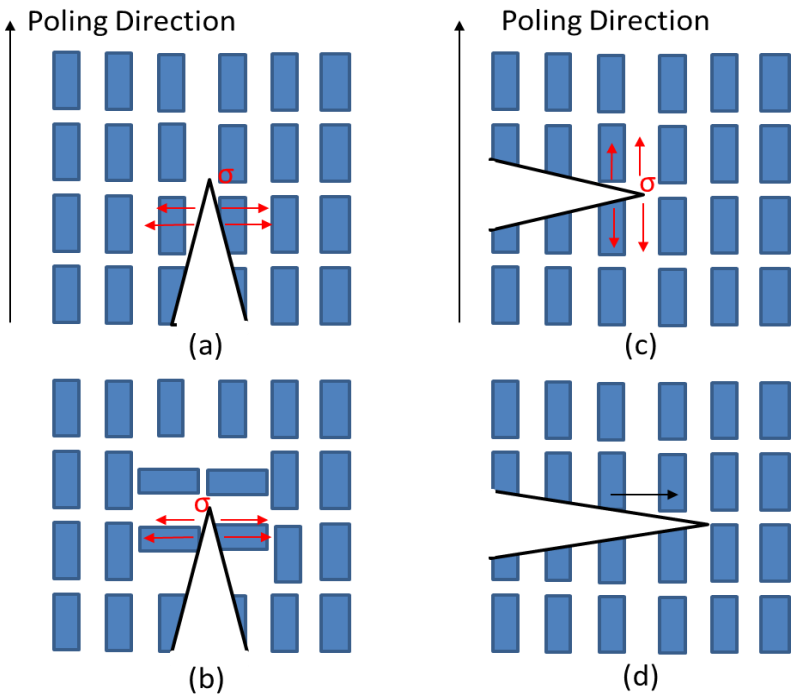

Figure 36. Switch Toughening Effect in Poled Ferroelectric Materials

4.1.2 Experimental Procedure

Poling induced anisotropy is evaluated using the most widely adopted method in the literature- indentation. With a package was reformed at 150°C for 30 minutes to eliminate the effect of aging or electrical tests prior to packaging on crystal/ domain orientations. With rated voltage of the MLCC under evaluation at 50V, samples are poled at 25V, 30V, 40V and 50V (Correspond to 2.5kV/mm, 3kV/mm, 4kV/mm and 5kV/mm respectively) for 30 minutes. Including the control samples that are not poled, 2 samples are used for each poling condition to account for part variability as shown in Table 11, and 20 indents were made in between the electrodes for each sample.

After poling, samples were potted in epoxy for sample preparation. Since an exposure to temperature above the Curie temperature can de-polarize the samples, potting compound systems with a minimal exothermal reaction over curing is selected. Potted samples are then ground and polished from 400 grit sandpaper until 0.05μm diamond suspension for an optical finish. Keysight G200 system was used for performing indentation in this part of the study. Indentations are made with 100mN measuring load. All the indents were imaged with Scanning Electron Microscopy (ESEM) at 6000X for crack length measurement. To account for the effect of aging, the time between the end of poling and the start of the first indent is kept within 48 hours for each sample.

Table 11. Test Matrix for Poling Voltage Dependence on Fracture Toughness Anisotropy

	Baseline	**25V**	**30V**	**40V**	**50V**
MLCC-As	2	2	2	2	2

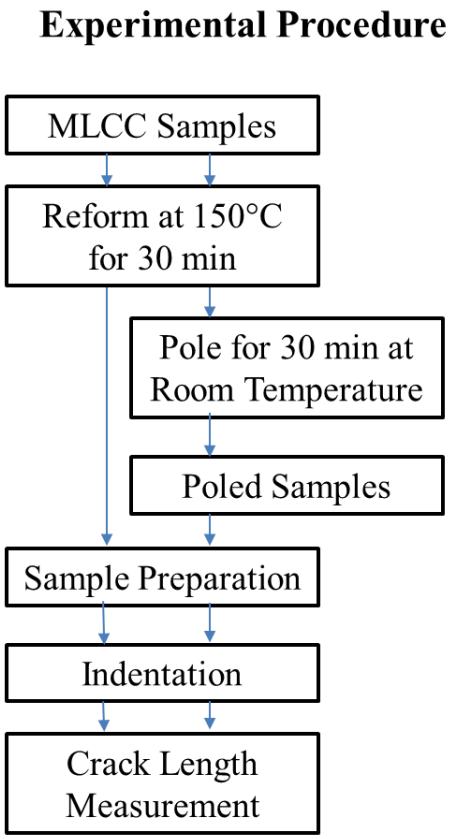

Figure 37. Experimental Procedure for Evaluation of Poling Induced Fracture Toughness Anisotropy

4.1.3 Indentation Results

Crack lengths that are perpendicular (cracks ⊥ pol) and parallel to the poling directions (cracks ∥ pol) are measured from one end of the crack to the other end through an indent, and they are represented by red triangles and blue circles in Figure 38. Data at 0 poling field represents crack lengths on samples which have not been poled. For indents made on unpoled samples, cracks ⊥ pol are measured to be slightly shorter than cracks ∥ pol. As the poling voltage increases, the deviation of crack lengths from the two directions increases as shown in Figure 38.

It is also observed that except for the difference in crack lengths, the widths of cracks ⊥ pol also appears to be larger than that of cracks ⊥ pol. Representations of indents on MLCCs with different voltage histories are shown in Figure 39.

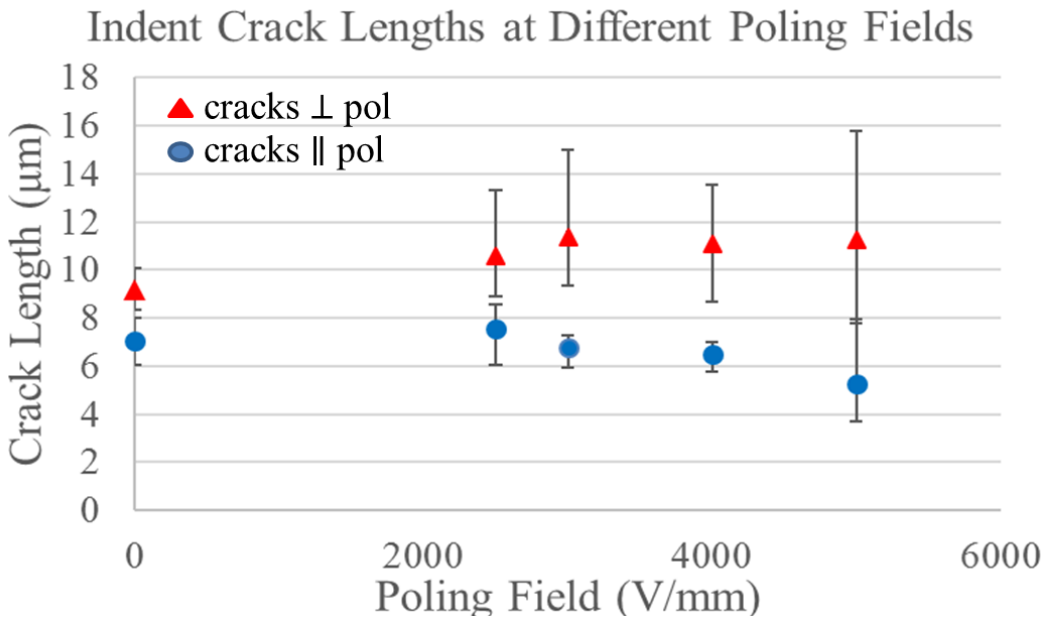

Figure 38. Effect of Poling Field on Crack Lengths

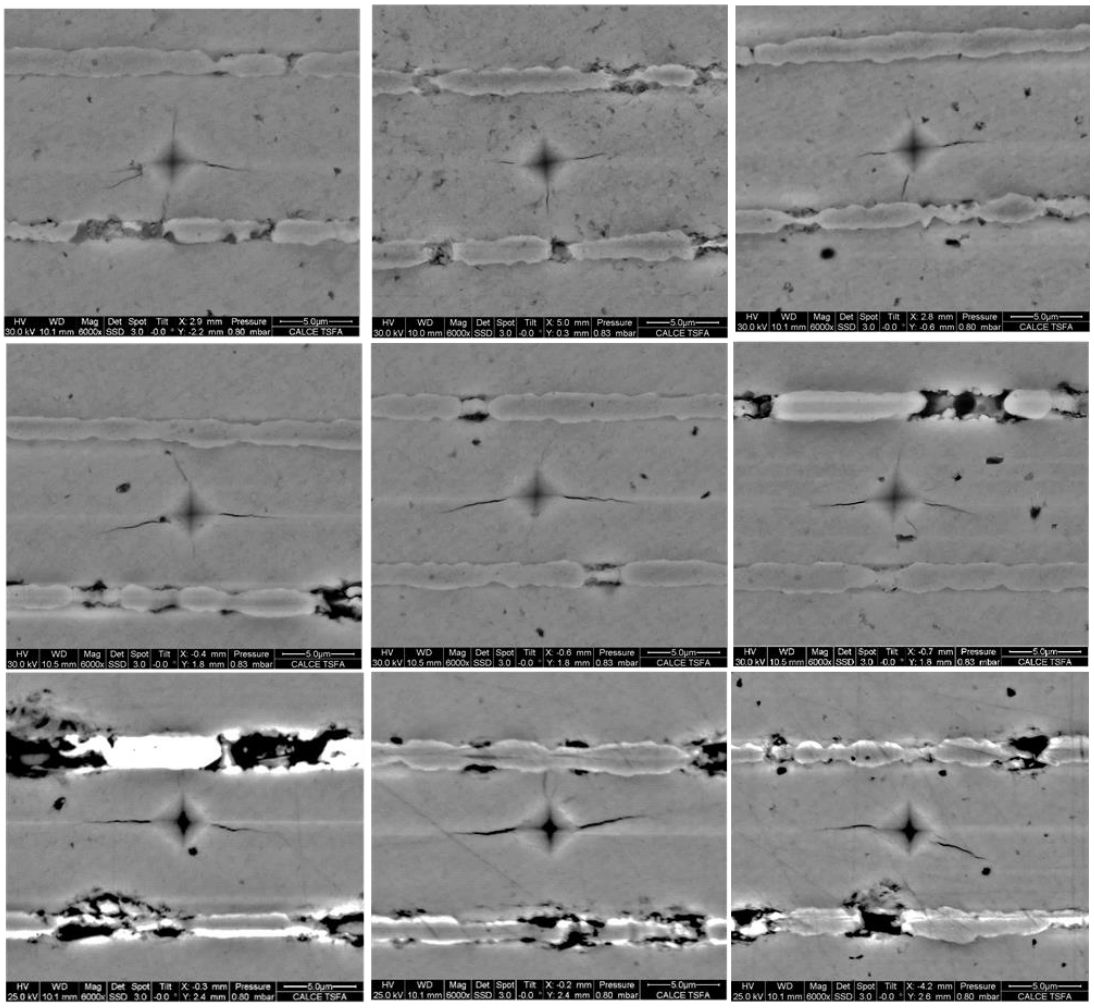

Figure 39. Representations of Indents on MLCCs which are Not Poled (First Row), Poled with 2.5kV/mm (2nd Row), and 5kV/mm (3rd Row)

4.1.4 Discussion

As discussed in Section 2.2 and 4.1.1, an unpoled ferroelectric material should exhibit isotropic fracture toughness due to the random orientations of domains at a "stress free" condition. From the measurements, cracks ⊥ pol are measured to be slightly shorter than cracks ∥ pol. As the unpoled units have been reformed above

Curie temperature prior to the indentations were made, polarizations due to electrical stress should be minimized. Also, cracks ∥ pol for most indents end before meeting the electrodes at the controlled measuring load (100mN). Therefore, the difference in crack lengths for unpoled MLCCs indicate the existence of mechanical residual stress in the unit.

In-plane compressive stress in MLCCs is widely demonstrated in the literature. Park et al. [108] used finite element analysis to evaluate thermal residual stress in MLCCs, and concluded an in-plane compressive stress and out-of-plane tensile stress in effective dielectric layers. Due to the ferroelastic effect, an in-plane compressive stress aligns domains in the out-of-plane direction of an MLCC. Therefore, cracks in the thickness direction can be inhibited by domain switching at the crack tip, but not for cracks along the electrode directions. Hence, the observation of fracture toughness anisotropy in the unpoled MLCCs agrees with the demonstrated residual stress distribution from the literature.

After poling, cracks ⊥ pol to grew longer and cracks ∥ pol appeared to be inhibited to a greater extent. The deviances between crack lengths in the two directions grow larger for MLCC samples poled at a higher voltage. As an MLCC is poled, more domains are further aligned with the poling direction, in addition to the ones that have been aligned by the in-plane compressive stress. Therefore, there will be more domains with orientations for switch toughening effect for cracks ∥ pol, and less for cracks ⊥ pol, resulting in the shorter crack lengths for cracks ∥ pol and longer crack lengths for cracks ⊥ pol respectively. With higher poling voltage, the domains will be further aligned and strengthen the effect of fracture toughness anisotropy. It

should be noted that except for crack lengths, the average widths of the cracks are larger for cracks ⊥ pol and smaller for cracks ∥ pol. This effect also appears to strengthen for MLCCs poled with higher voltages.

4.2 Effect of Poling Induced Material Properties Change of Effective Dielectric

As discussed in Section 2.3.1, material properties change from isotropic to approaching transversely isotropic as a ferroelectric material is subjected to a DC voltage larger than a threshold value. In this section, the effect of voltage induced texture in effective dielectric on stress distribution of MLCC body under 3 point bending is evaluated. In section 4.2.2, crystal orientation before and after the application of an electric field is shown by Electron Backscatter Diffraction (EBSD) on a commercial MLCC unit. Using the orientation average estimated elastic moduli of polycrystalline $BaTiO_3$ with different degree of texture, finite element model and stress analyzes on an MLCC under 3-point bending (AEC-Q200-003) are discussed in Section 4.3.1 and 4.3.2 respectively. With the same degree of texture, impact of ineffective to effective dielectric thickness ratio is evaluated.

4.2.1 Experimental Procedure

A commercial MLCC with X7R dielectric, rated for 50V, is used for evaluation. The sample was brought up to 150°C for 15 minutes before surface preparation to

remove any aging-induced polarization or polarization resulting from electrical tests performed by manufacturer. Sample was then soldered onto a printed circuit board for external electrical connection after potting. To ensure a smooth finish for EBSD analysis, diamond suspensions down to 50nm particle size were used for polishing after effective dielectric in the capacitor is revealed by mechanical grinding.

After surface preparation, electron backscatter diffraction (EBSD) scan is performed in between positive and negative electrodes as indicated in the square box in Figure 42 for "baseline" characterization before application of voltage. Tan et al. [118] compared coercive field of 13 polycrystalline $BaTiO_3$ with grain size varied from 0.8 to 32μm and showed that coercive field for all samples were smaller than 0.4kV/mm. $10V_{DC}$ was selected as the poling voltage (~0.5kV/mm) which was applied to the capacitor via the external connections for 30 minutes to evaluate the effect of poling on crystal reorientation. EBSD scan is performed in the same area for result comparison.

4.2.2 Electron Backscatter Diffraction (EBSD) Working Principle

Electron Backscatter Diffraction, as the name suggests, makes use of backscatter electrons (BSE) to study crystal orientation in a specimen.

When an electron beam strikes a specimen, two primary electronics: secondary electrons (SE), BSE, along with radiations such as X-Ray and Cathodoluminescence (CL) are generated. BSE, out of all other emissions, are

widely adopted for crystallographic orientation determination of a specimen because of their interaction with the crystallographic planes in a specimen.

Backscatter electrons are generated when the primary electrons have dispersed beneath the surface of the sample and diffracted by the inner crystallographic planes with an elastic collision. For an EBSD set up, the sample is tilted at about 70 degrees with respect to the horizontal to increase the yield of electrons that are backscattered from the sample and undergo diffraction effects [111] as shown in Figure 40. These diffracted electrons go through constructive interference and produce a pattern composed of intersecting bands known as the Kikuchi pattern [110], from which the orientation of the corresponding crystal lattice with respect to the reference frame can be calculated.

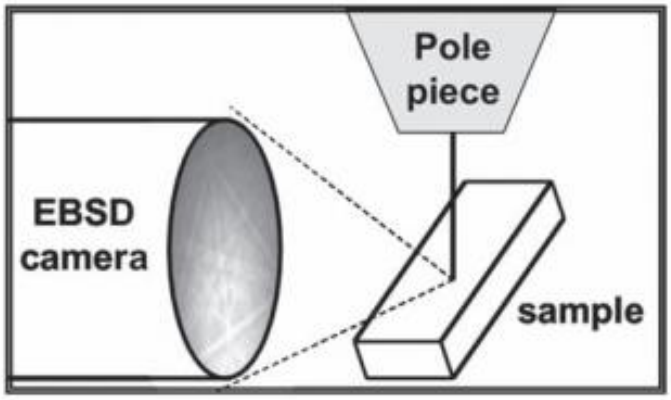

Figure 40. Sample Configuration for EBSD

Crystal orientation distributions is usually defined with respect to a reference frame. In one of the most popular application of EBSD, reference frame of sheet metal evaluation is typically set with respect to normal direction (ND) of the specimen rolling direction (RD) and transverse direction (TD). To study the effect of voltage

history on crystal orientations, reference frame is defined with respect to the normal direction (ND), poling direction (PD), and transverse direction (TD) in this study.

Pole figure is a stereographic projection of selected crystal directions (3 dimensional) onto a 2 dimensional plane. When the projection plane is set to align with a reference frame which coincides with specimen axes, crystal direction with respect to specific axes of the specimen can be visualized using the pole figure. An example of a $BaTiO_3$ crystal in a 3D space is used to illustrate how a pole figure is constructed in Figure 41.

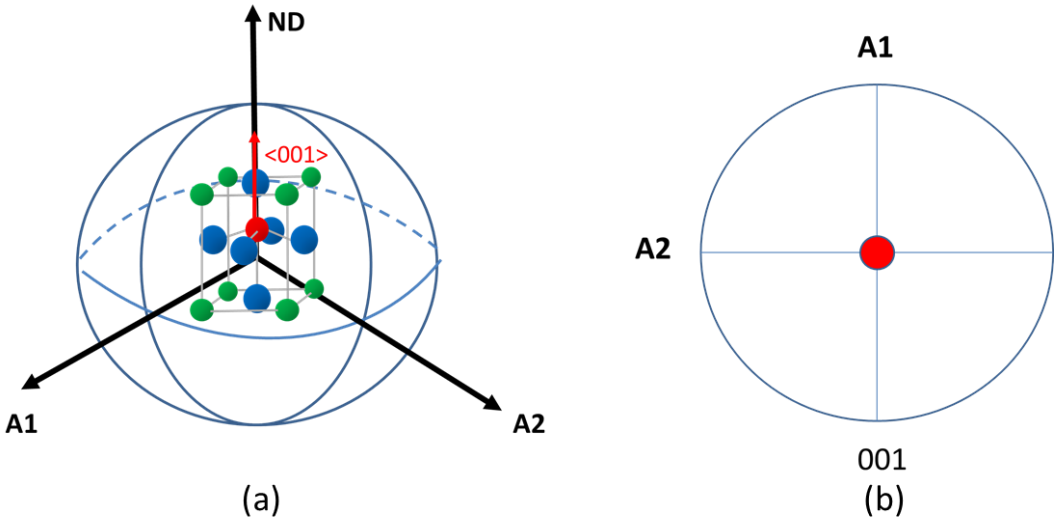

Figure 41. Stereographic Representation of Crystal Orientations- Pole Figure

In this figure we consider a $BaTiO_3$ crystal with <001> aligns with ND of the defined reference frame with the other two axes named A1 and A2. Pole figure can be thought of as the "top view" of with the axis of interest pointing out of paper, which is ND in this case. Therefore, ND would be the center of the pole figure as shown in Figure 41 (b).

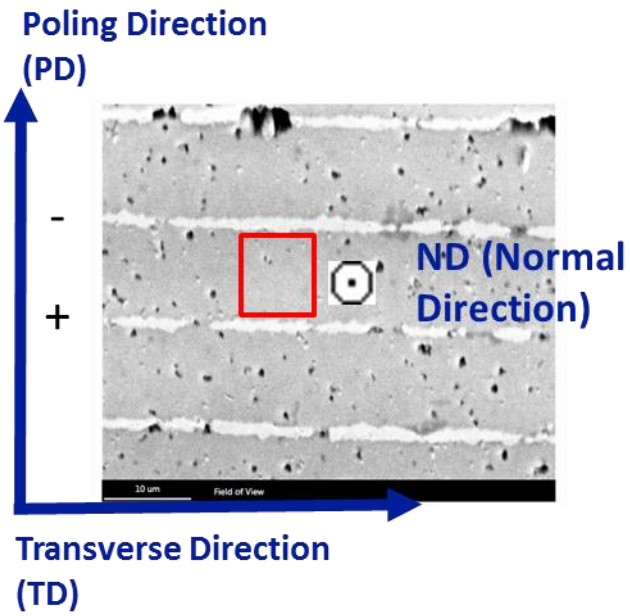

Figure 42. MLCC Surface for EBSD Analysis

As <001> aligns with ND, the vector is projected as a point at the center in the pole figure. Likewise, crystals with <001> directions pointing at different directions can be projected in corresponding locations in the pole figure. Therefore, from studying a pole figure, the distribution of crystal orientations in a specimen with respect to a defined reference frame can be evaluated. Population of crystal orientations are usually normalized and represented as multiples of a random (MOR) in different regions of the pole figure [107].

4.2.3 EBSD Results before Poling

(001) pole figure of the scanned area in Figure 42 for the MLCC before poling is shown in Figure 43. In this figure, it is evident that most of the intensity of <001> parallel to the poling axis is the highest (MOR ≈ 3.16), while intensity of <001>

parallel to ND is weak (MOR $\leq$ 0.825). This suggests that $BaTiO_3$ crystals in the effective dielectric are NOT randomly distributed for the MLCC under evaluation. Instead, there is a substantial preferred crystal orientation perpendicular to the electrodes.

This preferred orientation of crystals supports the findings of residual stresses in commercial MLCC units in the literature.

Park et al. [108] evaluated residual stresses developed in effective dielectric layer of MLCCs after sintering using FEA. From his analysis, in-plane residual stresses (σ_{11} and σ_{22}) in the dielectric layers are compressive. This is explained by the smaller CTE of $BaTiO_3$ than the electrodes. The in-plane compressive stress is also found to increase with the increase in number of layers in the MLCC. Under in-plane compressive stress, ferroelectric crystals and domains align perpendicular to the applied stress direction due to the ferroelastic switching effect. Therefore, preferred crystallographic orientations perpendicular to electrodes have confirmed the existence of in-plane compressive stress in effective dielectric layers in MLCCs.

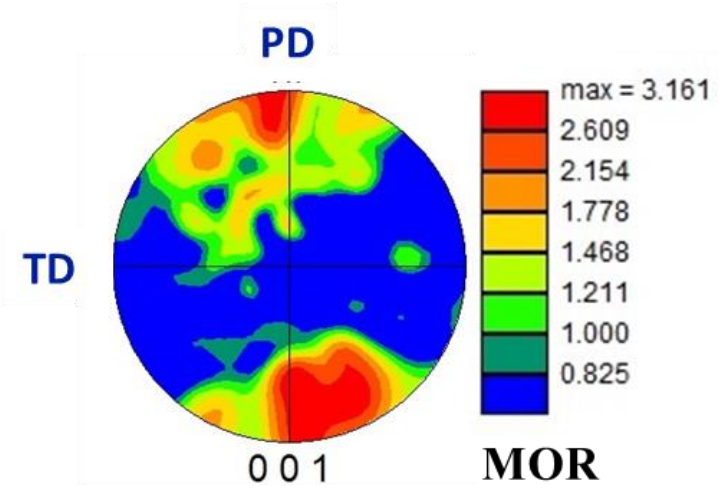

Figure 43. Pole Figure of Scanned Area in MLCC BEFORE Poling

4.2.4 EBSD Results after Poling

The pole figures under the same scanned area before and after poling is shown in Figure 44. Crystal directions <001> that were in the 1st and 4th quadrant of the pole figure (top half), were found to move closer to towards the top pole, and resulted in concentrated population at the proximity around the negative electrode, with the highest MOR going from around 3.16 to 4. <001> directions that were in the 2nd and 3rd quadrant of the pole figure (bottom half), were found to slightly move in the poling direction, resulting in an increase MOR in the islands separated away from the positive electrode.

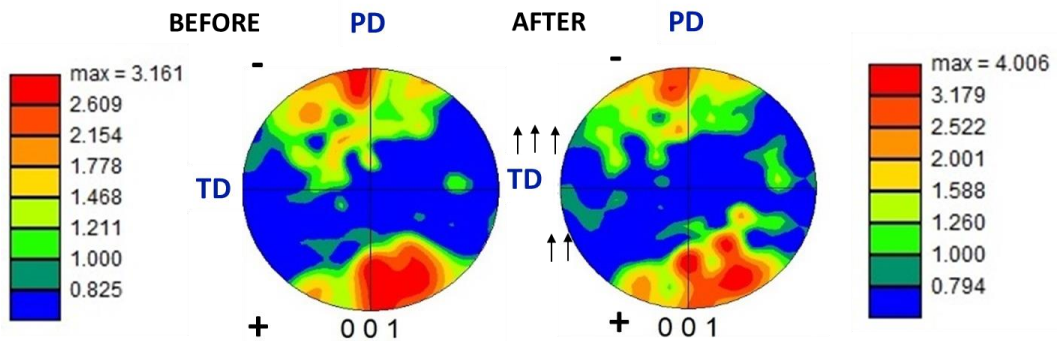

Figure 44. Pole Figure of Scanned Area BEFORE and AFTER Poling

Relative angular positions between <001> directions of $BaTiO_3$ crystals, and the normal axis (ND) are plotted to further illustrate the effect of poling in Figure 45. In this figure, perfect alignment between <001> of a $BaTiO_3$ crystal and the normal axis is given by 0°. From the distribution, it is clear that after poling, there is a higher population of <001> directions aligning further away from the normal axis as a result of remnant polarization. From this experiment, crystal reorientation after poling is evident.

It should be noted the poling process which introduced the extent of crystal re-orientation was performed at 10V for 30min on a cross-sectioned MLCC that is rated at 50V. Poling with higher voltage was attempted for a more remarkable crystal re-orientation result. However, the sample was burnt due to arcing. With the close proximity of opposite electrodes (<20µm), arcing takes place through the air as the breakdown voltage of air is around 3kV/mm. It is also possible that the electric field strength experienced by the scanned area is less than the applied value due to the electric field non-uniformity on a half sample. For a complete MLCC

unit, a higher degree of texture can be achieved with a higher poling voltage or longer poling time.

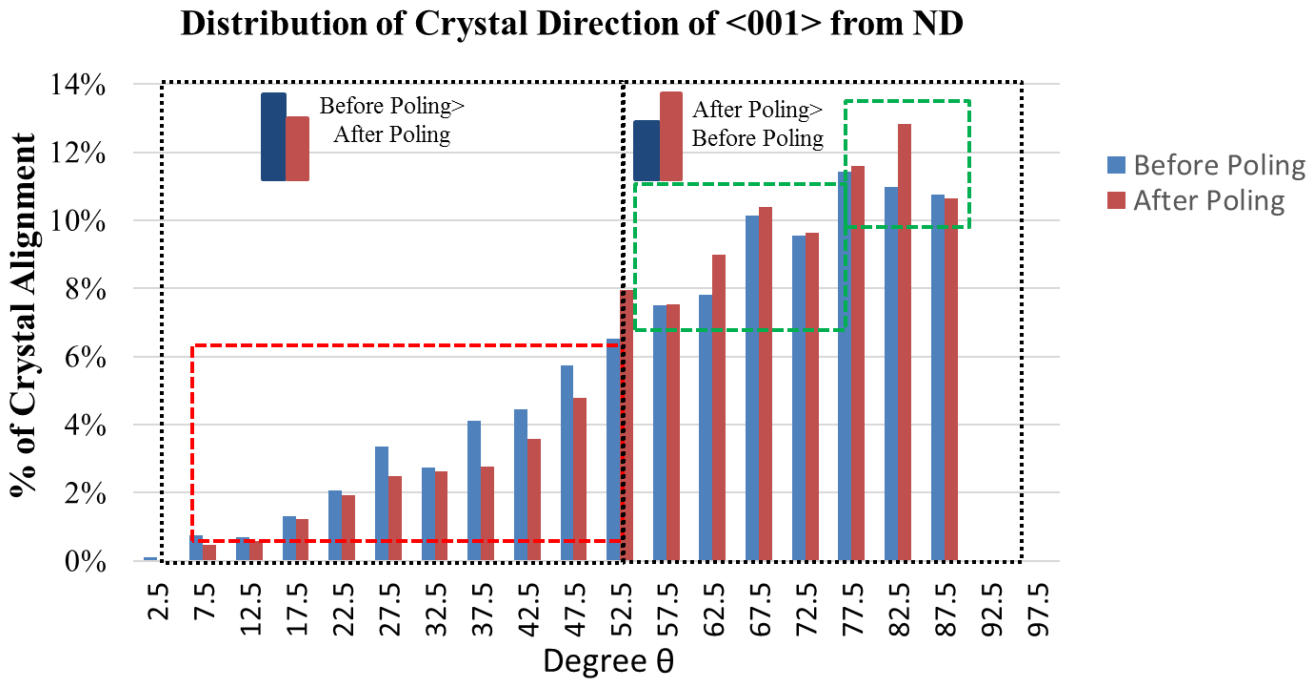

Figure 45. Distribution of Relative Angular Position between <001> Directions and Normal Axis

4.3 Stress Analysis with Change in Core Texture

In this section, the effect of core texture due to poling on stresses acting on an MLCC body under a three point bending load is evaluated. Linear elasticity (Hooke's Law) is assumed in this analysis and a general 3-D relationship is given as below, where σ_{ij} are the stress tensors, C is the stiffness matrix, and ε_{ij} are the strain tensors.

$$\begin{pmatrix}\sigma_{xx}\\ \sigma_{yy}\\ \sigma_{zz}\\ \sigma_{yz}\\ \sigma_{xz}\\ \sigma_{xy}\end{pmatrix}=\begin{bmatrix}C_{11} & C_{12} & C_{13} & C_{14} & C_{15} & C_{16}\\ C_{21} & C_{22} & C_{23} & C_{24} & C_{25} & C_{26}\\ C_{31} & C_{32} & C_{33} & C_{34} & C_{35} & C_{36}\\ C_{41} & C_{42} & C_{43} & C_{44} & C_{45} & C_{46}\\ C_{51} & C_{52} & C_{53} & C_{54} & C_{55} & C_{56}\\ C_{61} & C_{62} & C_{63} & C_{64} & C_{65} & C_{66}\end{bmatrix}\begin{pmatrix}\varepsilon_{xx}\\ \varepsilon_{yy}\\ \varepsilon_{zz}\\ \varepsilon_{yz}\\ \varepsilon_{zx}\\ \varepsilon_{xy}\end{pmatrix}$$

When a ferroelectric material is unpoled, there is no texture and it is considered isotropic due to the random domain orientations. For an isotropic material, C_{ij} matrix is reduced to the following form:

$$\begin{bmatrix}C_{11} & C_{12} & C_{12} & 0 & 0 & 0\\ C_{12} & C_{11} & C_{12} & 0 & 0 & 0\\ C_{12} & C_{12} & C_{11} & 0 & 0 & 0\\ 0 & 0 & 0 & C_{44} & 0 & 0\\ 0 & 0 & 0 & 0 & C_{44} & 0\\ 0 & 0 & 0 & 0 & 0 & C_{44}\end{bmatrix}$$

When a ferroelectric material is poled in axis-3, texture or crystallinity of the material increases, and it goes from isotropic to transversely isotropic with the direction of the polarization as the axis of symmetry. For a transversely isotropic material, C_{ij} matrix can be represented as the following form:

$$\begin{bmatrix}C_{11} & C_{12} & C_{13} & 0 & 0 & 0\\ C_{12} & C_{11} & C_{13} & 0 & 0 & 0\\ C_{13} & C_{13} & C_{33} & 0 & 0 & 0\\ 0 & 0 & 0 & C_{44} & 0 & 0\\ 0 & 0 & 0 & 0 & C_{44} & 0\\ 0 & 0 & 0 & 0 & 0 & C_{66}\end{bmatrix}$$

Based on the change in core texture associated change in elastic stiffness of the core dielectric, a finite element model is developed to evaluate the change in stress in the capacitor body under the same loading condition.

4.3.1 Finite Element Model Set Up for Stress Analysis

In this study, a three point bending test set up adopted from AEC-Q200-003 is constructed for stress analyzes on an MLCC body. This standard is designed for measuring breaking strength of surface mounted ceramic capacitors. A simplified 3D model for FEA is shown in Figure 46. A downward displacement of the loading pin is applied in the Z direction with a rate of 0.2mm/s. 0 displacement in the Z direction is applied on two edges at the bottom of the capacitor as support. Distance between two fixed supports is 55% of the whole capacitor width adopted from the same standard. In this study, the deformation behavior of the capacitor body (both core and face) is assumed to be elastic as ceramics are brittle materials that adhere to Hooke's law and deform reversibly under an applied load until the onset of cracking.

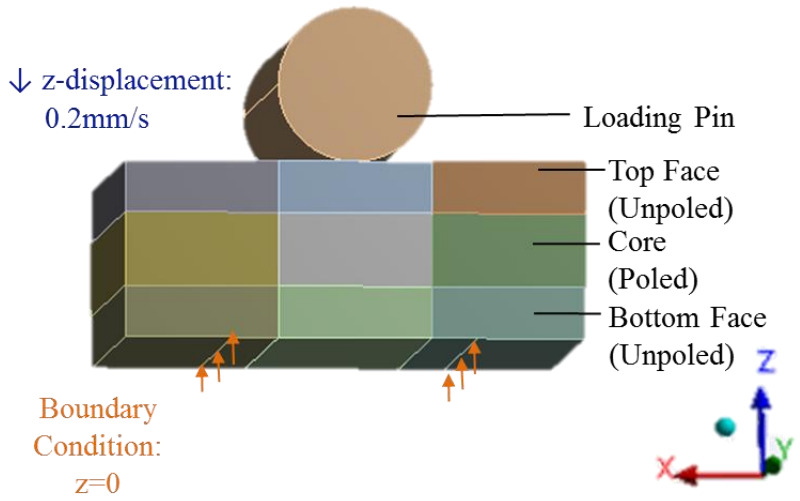

Figure 46. Simplified 3D Model for Stress Analyzes of MLCCs under 3 Point Bending

For material properties, loading pin is assigned as stainless steel. Dielectric that is outside of electrodes (Top and bottom face) does not experience sufficient electric field and therefore is modeled as unpoled $BaTiO_3$ (no texture), while dielectric that is within electrodes (Core) are modeled with different degree of texture depending on the voltage history. The elastic stiffness matrices representing different textures used as inputs in the simulation is discussed in detail in Section 4.3.2.

During bending, top side of the specimen under compressive stress and bottom side is under tensile stress. Since compressive strength is typically 10 times more than tensile strength for ceramics, fracture typically occurs at the bottom side of brittle materials under a bending load. Therefore, tensile and shear stresses at the core and bottom are selected for evaluation

4.3.2 Poling Induced Texture in $BaTiO_3$ Polycrystals

Estimation of effective elastic moduli of polycrystals typically involves orientational volume averages of crystallites, which can be assessed through orientation distribution functions (ODF). As domains are aligned by an electric field in a polycrystal, the properties of the material approach that of a single crystal. Using orientation averages, bulk material properties of a polycrystal can be estimated and the results by Li [117] for $BaTiO_3$ is used in this study to represent different texture of dielectric in an MLCC. In Li's study, ODF is approximated by a Gaussian distribution function with a parameter α indicating degree of texture. $\alpha = 0$ represents maximum texture of the polycrystal, and degree of texture reduces as α increases until it reaches zero texture ($\alpha = 10$). Elastic moduli of polycrystalline $BaTiO_3$ as a function of α from Li's study is shown in Figure 47 and the elastic moduli correspond to α= 10, 1, 0.5, 0.3, 0 is tabulated in

Table 12. Tabulated Elastic Moduli of Polycrystalline

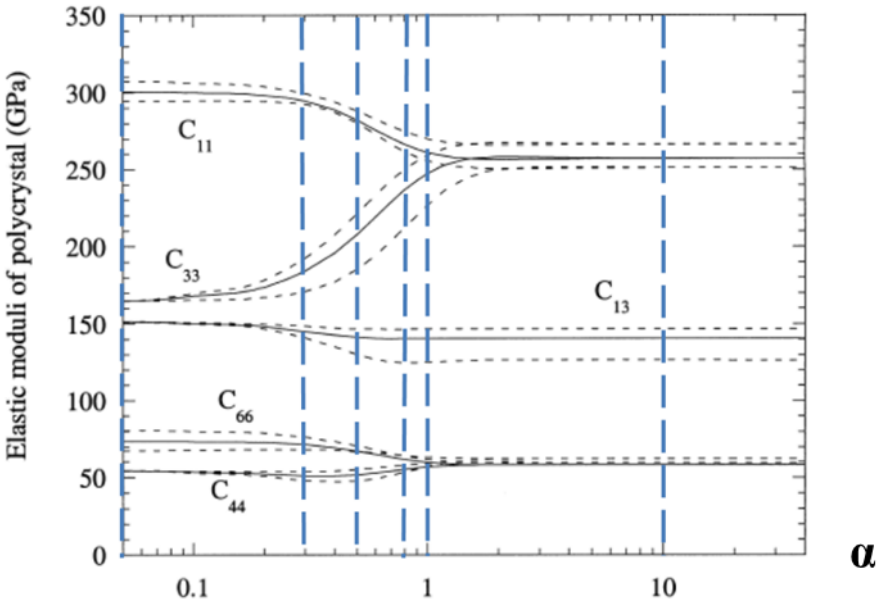

Figure 47. Elastic Moduli of Polycrystal $BaTiO_3$ as a Function of Texture [117]

Table 12. Tabulated Elastic Moduli of Polycrystalline $BaTiO_3$ from Figure 47.

α	C11/C22	C33	C12/C21	C13/C23	C44/C55	C66	C31/C32
0	300	165	154	150	54	73	150
0.3	294	182	154	145	50	70	145
0.5	281	210	151	142	50	65	142
0.8	265	240	145	140	53	60	140
1	260	246	144	140	56	58	140
10	255	255	140	140	58	58	140

4.3.3 Effect of Core Texture on Stresses under 3 Point Bending

The effect of core texture on stresses induced on the capacitor body is evaluated by varying the 6 by 6 elastic stiffness matrices represented by α value at 10, 1, 0.5, 0.3, 0, representing an increasing degree of texture. Tensile and shear stress distributions in core and bottom part of the MLCC body at 1mm displacement of the loading pin is shown in Figure 48. Stress distributions remain the same as core texture is varied in this section and as core to height ratio is varied in Section 4.3.4.

To compare the effect of core texture and core to height ratio of the MLCC, maximum tensile and shear stress which takes place at the same location is compared as the parameters were varied. For shear stress at the bottom part of the MLCC, the maximum stress shown by FEA does not converge due to stress singularity. Therefore, the stress at the middle part of the edge that is mesh size independent was used for comparison as the maximum stress at the bottom. Mesh convergence study is shown in Section 4.3.5.

Maximum tensile and shear stress at the bottom face is two to three times higher than that on the core dielectric. Brittle material failures are sensitive to defects. Assuming the same distribution of defects throughout the capacitor body, the bottom face are more likely to fail as expected since the critical crack length will become smaller based on Griffith's equation in fracture mechanics.

With the increase in texture (α goes from 10 to 0), a reduction in maximum tensile and shear stress experienced by the bottom face is observed. Maximum shear stress

experienced by core dielectric also shows a decreasing trend as texture increases, while maximum tensile stress remains almost unchanged.

The result suggests that as an MLCC is poled, or has been subjected to a DC voltage history with a sufficient electric field, the bending strength under a 3 point bending load can be increased due to the lower maximum stresses experienced by the bottom side of the capacitor. It should be noted that since loads and supports are acted on the ceramic capacitor bodies directly, as opposed to other experimental setups in which the loads and supports are imposed on the PCB with the MLCC mounted, the stresses on the MLCCs are much higher than that from similar studies in the literature.

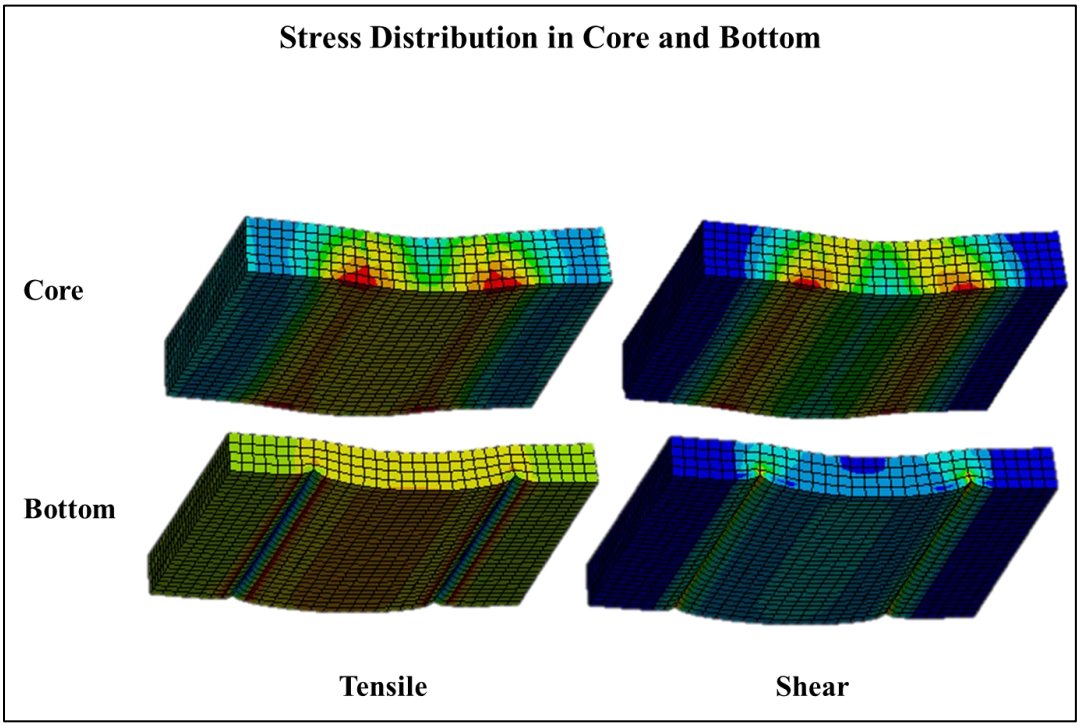

Figure 48. Stress Distribution in Core and Bottom Part of MLCC from FEA

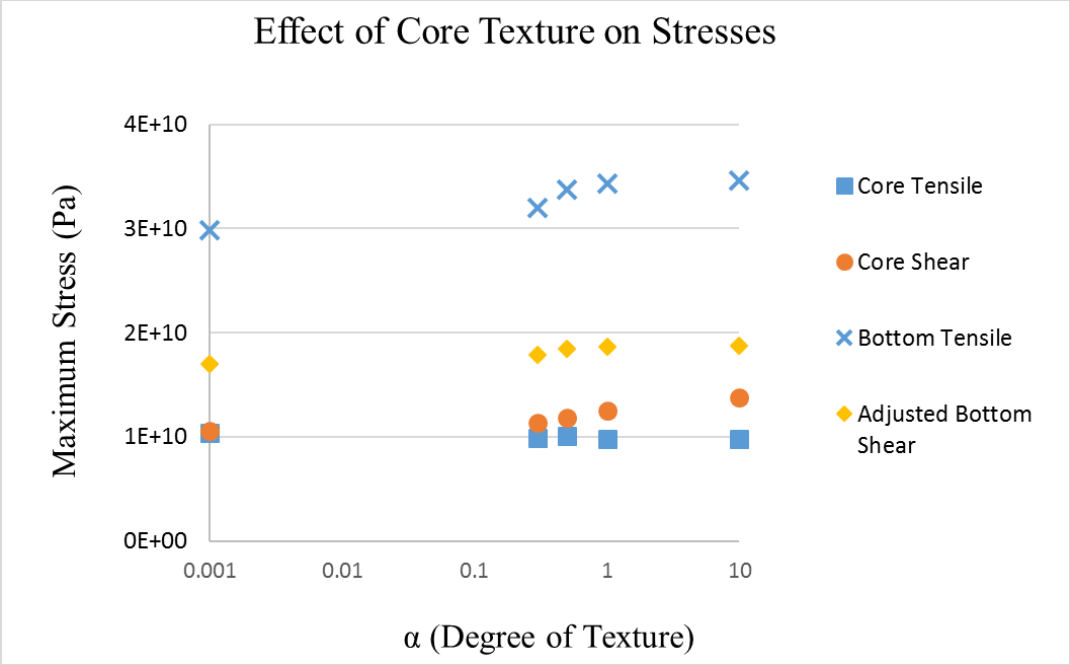

Figure 49. Effect of Core Texture on Max. Stress under 3 Point Bending

4.3.4 Effect of Core Thickness to Height Ratio on Stresses under 3 Point Bending

Although footprints of MLCCs are standardized, their internal structures vary. In this section, the effect of core thickness to height ratio (c/h) on stresses under the same three point loading condition is evaluated. For polycrystal, fully poled (α=0) or fully unpoled (α=10) are impractical. Therefore, maximum stresses experienced by the bottom face are computed for α=0.3 and α=0.8 to simulate a potential change in mechanical properties due to crystal or domain re-orientation after a DC voltage history. Then, the percentage reduction in maximum stresses from α=0.8 to α=0.3 is compared for common c/h configurations as shown in Figure 50. Only maximum tensile and shear stresses experienced by the bottom face are evaluated in this part

as it was evident from the previous part that the stresses at the bottom are significantly higher.

As c/h is increased, percentage reduction for both in maximum tensile and shear stresses increase significantly, showing an exponential relationship (R^2= 0.99 and 0.95 respectively). This suggests that MLCCs with high c/h (high volumetric ratio of effective dielectric) are much more likely to have an increase in bending strength after a DC voltage history.

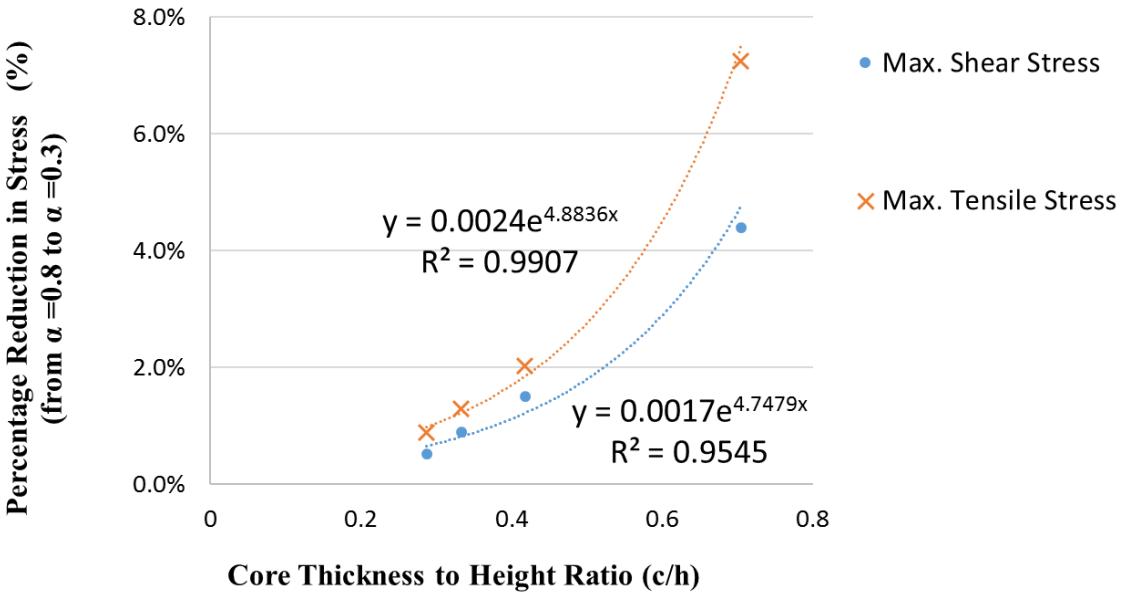

Figure 50. Effect of Core Thickness to Height Ratio (c/h) on Max. Tensile and Shear Stress at Bottom Face of Capacitor

4.3.5 Mesh Convergence Evaluation

Since maximum stresses are used as the metric for crack susceptibility evaluation, it should be confirmed that stress singularity does not have an effect on the maximum stress. With stress singularity, stress does not converge as the mesh is refined. With the increase in number of elements in the corresponding bodies, it was found that the maximum tensile stress and shear stress at the core dielectric, and the maximum tensile stress at the bottom converges with the increase in number of elements. However, the maximum shear stress at the bottom increases as the number of elements increases as shown in Figure 51.

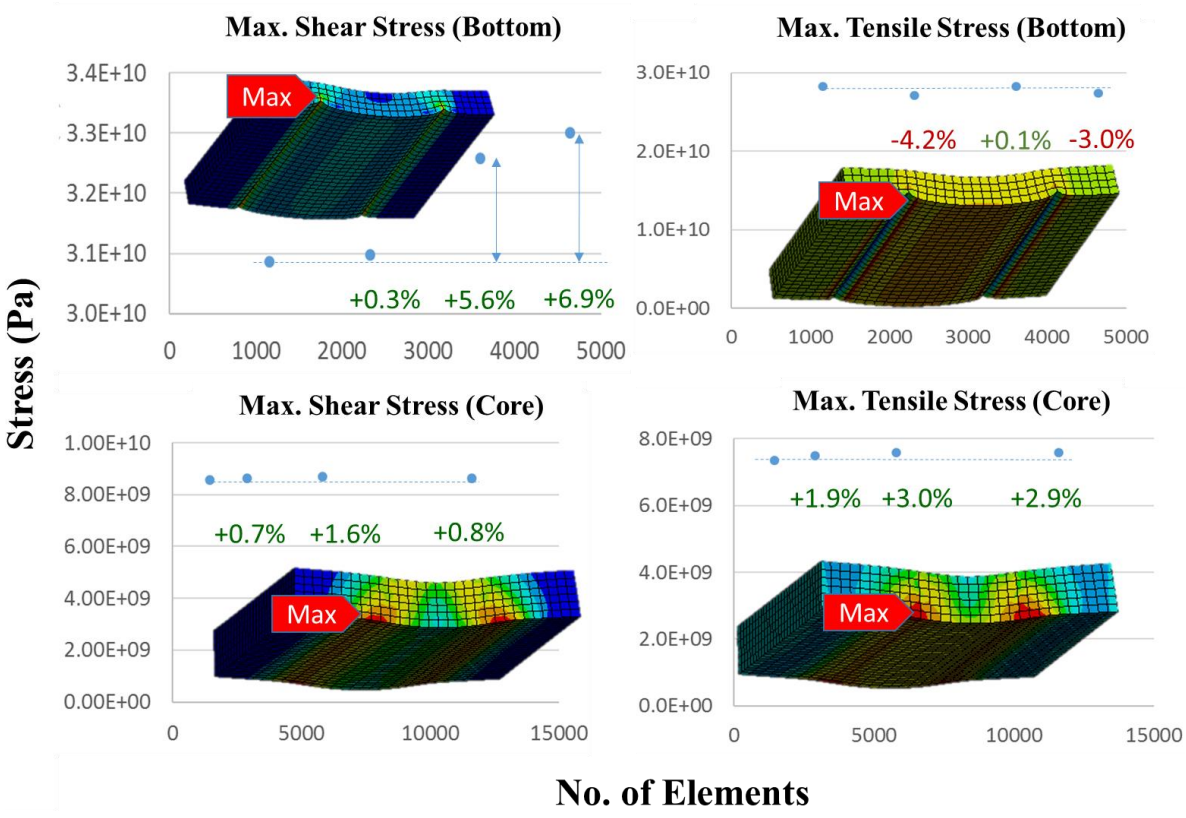

Figure 51. Mesh Convergence Evaluation

As the maximum shear stress at the bottom is distributed on the edges of support as indicated by the red dotted line in Figure 52, shear stress convergence along the edge was evaluated. In Figure 53, shear stress is plotted along the length of the supporting edge with different number of elements. It is obvious that towards the ends of the edge, shear stress increases with the number of elements, while in the middle regions of the edge, the shear stress is independent of the number of elements. The independence of shear stress with the number of elements at the mid-point of the edge is shown in Figure 54. Therefore, shear stress at the mid-point of the edge is taken as the maximum shear stress for comparison.

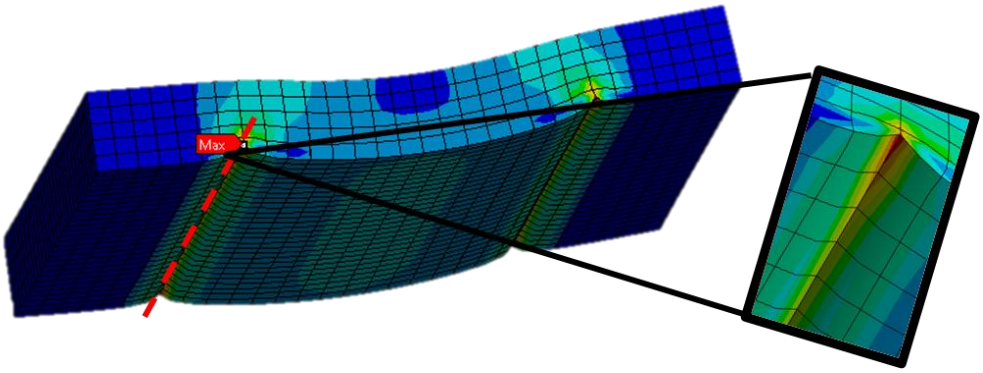

Figure 52. Shear Stress along Edge of Support

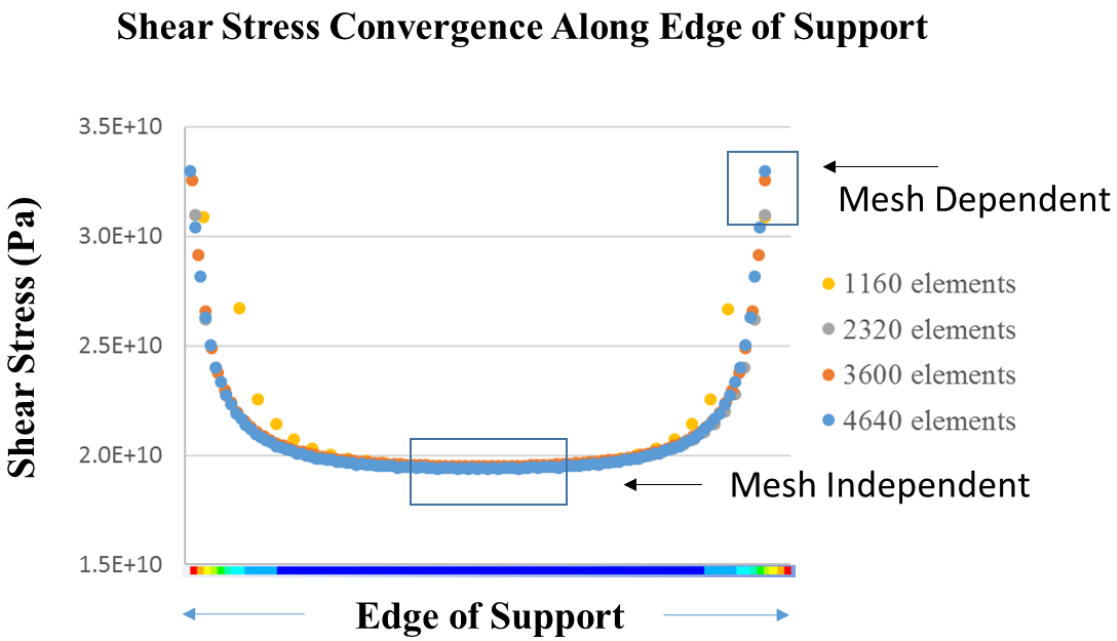

Figure 53. Shear Stress Convergence along Bottom Edge of Support

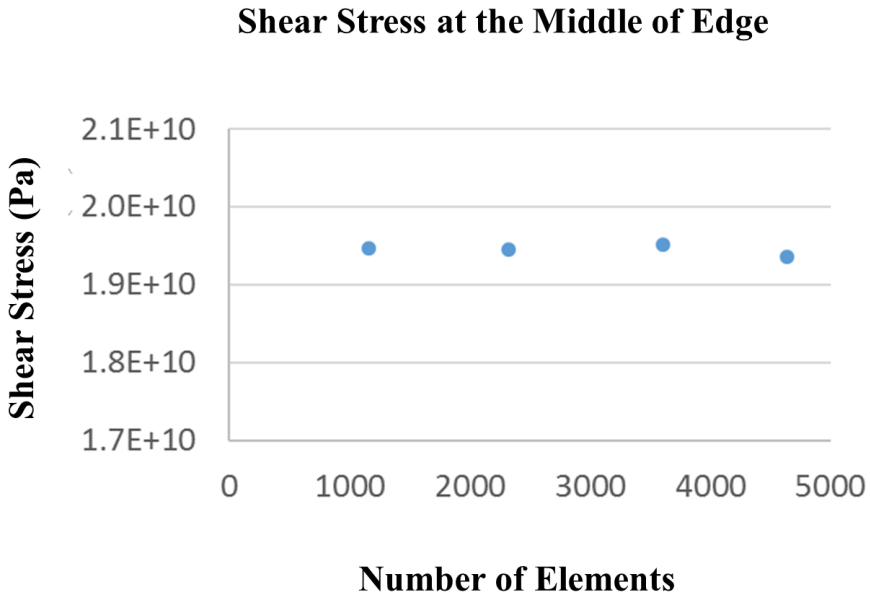

Figure 54. Shear Stress at the Middle of Edge

4.4 Conclusion

In this section, crystallographic orientation of a commercial MLCC unit before and after poling was evaluated and the effect of poling induced dielectric texture on mechanical response of MLCC under 3 point bending is evaluated using finite element analysis.

From the results of EBSD, a preferential texture along poling axis was shown in the effective dielectric of the tested MLCC even before poling, which is a supporting evidence for the existence of the in plane residual compressive stress in these units. After poling, more <001> crystal directions align with the poling direction. As the MLCC under poling was cross-sectioned, and only a 10V poling voltage was applied, it can be deduced that a much stronger crystal alignment can be expected with higher voltage on a complete MLCC unit.

Using finite element analysis to evaluate stresses on MLCC body under a three point bending load, it was found that maximum tensile and shear stress at the bottom face of an MLCC are found to be critical for failures under the 3 point bending load in this study. With the elastic stiffness matrix corresponds to different $BaTiO_3$ texture as an input, it was found that both stresses reduce as degree of texture increase in the effective dielectric and the reduction is more significant for MLCCs with a high core thickness to height ratio (c/h), indicating flexural strengths of MLCCs with a higher volumetric ratio of effective dielectric are more affected by voltage history.

5 Effect of Voltage History on MLCC Flexural Strength

From Section 3, the two mechanisms are proven through experiment and the effect of poling induced core dielectric texture on stresses on an MLCC under 3-point bending load is evaluated. In this section, a 3-point bending test set up as described in AEC-Q200-003 [119] is used to evaluate flexural strengths of commercial MLCCs after different voltage levels of poling.

Flexural strength (σ_{FS}) is a material property defined as the stress in a material just before it yields or fracture in a flexure test. Three point bending set up is often used to assess flexural strength of materials σ_{FS} of a rectangular sample under a three point bending setup is given by

$$\sigma_{FS} = \frac{3F_{max}L}{2bd^2}$$

F_{max}: Maximum force at the fracture point

L: Length of the support span

b: Sample width

d: Sample thickness

A typical force vs deflection relationship of a rectangular beam under a 3-point bending load is shown in Figure 55. By capturing the maximum load before fracture, σ_{FS} can be calculated.

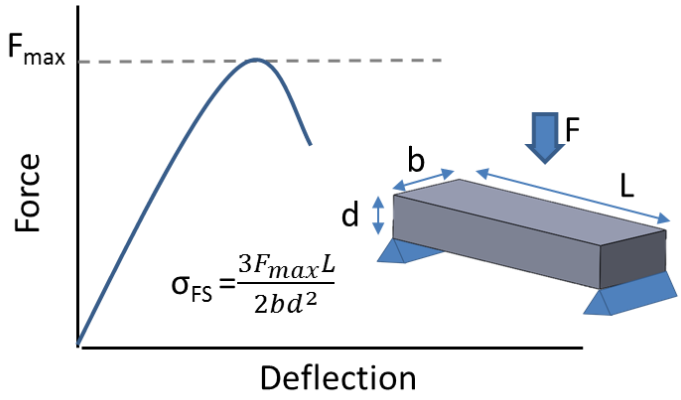

Figure 55. Flexural Strength of Rectangular Beam from 3 Point Bending Test

5.1 Experimental Set Up

To evaluate the effect of poling on flexural strength (σ_{FS}) of MLCCs, a 3 point bending set up as described in AEC-Q200-003 is used. This test is used to evaluate if breaking strengths of MLCC lots satisfy minimum force requirements specified by users. A loading pin and a fixture were machined according to the description in the standard as shown in Figure 56. The end of the loading pin is rounded with a radius of 0.5mm, and the seat for the tested MLCC is separated with a gap of 55% length of the MLCC length to allow bending. An Instron universal tester 5944 as shown in Figure 57 was used for conducting this test.

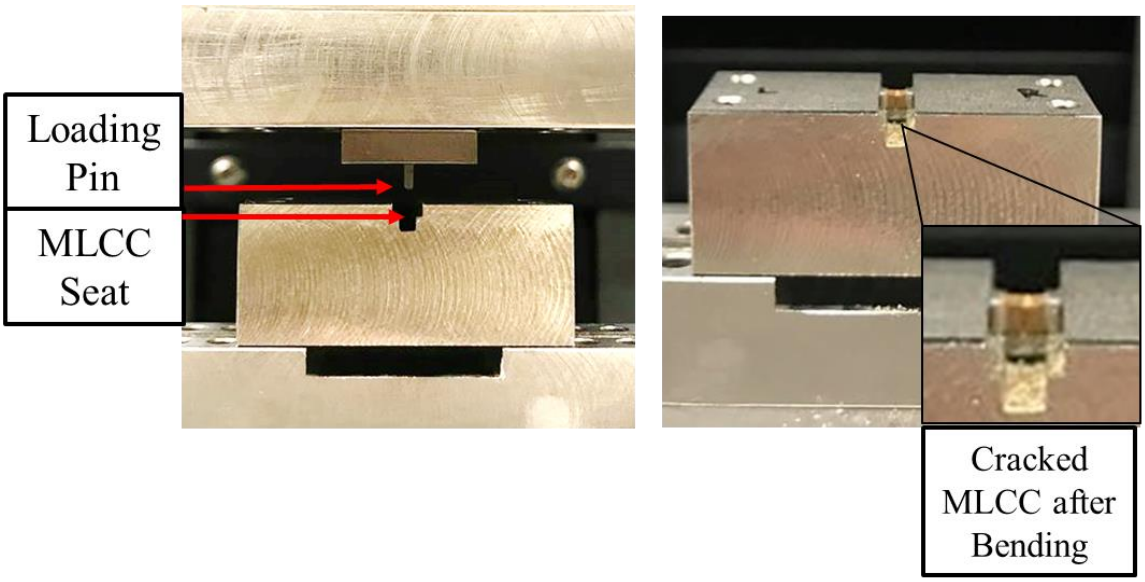

Figure 56. Loading Pin and Test Fixture Machined According to AEC-Q200-003

Figure 57. Instron Universal Tester used for 3 Point Bending Test

5.2 Experimental Procedure

An Inston tester is used for applying a constant strain rate at 0.2mm/s until failure of the unit. The test is set to stop after the recorded load drops by 10% after hitting the peak. In this test, the peak load (F_{max}) before fracture is recorded σ_{FS} comparison. MLCCs from 4 different manufacturers and different c/h ratio are selected for this study. All MLCCs were chosen to have the same length and same rated voltage, and 30 MLCCs are used for each pre-test condition. Test matrix for this experiment is shown in Table 13. A typical load vs displacement curve as an output of the test is shown in Figure 58.

Table 13. Test Matrix for 3 Point Bending Test of MLCCs

MLCC Groups	**Rated Voltage (V)**	**c/h**	**h**	**Poling Voltage**				
				Not Poled	10V	25V	50V	75V
I	50	0.27	0.75	30	30	30	30	30
II	50	0.35	1.15	30	30	30	30	30
III	50	0.53	0.8	30	30	30	30	30
IV	50	0.7	1.15	30	30	30	30	30

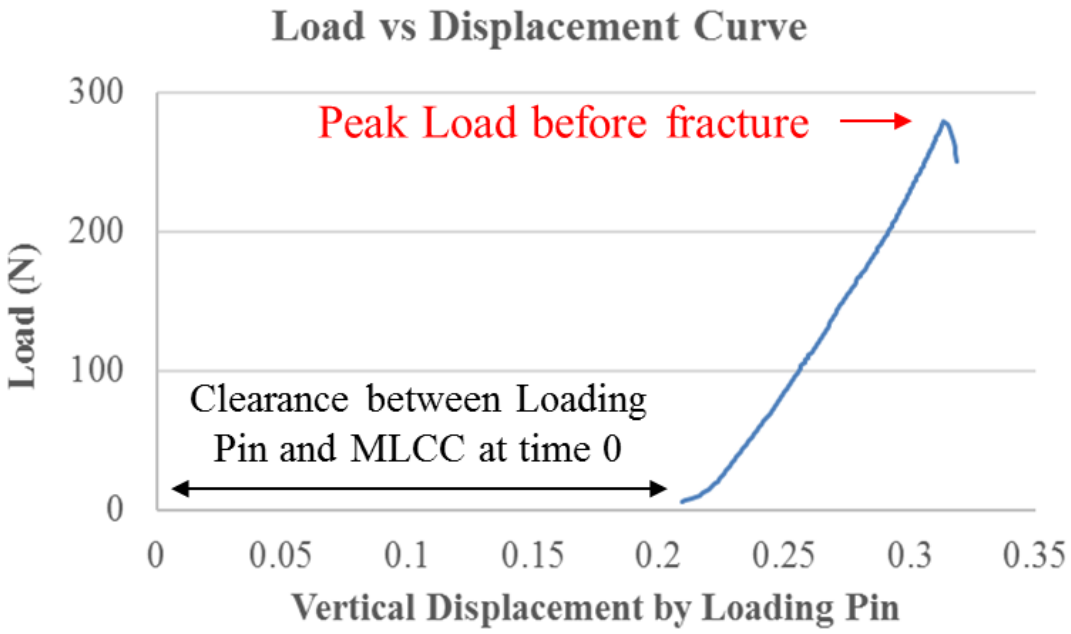

Figure 58. Typical Load vs Displacement Curve during 3 Point Bending of MLCC Units

5.3 Results

In this section, the change in flexural strength of MLCCs that are poled at different voltage levels, and of different c/h using the 3-point bending set up as described in Section 5.1 are presented.

5.3.1 Effect of Applied Voltage Level on Flexural Strengths of MLCCs with different Core to Height Ratios

Flexural strength data is presented with box and whisker plots from Figure 59 to Figure 62 for MLCC group I to IV. The ends of the box indicate upper and lower quartiles of the data, and the medians and means of the data are marked with the line, and the cross in the middle of the box. The end of the whisker indicates the highest and lowest values in the datasets.

Voltage level used in poling prior to 3 point bending test is indicated in different colors in the figures as multiples of rated voltage, i.e. 0.1 represents 0.1*50 =10V. Y-axes are set for the same range for visual comparison of results from the 4 groups.

The change in flexural strength with different poling conditions in Group I is minimal. However, when the means of the datasets are compared, a slight increase is reckoned. From the data of group II, III and IV, it appeared that as c/h of an MLCC is higher, the increase in flexural strength due to voltage history is of a greater extent. The percentage increase in the mean of flexural strengths with different poling conditions are plotted for each group in Figure 63. Comparing the means between As-Is and poling at rated voltage (50V) for MLCC groups A to D, the increase is found to be 4.38%, 5.24%, 7.52% and 8.91% respectively.

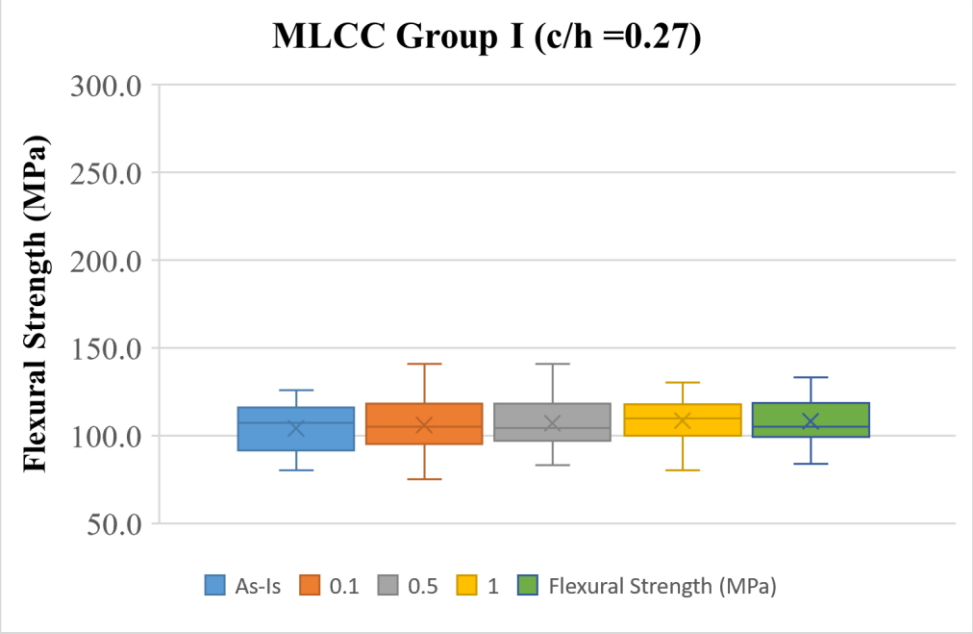

Figure 59. Flexural Strength of Group I MLCCs after Poling at Various Voltage Levels

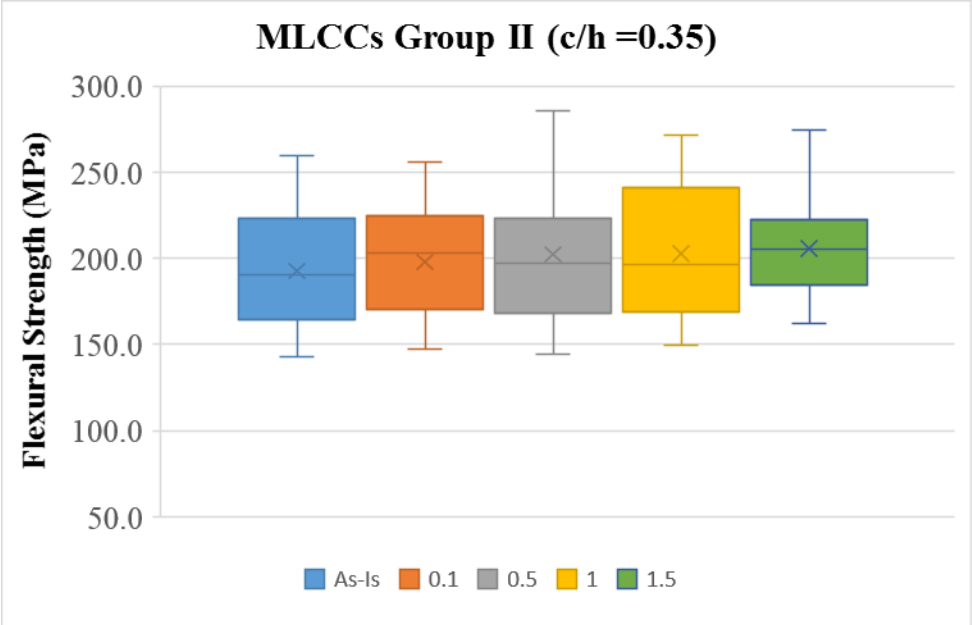

Figure 60. Flexural Strength of Group II MLCCs after Poling at Various Voltage Levels

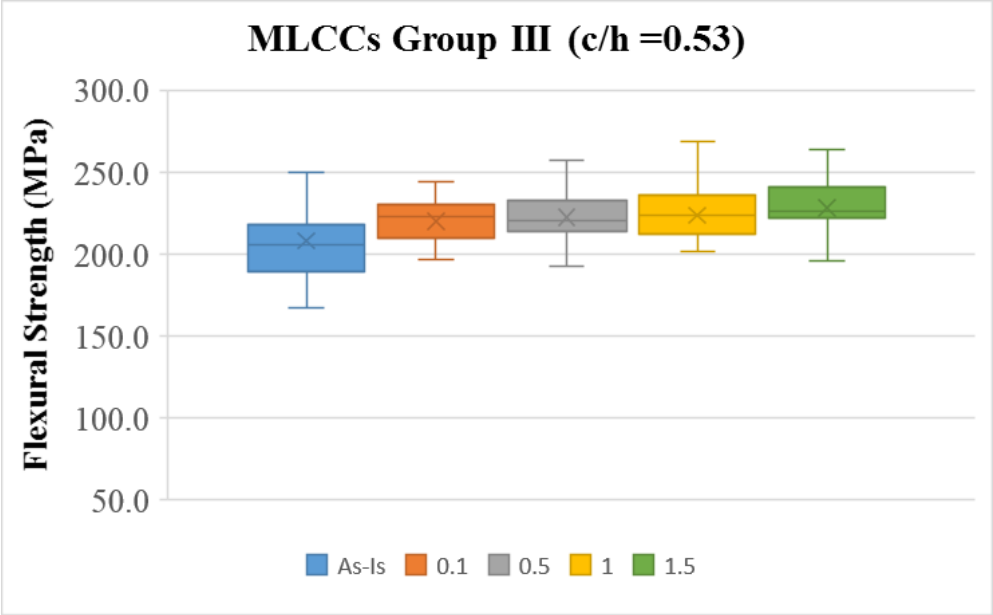

Figure 61. Flexural Strength of Group III MLCCs after Poling at Various Voltage Levels

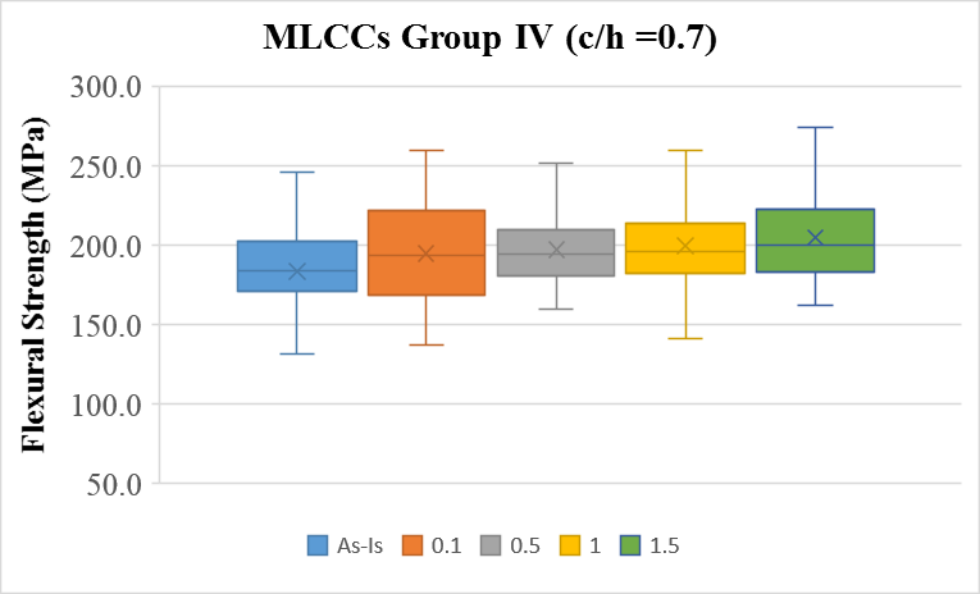

Figure 62. Flexural Strength of Group IV MLCCs after Poling at Various Voltage Levels

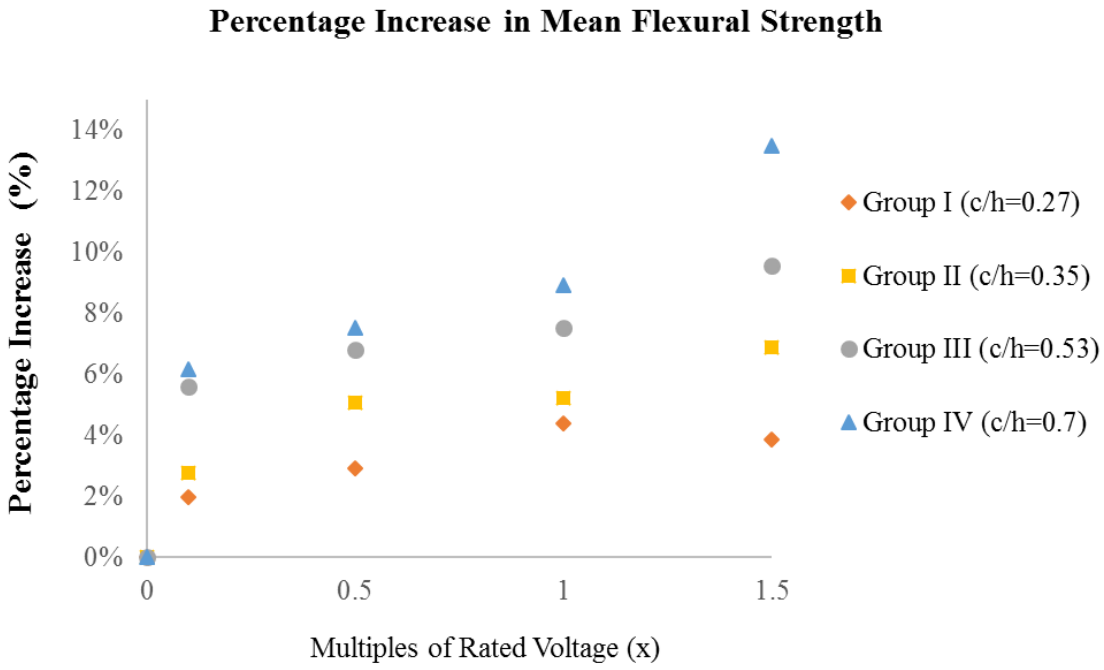

Figure 63. Percentage Increase in Mean Flexural Strengths

5.3.2 T-Test Results of Flexural Strength before and after Poling

T-test is typically used in data analysis to evaluate statistical significance between the means of two datasets considering the variances. T-test is also mathematically equivalent to the one-way analysis of variance (ANOVA) procedure with two groups [120]. Mathematically, the t-test takes a sample from each of the two sets and establishes the problem statement by assuming a null hypothesis that the two means are equal (H_0: $\mu_1=\mu_2$). The outcome of the t-test produces a t-value that is compared against a value obtained from the T-distribution table. The most common parameter that is used for determining statistical significance is the p-value from T-distribution table corresponding to a certain t-value.

Assuming unequal variances in two populations, t value is represented as the formula below [121]:

$$t = \frac{\bar{x}_1 - \bar{x}_2}{\sqrt{\frac{{S_1}^2}{n_1} + \frac{{S_2}^2}{n_2}}}$$

$\bar{x}_1, \bar{x}_2$: Sample means for two datasets

${S_1}^2, {S_2}^2$: Sample variance for two datasets

n_1, n_2: Sample size for two datasets

Sample for a population is given by the equation below:

$${S_i}^2 = \frac{\sum_{j=1}^{n_j} x_j - \bar{x}_i}{n_i - 1}$$

Degree of freedom (df) used in T-distribution table is given by the below equation:

$$df = \frac{[\frac{{S_1}^2}{n_1} + \frac{{S_2}^2}{n_2}]^2}{\sqrt{\frac{({S_1}^2/n_1)^2}{n_1 - 1} + \frac{({S_2}^2/n_2)^2}{n_2 - 1}}}$$

Having computed the above parameters, p- value can be looked up from t-distribution table.

In this section, t-test is performed on flexural strength data from unpoled MLCCs, and MLCCs poled at different levels, one pair at a time. Instead of using t-test as a means to accept or reject datasets based on a universal p-value cut-off (0.1, 0.05, or 0.01), the variation of p-values at various voltage level is compared for both 2-tail and 1-tail analysis to see how statistical significance evolve with the increase in poling voltage level as shown in Figure 64 and Figure 65 respectively.

From the results, it is obvious that as the poling voltage increases, p value reduces for MLCCs from all groups, meaning the differences between the unpoled samples and the poled samples become more statistically significant as a higher poling voltage was used. P-values obtained from Group C and Group D are also found to be much lower than that from Group A and C, indicating the same poling conditions have induced a more significant change in flexural strengths in MLCC samples with a higher c/h.

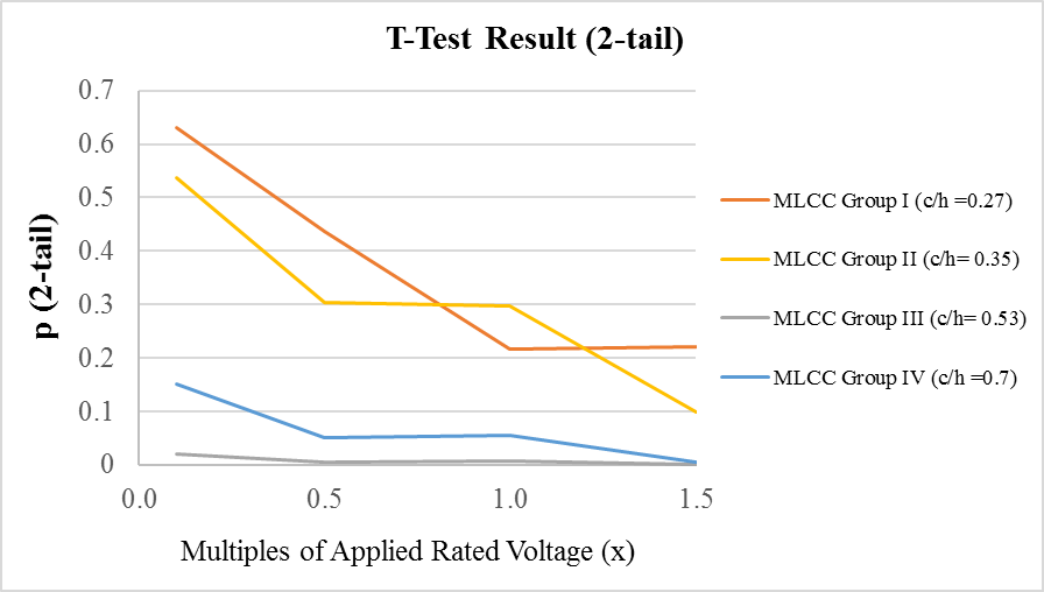

Figure 64. T-Test Result (2-Tail)

1-tail analysis of t-test results are typically not recommended because it generates a higher statistical significance by comparing only one-tail (end) of the distributions, and it neglects the change on the other tail of the distribution. It is included here as a reference because a directional change is expected (increase) due to poling. Another reason is the fact that the units exhibit the lowest flexural strengths in the dataset could have failed due to defects, or pre-existing cracks in the dielectric material, which may not be affected by the process of poling.

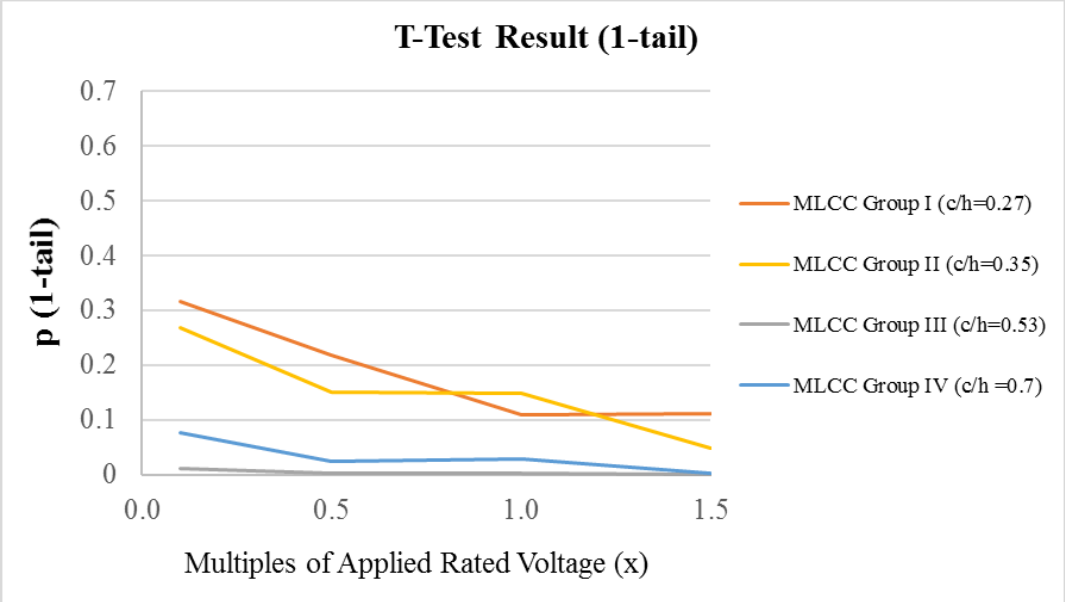

Figure 65. T-Test Result (1-Tail)

5.4 Empirical Model Development from 3 Point Bending Test Data

In this section, an empirical model to relate the increase in mean flexural strengths, poling voltage as a multiple of rated voltage, and core to height ratio of an MLCC sample is developed by using the 3-point bending data presented in Section 5.3.1. Regression is performed on the percentage increase in mean flexural strength with poling voltage shown in Figure 63, and the data follows a logarithmic trend for all MLCC groups which can be expressed with the following relationship, with x as the multiples of rated voltage used in poling. k and m are the fitted model parameters.

$$\%\ Increase\ in\ \overline{\sigma_{FS}} = \boldsymbol{k}ln(x) + \boldsymbol{m}$$

The fitted model parameters k and m for the means of each group and the goodness of fit are included in Table 14. R^2 values are in the range of 0.88 to 0.97, indicating a good fit of the model to the data.

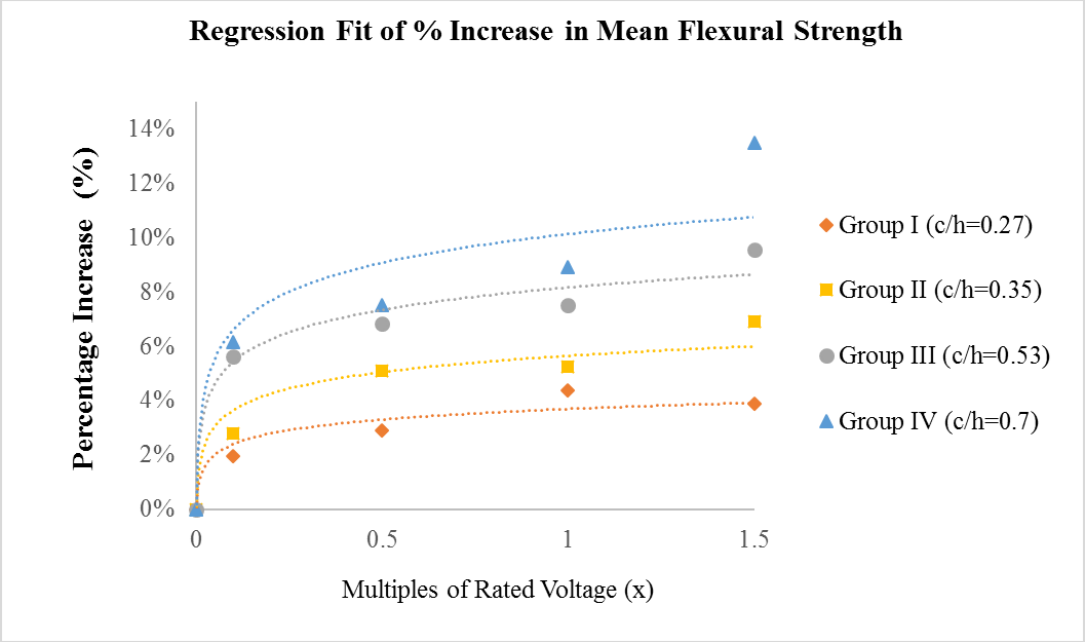

Figure 66. Regression Fit of Percentage Increase in Flexural Strength with Multiples of Rate Voltage

Table 14. Fitted Model Parameters and Goodness of Fit

	c/h	k	m	R^2
MLCC Group I	0.27	0.0056	0.0369	0.93
MLCC Group II	0.35	0.0087	0.0565	0.94
MLCC Group III	0.53	0.0119	0.0816	0.97
MLCC Group IV	0.7	0.0153	0.1013	0.88

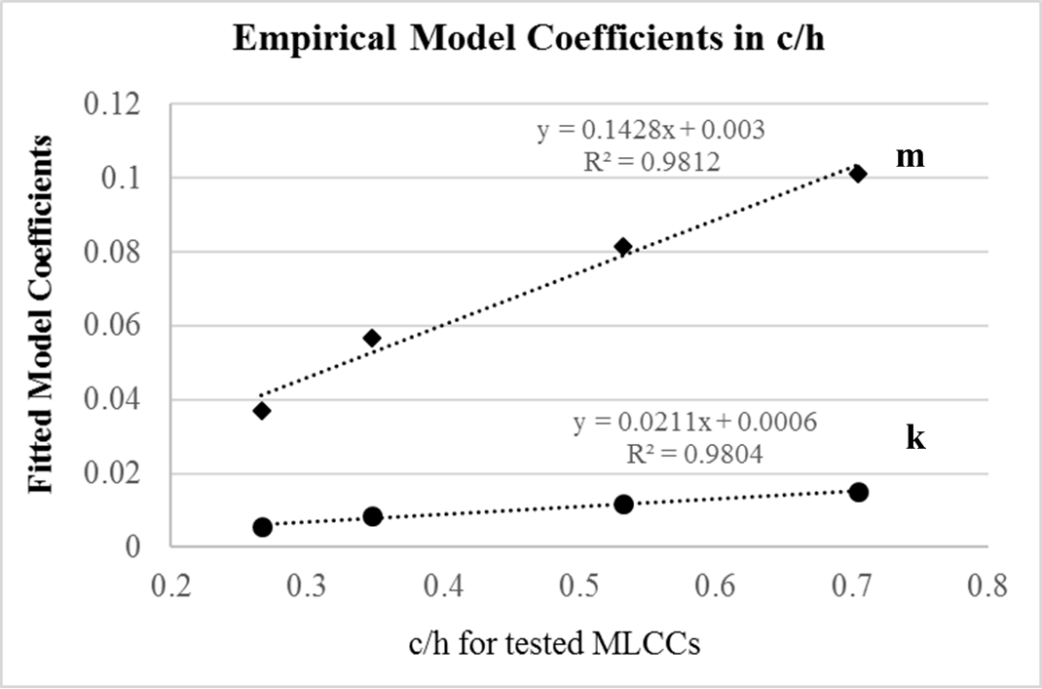

Figure 67. Empirical Coefficients k and m as a Function of c/h

Fitted model parameters k and m follow a linear relationship with c/h as shown in Figure 67. k and m can be approximated as 0.02(c/h) and 0.14(c/h) respectively. Therefore, percentage increase in flexural strength of an MLCC under 3 point bending, of a particular c/h, that is poled at a multiple x of its rated voltage can be represented with the following empirical model:

$$\%\ Increase\ in\ \overline{\sigma_{FS}} = 0.02\left(\frac{c}{h}\right) ln(x) + 0.14(\frac{c}{h})$$

5.5 Conclusion

In this section, effect of poling on flexural strength of commercial MLCCs is evaluated using a three point bending set up. Test fixture and loading pin were machined so that the setup is in accordance with AEC-Q200-003B for evaluating breaking strength of surface mounted ceramic capacitors. Commercial MLCCs with four different core thickness to height ratio (c/h) were selected for the test. Flexural strengths of MLCCs that are unpoled, and poled using different voltage levels were compared.

With 30 MLCC samples used for each poling condition, flexural strengths of all 4 groups of MLCCs were observed to increase after they are poled. Flexural strengths are also found to increase with the increase in voltage used for poling.

The change in flexural strength with different poling conditions in Group A is minimal. However, when the means of the datasets are compared, a slight increase can be reckoned. From the data of group B, C and D, it appeared that as c/h of an

MLCC is higher, the increase in flexural strength due to voltage history is of a greater extent. The experimental result is in agreement with the two major conclusions from the finite element analysis that poling increases flexural strength of an MLCC and the effect is more significant for MLCC units with a large c/h.

Then, an empirical model is developed based on the experimental data of 600 tested MLCCs. The model relates percentage increase in flexural strength of an MLCC, with c/h of the unit, and poling voltage as a multiple x of the rated voltage.

6 Contributions

The first part of this study focuses on mechanical properties characterization using indentation with the Oliver-Pharr method under different test parameters and treatment parameters of MLCCs. For test parameters, elastic modulus of commercial MLCCs demonstrated a continuous increase from terminal to the middle of an MLCC which is in agreement with the transition in residual stress along the length reported for these units. Hardness and Young's modulus measured with Berkovich indenter tips yield higher value than that by Vickers tips for the tested MLCC units with a h_f/h_{max} of 0.87 ± 0.03, which may suggest that the tip geometry effect has a wider h_f/h_{max} ratio coverage than reported (< 0.65) in the literature. Also, properties such as porosity and quality of an MLCC (symmetry of residual stress) can be reflected from the dataset of indentation characterized mechanical properties.

For treatment parameters, it was found that aging and reforming does not show a noticeable impact on indentation characterized mechanical properties. It is also found that the indentation characterized elastic modulus and hardness decreases with an increase in poling voltage due to electrical mechanical coupling effects.

From the literature, flexural strength of poled ferroelectrics are reported to increase compared to unpoled ferroelectrics. In the second part of the study, two mechanisms are evaluated for an potential flexural strength increase in MLCCs with DC voltage history. First one is the domain switching induced fracture toughness anisotropy, which can cause a shorter crack in the thickness direction of

a poled MLCC. Crack lengths were measured for indents made in between electrodes of MLCCs that were unpoled, and MLCCs that were poled at different voltage levels. A difference in crack length was observed for unpoled MLCCs, which confirms the existence of in-plane compressive stress as reported in the literature. For poled MLCCs, it was observed that for MLCCs that are poled at higher voltages, the difference in crack lengths that are parallel and perpendicular to the poling direction becomes larger, indicating fracture toughness anisotropy becomes more prominent with a higher poling voltage. This confirms that fracture toughness anisotropy effect increases with the increase in poling voltage, with the existence of in-plane compressive stress perpendicular to the poling direction in the tested units.

The second evaluated mechanism was the change in core texture of the effective dielectric impacting stresses experienced by the MLCC body under flexural stresses. Electron Backscatter Diffraction (EBSD) was used to evaluate crystallographic orientations before and after a cross-sectioned MLCC sample was poled. It was found that crystal directions were not randomly distributed prior to the poling treatment. Instead, the <001> directions align within a close proximity to the poling axis, which reflects the alignment of domains due to ferroelastic effect caused by the in-plane compressive stress. After poling, the <001> directions have aligned towards the poling direction. With the evidence of domain alignment towards poling field after voltage history, elastic stiffness matrix as a function of $BaTiO_3$ polycrystals from the literature was used to evaluate the effect of core texture on stresses experienced by an MLCC under a flexural/bending load using finite

element analysis. Under a three point bending load, it was found that maximum tensile stress, shear stress take place at the bottom dielectric (ineffective), indicating failure is likely to initiate at the bottom of the MLCC under such loading condition. It was also found that all the stresses under evaluation for core and bottom decreases as the texture of the core dielectric increases, indicating as an MLCC is poled, stresses experienced by the MLCC body reduces, thus implying a higher flexural strength.

After that, the volumetric ratio of effective dielectric to overall MLCC thickness is considered. The same stress analysis was performed with core (effective dielectric) thickness varied with the overall thickness of an MLCC held constant. Under the same amount of core texture increase, it was observed that the stress reduction becomes more significant for MLCCs with a higher core to height ratio. In another words, MLCCs with a higher core to height ratio are more prone to changes in flexural change under the same poling treatment.

Then, the effect of poling voltage on flexural strength was evaluated using the 3 point bending set up in accordance with AEC-Q200-003B. Four commercial MLCCs with different core to height ratio are used in the study. Poling voltage up to 1.5 multiples of the rated voltage was applied for 30 minutes. It was found that for MLCCs with a higher core to height ratio, the increase in flexural strength with poling voltage becomes more significant, which is in agreement with the results from FEA. With the 3 point bending test data that involved 600 MLCCs from 4 different manufacturers, an empirical model is developed to relate the increase in

percentage flexural strength, with multiples of poling voltage and core to height ratio of the MLCC being considered.

7 Future Work

Apart from the macroscopic feature c/h, other Class II MLCC ceramic design variables such as porosity, additives, number of electrodes can also be included as an extension to this study. Also, the effect of poling duration can be used as an additional test parameter to investigate how poling for different durations can affect mechanical response of the effective dielectric.

The effect of in-situ electric field application during mechanical testing is another stress condition that is widely studied for ferroelectric and piezoelectric materials. Often attributed to the clamped domain orientations by the electric field, the bending strength of specimen are reported to reduce. This effect on mechanical behavior of Class II MLCCs can be another interesting study in the future.

Apart from the effects due to DC voltage and DC voltage history, fatigue crack growth due to an applied AC voltage is also widely reported for ferroelectric and piezoelectric materials. It can potentially be a failure mechanism in MLCCs. This effect can be studied by subjecting cross-sectioned MLCC units with indents made to an AC voltage for crack growth evaluation as a future study.

8 Publications

[1] McCluskey P., Li N., “Eliminate Infant Mortality in Metallized Film Capacitors by Defect Detection”, *Microelectronics Reliability,* vol. 54, no. 9-10, pp.1818-1822, 2014

[2] Li N., Das D., “Critical Review of U.S Military Environmental Stress Screening (ESS) Handbook”, *Proceedings of the IEEE ASTR Conference,* FL, 2016

[3] Li N., Das D., Pecht M., “Shelf Life Evaluation Method for Electronic and Other Components using a Physics of Failure (PoF) Approach”, *Proceedings of the MFPT Conference,* VA, 2017

[4] Li N., Manoharan S., Das D., Mccluskey F.P., “Analysis of Indentation Measured Mechanical Properties on Multilayer Ceramic Capacitors (MLCCs)”, *Microelectronics Reliability*, vol. 88, pp. 528-533, 2018

[5] Manoharan S., Li N., Patel C., Hunter S., McCluskey F.P., “Mechanics of Copper Wire Bond Failure due to Thermal Fatigue”, *Proceedings of the EPTC Conference,* Singapore, 2018

[6] Li N., Das D., McCluskey P., "Review of Shelf Life Evaluation Methods and a Physics of Failure Approach for Shelf Life Estimation for Electronic Components", vol. 99, pp. 152-160, 2019

9 References

[1] Kemet, Kemet Online Education Resource. Available at: https://ec.kemet.com/terms/surface-mount-mlcc. [Last accessed: 5/10/2019]

[2] Courtesy: Mr. Dennis Zogbi from Paumanok Publications.

[3] Quartz, "The Global Shortage of Capacitors Impacts all Consumer Electronics " Available at: https://qz.com/1575735/a-mlcc-shortage-is-stifling-electronics-hardware-auto-makers/. [Last Accessed: 5/28/2019]

[4] EIA Standard, "Ceramic Dielectric Capacitors Class I, II, III and IV- Part I: Characteristics and Requirements", EIA-198-1-F, 2002.

[5] IEC Standard, "Fixed Capacitors for Use in Electronic Equipment- Part 1: Generic Specification", IEC 60384-1, 2016

[6] AVX, "Multilayer Ceramic Capacitor-Materials and Manufacture", Technical Information. Available at: http://www.avx.com/docs/techinfo/CeramicCapacitors/mlcmat.pdf. [Last accessed: May 30, 2019]

[7] Johnson Dielectric Inc., "Ceramic Capacitor Aging Made Simple". Available at: https://www.johansondielectrics.com/ceramic-capacitor-aging-made-simple.html. [Last Access: 5/14/2019]

[8] Wikipedia contributors. Ceramic capacitor [Internet]. Wikipedia, The Free Encyclopedia; 2019 Apr 23, 20:43 UTC. Available at: https://en.wikipedia.org/w/index.php?title=Ceramic_capacitor&oldid=893828687. [Last Accessed:5/14/2019]

[9] Zogbi D.M., “Global Market Update for 16 Types of Capacitor”, TTTI Resources. Available at: https://www.ttiinc.com/content/ttiinc/en/resources/marketeye/categories/passives/me-zogbi-20181106.html. [Last accessed: 5/12/2019]

[10] Prymak, J. D., and Berganthal, J., “Capacitance monitoring while flex testing,” *IEEE Transactions on Components, Packaging, and Manufacturing Technology*, Part A, vol. 18, No. 1, pp. 180-186, 1995

[11] Keimasi, M., Azarian, M. H., and Pecht, M., “Isothermal aging effects on flex cracking of multilayer ceramic capacitors with standard and flexible terminations,” *Microelectronics Reliability*, vol. 47, no. 12, pp. 2215-2225, 2007.

[12] J. M. Blamey and T. V. Parry, "The effect of processing variables on the mechanical and electrical properties of barium titanate positive temperature coefficient of resistance ceramics. 2. Sintering atmospheres.," *Journal of Materials Science*, vol. 28, pp. 4317-4324, 1993.

[13] Al-Saffar, R., Freer, R., Tribick, I., and Ward, P., “Flexure strength of multilayer ceramic capacitors,” British Ceramic Transactions, Vol. 98, No. 5, pp. 241-245, 1999.

[14] Keimasi M., Azarian M., Pecht M., “Flex Cracking of Multilayer Ceramic Capacitors Assembled with Pb-Free and Tin-Lead Solders”, *IEEE Transactions on Device and Materials Reliability*, vol.8, no.1, pp. 182-192, 2008.

[15] Ahmar J., Wiss E., Wiese S., “Fracture Probability of MLCC in Dependence of Solder Fillet Height”, *International Conference on Thermal, Mechanical Multi-physics Simulation and Experiments in Microelectronics and Microsystems (EuroSimE)*, 2017.

[16] Berganthal, J., “Ceramic chip capacitors “flex cracks”: understanding & solutions,” Kemet Electronics Corporation, Document No.: F-2111, January 1998.

[17] Blattau N., Gormally P., Innaccone V., Harvilchuck L., Hillman C., Robustness of Surface Mount Multilayer Ceramic Capacitors Assembled with Pb-Free Solder”, *Proceedings of CARTS-Conference*, vol.26, pp.25, 2006.

[18] Nies, C., and Maxwell, J., “Important factors in board flexure testing of surface mount capacitors,” *Proceedings of CARTS-Conference*, Asia, Singapore, pp. 75-82, 1991

[19] Keimasi, M., “Flex Cracking and Temperature-Humidity-Bias effects on Reliability of Multilayer Ceramic Capacitors”, PhD Thesis, University of Maryland – College Park, Mechanical Engineering Department, Maryland, USA,2006.

[20] Sato, K., Ogata, Y., Ohno, K., and Ikeo, H., “Mechanism of ceramic capacitor leakage failures due to low DC stress,” *Proceedings of the 18th International Reliability Physics Symposium*, pp. 205-212, 1980.

[21] Freiman, S. W., and Gonzalez, A. C., “Electrical failures due to cracks in multilayer ceramic capacitors,” *Advances in Ceramics*, vol. 19, Multilayer ceramic devices. Edited by Blum, J. B., and Cannon, W. R., American

Ceramic Society, Westerville, OH, pp. 191-201, 1986.

[22] Ling, H. C., and Jackson, A. M., “Correlation of silver migration with temperature-humidity-bias (THB) failures in multilayer ceramic capacitors,” *IEEE Transactions on Components, Hybrids, and Manufacturing Technology*, vol. 12, No. 1, pp. 130-137, March 1989.

[23] Herzberger J., Teverovsky A., “Dendritic Growth in BME and PME Ceramic Capacitors”, *Proceedings of CARTS-Conference, Houston, TX, pp. 1-21,* 2013.

[24] Ciccotti M., George M., Ranieri V., Wondraczek L., and Marlière C., "Dynamic condensation of water at crack tips in fused silica glass," *Journal of Non-Crystalline Solids,* vol. 354, pp. 564-568, 2008

[25] Munikoti, R., and Dhar, D., “Low-voltage failures in multilayer ceramic capacitors: a new accelerated stress screen,” *IEEE Transactions on Components, Hybrids, and Manufacturing Technology*, vol. 11, No. 4, pp. 346-350, 1988.

[26] Munikoti, R., and Dhar, D., “Highly accelerated life testing (HALT) for multilayer ceramic capacitor qualification,” *IEEE Transactions on Components, Hybrids, and Manufacturing Technology*, vol. 11, No. 4, pp. 342-345, December 1988.

[27] Rawal, B. S., and Chan N. H., "Conduction and failure mechanisms in barium titanate based ceramics under highly accelerated conditions." *Proceedings of the 34th Electronic Components Conference, New Orleans*, pp. 184-188. 1984.

[28] Liu, D., “Highly accelerated life stress testing (HALST) of base-metal electrode multilayer ceramic capacitors.” *Proceedings of CARTS-Conference*, pp. 235-248. 2013.

[29] Liu, D., Sampson, M., “Reliability evaluation of base-metal-electrode multilayer ceramic capacitors for potential space applications,” *Proceedings of CARTS-Conference*, pp. 45-63, 2011.

[30] Chen, W. P., Jiang, X. P., Wang, Y., Peng, Z., and Chan, H. L. W., “Water- induced degradation of barium titanate ceramics studied by electrochemical hydrogen charging,” *Journal of American Ceramic Society*, vol. 86, No. 4, pp. 735- 737, 2003.

[31] Donahoe, D. N., Hillman, C. D., and Pecht, M. G., “Failures in base metal electrode (BME) capacitors,” *Proceedings of CARTS-Conference*, pp. 129-133, March/April 2003.

[32] Donahoe, D., “Moisture in multilayer ceramic capacitors,” PhD Thesis, University of Maryland – College Park, Mechanical Engineering Department, Maryland, USA, 2005.

[33] Fu D., Itoh M., “Role of Ca off-Centering in Tuning Ferroelectric Phase Transitions in Ba(Zr,Ti)O3 System”, Ferroelectric Materials- Synthesis and Characterization, Ch. 5, Barranco, A.P., Ed., Intech: Rijeka, Croatia, 2015.

[34] Mason, W. P., and Baerwald H., "Piezoelectric crystals and their applications to ultrasonics." *Physics Today* vol.4, no.12, 1951.

[35] Rupitsch, Johann S., “Piezoelectricity”, Piezoelectric Sensors and Actuators, Ch.3, Ed.1, Springer: Berlin, 2019

[36] Haertling, Gene H. "Ferroelectric ceramics: history and technology." *Journal of the American Ceramic Society,* vol. 82, no. 4, pp. 797-818, 1999

[37] Kao K.C., “Ferroelectrics, Piezoelectrics and Pyroelectrics”, Dielectric Phenomena in Solids, Ch.4, Ed.1, Academic Press: San Diego, pp. 213–282, 2004.

[38] Whatmore R., Ferroelectric Materials. In: Kasap S., Capper P. (eds) Springer Handbook of Electronic and Photonic Materials. Springer Handbooks. Springer, Cham, 2017

[39] Acosta M., Novak N., Rojas V., Patel S., Vaish R., Koruza J., Rosesetti G. A., Rodel J., “$BaTiO_3$-based Piezoelectrics: Fundamentals, Current Status, and Perspectives”, *Applied Physics Reviews,* vol. 5, 041305, 2017.

[40] Kwei G.H., Lawson A.C., Billinge S.J.L., “Structures of the Ferroelectric Phases of Barium Titanate”, *Journal of Physical Chemistry*. vol. 97, no. 10, pp. 2368-2377, 1993.

[41] Tan Y., Zhang J., Wu Y., Wang C., Koval V., Shi B., Ye H., McKinnon R., Viola G., Yan H., “Unfolding Grain Size Effects in Barium Titanate Ferroelectric Ceramics”, *Scientific Reports,* vol. 5, no. 9953, 2015.

[42] Marsillius M., Granzow T., Jones J.L., “Effect of Electrical and Mechanical Poling History on Domain Orientation and Piezoelectric

Properties of Soft and Hard PZT ceramics", *Science and Technology of Advanced Materials*, vol. 12, no.1, 2011.

[43] Marsilius, M., Webber, K. G., Aulbach, E., & Granzow, T. (2010). "Comparison of the temperature-dependent ferroelastic behavior of hard and soft lead zirconate titanate ceramics", *Journal of the American Ceramic Society*, vol. *93, no.*9, pp. 2850-2856, 2010.

[44] Genenko Y.A., Glaum J., Hoffmann M.J., Albe K., "Mechanisms of Aging and Fatigue in Ferroelectrics", *Journal of Material Science and Engineering: B*, vol. 192, pp. 52-82, 2015.

[45] Vladimir Koval, Giuseppe Viola and Yongqiang Tan., Biasing Effects in Ferroic Materials, Ferroelectric Materials - Synthesis and Characterization, Dr. Aimé Peláiz-Barranco (Ed.), InTech, 2015. Available from: https://www.intechopen.com/books/ferroelectric-materials-synthesis-and-characterization/biasing-effects-in-ferroic-materials . [Last Accessed: 5/12/2019]

[46] Ulrich R., Schaper L., "Comparison of Paraelectric and Ferroelectric Materials for Applications as Dielectrics in Thin Film Integrated Capacitors", *The International Journal of Microcircuits and Electronic Packaging*, vol. 23, no.2, 2000.

[47] Koval V., Viola G., Tan Y., Biasing Effects in Ferroic Materials, Ferroelectric Materials- Synthesis and Characterization, Dr. Aime Paliz-Barranco (Ed.), Intech, 2015.

[48] Ikegami S., Ueda I., "Mechanism of Aging in $BaTiO_3$", *Journal of Physical Society of Japan*, vol. 22, no.3, pp.725-734, 1967.

[49] Bradt R.C. et al., "Aging in Tetragonal Ferroelectric Barium Titanate", *Journal of the American Ceramics Society*, vol. 52, no.4, pp. 192-199, 1968

[50] J. Stankowska and J. Stankowski, "Aging Process in Triglycerine Sulfate," *Proceedings of the Physical Society (London),* vol. 75, pp. 455- 456, 1960

[51] J. Stankowski, "Aging in $BaTiO_3$ Ceramics," Bull. SOC. Amis. Sci. Lettres Pozman Ser. B 16, 27-59, 1962.

[52] F. W. Cooke, "Microstructure, Precipitation, and Dielectric Aging in the System $BaTiO_3$-CaTiO,"; Ph.D. Thesis, Rensselaer Polytechnic Institute, 1965.

[53] Takahashi M., "Space Charge Effect in Lead Zirconate Ceramics Caused by the Addition of Impurities", *Japanese Journal of Applied Physics,* vol. 9, pp.1236-1246, 1970.

[54] Thomann H., "Stabilization Effects in Piezoelectric Lead Titanate Zirconate Ceramics," *Ferroelectrics,* vol.4, pp.141-146, 1972.

[55] Lambeck P.V., Jonker G.H., "The Nature of Domain Stabilization in Ferorelectric Perowskites," *Journal of Physics Chemistry of Solids,* vol. 47, pp. 453-461, 1986

[56] Hagemann H.J., ''Loss Mechanisms and Domain Stabilisation in Doped $BaTiO_3$,'' *Journal of Physics. C: Solid State Physics*., vol. 11, pp. 3333–3344 , 1978.

[57] Murata, “Ceramic Capacitors FAQ”. Available from: https://www.murata.com/enus/support/faqs/products/capacitor/mlcc/char/0006 [Last Accessed: 5/20/2019]

[58] Robels U., and Arlt G, ‘‘Domain Wall Clamping in Ferroelectrics by Orientation of Defects,’’ *Journal of Applied Physics.*, vol. 73, pp. 3454–3460, 1993.

[59] Mason W.P., “Aging of the Properties of Barium Titanate and Related Ferroelectric Ceramics”, *The Journal of the Acoustical Society of America*, vol. 27, pp. 73-85, 1955

[60] Zhang K., Zeng F., Wang H., Lin H.T., “Strength Properties of Aged Poled Lead Zirconate Titanate Subjected to Electromechanical Loadings”, *Smart Materials and Structures*, vol.21, no.11, 2012.

[61] Cohen A. et al., “Dielectric Aging in Tetragonal Solid Solutions of Calcium Titanate in Barium Titanate”, *Journal of American Ceramic Society*, vol. 53, no. 7, pp. 396-398, 1970.

[62] Okayasu M., Sato Y., Mizuno M., Shiraishi “Effect of Domain Wall Characteristics on Material Properties of Lead Zirconate Titanate Piezoelectric Ceramics”, *Advances in Applied Ceramics*, vol. 111, no.4, pp. 187-195.

[63] Jones J.L. et al., “Crack Tip Process Zone Domain Switching in a Soft Lead Zirconate Titanate Ceramic”, *Acta Materialia*, vol. 55, pp.5538-5548, 2007.

[64] Deluca M. et al., “Raman Spectroscopy for the Investigation of Indentation-Induced Domain Texturing in Lead Zirconate Titanate Piezoceramics”, *Scripta Materialia,* vol. 63, pp.343-346, 2010.

[65] Tanimoto T., Okazaki K., Yamamoto K., “Tensile Stress-Strain Behavior of Piezoelectric Ceramics”, *Japanese Journal of Applied Physics,* vol. 32, no. 9B, pp. 4233-4236, 1993.

[66] Ogawa T., Ikegaya T., “Elastic Constants Measured from Acoustic Wave Velocities in Barium Titanate Piezoelectric Ceramics”, *Japanese Journal of Applied Physics,* vol. 54, no. 1, 2014.

[67] Herbeit R., Tenbrock H., Arlt G., “The Aging Behavior of the Complex Material Parameters ε, d and s in Ferroelectric PZT Ceramics”, *Journal of Ferroelectrics,* vol. 76, no. 1, 1987.

[68] Zhang L., Xeng F., Wang H., Lin H.T., “Strength Properties of Aged Poled Zirconate Titanate Subjected to Electromechanical Loading”, *Smart Materials and Structure,* vol. 21, no. 11, 2012.

[69] Seo, S., and Kishimoto A., "Effect of polarization treatment on bending strength of barium titanate/zirconia composite." *Journal of the European Ceramic Society* vol.20, no.14-15 pp. 2427-243, 2000

[70] Kishimoto A., Seo S., “Polarization Dependent Mechanical Strength of Zirconia Base Composites Dispersed with Barium Titanate”, *Journal of Materials Science Letters,* vol. 20, pp.97-99, 2001.

[71] Efe C., Yilmaz H., Tur Y.K., Duran C., "Mechanical Property Characterization of Na1/2Bi1/2TiO3-$BaTiO_3$ Ceramics", *International Journal of Chemical Engineering and Applications*, vol. 5, no. 5, 2014

[72] Rattanachan S., Miyashita Y., Mutoh Y., "Fracture Toughness of $BaTiO_3$ and $BaTiO_3$-Al_2O_3 Composite under Electric Field", *Fracture Mechanics of Ceramics*, pp. 297-305, New York, 2005.

[73] Calderon-Moreno J.M., Meredith F.G., Reece M.J.," Fracture Toughness Anisotropy of PZT", *Materials Science and Engineering: A*, vol. 234-236, pp. 1062-1066, 1997.

[74] Lan C.F. et al., "Effects of Poling State and Pores on Fracture Toughness of $Pb(Zr_{0.95}Ti_{0.05})O_3$ Ferroelectric Ceramics", *Advances in Applied Ceramics*, vol. 112, no.5, pp. 306-310, 2013.

[75] Warren W.L., Dimos D., Tuttle B.A., Nasby R.D., Pike G.E., "Electronic Domain Pinning in Pb(Zr,Ti)O3 Thin Films and Its Rolw in Fatigue", *Applied Physics Letter*, vol. 65, no. 8, 1994.

[76] AEC-Q200-005 Rev A, "Passive Component Surface Mounted Ceramic Capacitors Board Flex Test", Automotive Electronics Council, 2010.

[77] Chen K. Y., Huang C. W., "Advanced characterization of mechanical properties of multilayer ceramic capacitors", *Journal of Materials Science: Materials in Electronics*, vol.25 no.2, pp.627–634, 2014.

[78] Kim D., Kang J., Park S., Kim J., Jung Y., Paik U., "Crack formation in MLCCs depending on position with and without post-heat treatment", *Journal of Electroceramics*, vol.17, no.2-4, pp.381-385, 2006.

[79] Wereszczak A., Riester L, Breder K., "In-Situ Mechanical Property Evaluation of Dielectric Ceramics in Multilayer Capacitors", SAE Technical Paper, no.2000-01-1535, 2000.

[80] Ryu S., Kim H., Kim H., Kim S., "Characterization of mechanical properties of $BaTiO_3$ ceramics with different types of sintering aid by nano-indentation", *Journal of the Ceramic Society of Japan*, vol. 117, no.7, pp. 811–814, 2009.

[81] Shin Y., Kang K., Jung Y., Yeo J., Lee S., Paik U., "Internal Stress in $BaTiO_3$/Ni MLCCs", *Journal of the European Ceramic Society*, vol. 23, pp. 1425-1434, 2003.

[82] Manoharan S., Patel C., Dunford S., Morillo C. G., McCluskey P., "Aging characteristics of green molding compound for use in encapsulation of microelectronic devices", *Electronic Components and Technology Conference (ECTC)*, San Diego, CA, pp. 1762–1767, 2018

[83] Menčík J., Uncertainties and errors in nanoindentation, in: J. Nemecek (Ed.), Nanoindentation in Materials Science, InTech, pp. 53–86, 2012

[84] Sahin O., "Indentation load effect on young's modulus and hardness of porous SiAiOn ceramic by depth sensing indentation tests", *Chinese Physics Letters*, vol.24, no.11, 2007.

[85] Chicot D., Tricoteaux A. Mechanical Properties of Ceramic by Indentation: Principle and Applications, Ceramic Materials, Wilfried Wunderlich (Ed.), InTech Open, 2010

[86] Cheng Y., Cheng C., "Scaling dimensional analysis, and indentation measurements", *Materials Science and Engineering: B*, vol.44, no.4–5, pp. 91-149, 2004.

[87] Peng Z., Gong J., Miao H., "On the Description of Indentation Size Effect in Hardness Testing for Ceramics: Analysis of the Nanoindentation Data", *Journal of the European Ceramic Society*, vol. 24, no. 8, pp. 2193-2201, 2004.

[88] Bull S. J., "An Explanation of the Indentation Size Effect in Ceramics", Philosophical Magazine Letters, vol. 59, no. 6, pp. 281-288, 1989.

[89] Gong J, Wu J., Guan Z., "Examination of the indentation size effect in low-load Vickers hardness testing of ceramics", *Journal of the European Ceramic Society*, vol.19, pp. 2625-2631, 1999.

[90] Li H., Bradt R., "The microhardness indentaton load/size effect in rutile and cassiterite single crystals", *Journal of Materials Science*, vol.28, pp. 917-926, 1993.

[91] Tsui T. Y., Oliver W.C., Pharr G.M., "Influences of stress on the measurement of mechanical properties using nanoindentation: I. Experimental studies in an aluminum alloy", *Journal of Materials Research*, vol. 11, no.752, 1996

[92] Kamble S.N., Kubair D.V., Ramamurty U., "Indentation Strength of a Piezoelectric Ceramic: Experiments and Simulations", *Journal of Materials Research*, vol. 24, no.3, 2009.

[93] Oliver W. C., Pharr G. M., "An Improved Technique for Determining Hardness and Elastic Modulus using Load and Displacement Sensing Indentation Experiments", Journal of Materials Research, vol. 7, no. 6, 1992

[94] Zhou H., Pei Y., Li F., Luo H., Fang D., "Electric-field-tunable Mechanical Properties of Relaxor Ferroelectric Single Crystal by Nanoindentation", *Applied Physics Letters*, vol. 104, no. 6, pp.61094, 2014.

[95] Prume K., Franken K., Bottger U., Waser R., Maier H., "Modelling and numerical simulation of the electrical, mechanical, and thermal coupled behavior of multilayer capacitors (MLCs)", *Journal of the European Ceramic Society*, vol.2, no.8, pp. 1285-1296, 2002.

[96] S.Y. Chang, Y.C. Huang, C.H. Chang, "Effect of residual stress on mechanical properties and interface adhesion strength of SiN thin films", *Thin Solid Films*, vol. 517, no. 17, pp. 4857-4861, 2009.

[97] Chen, X., Yan, J., & Karlsson, A. M. "On the determination of residual stress and mechanical properties by indentation" *Materials Science and Engineering: A*, vol. *416*, *no.*1-2, pp. 139-149, 2006

[98] Yan W., Pun C. L., Simon G. P., "Conditions of applying Oliver-Pharr method to the nanoindentation of particles in composites", *Composite Science and Technology*, vol. 72, pp.1147-1152, 2012.

[99] Sakharova N.A., Fernandes J.V., Antunes J.M., Oliveira M.C., "Comparison between Berkovich, Vickers and Conical indentation tests: a three-dimensional numerical simulation study", *International Journal of Solids and Structures.*, vol. 46, no. 5, pp.1095–1104, 2009

[100] T. Granzow, A. B. Kounga, E. Aulbach, and J. Rodel, "Electromechanical poling of piezoelectrics," *Applied Physics Letters*, vol. 88, 252907, 2006.

[101] A. B. Kounga Njiwa, E. Aulbach, T. Granzow, and J. Rödel, "Influence of radial stress on the poling behaviour of lead zirconate titanate ceramics," *Acta Materialia*, vol. 55, no. 2, pp. 675–680, 2007.

[102] Li Y. W., and Li . X. : 'Large anisotropy of fracture toughness in mechanically poled/depoled ferroelectric ceramics', *Scripta Materialia.*, vol. 62, pp.313-316, 2010

[103] Fett T., Munz D., Thun G., "Bending strength of a PZT ceramic under electric fields", *Journal of the European Ceramic Society*, vol. 23, pp. 195-202, 2003.

[104] Schneider G.A., Heyer V., "Influence of the electric field on Vickers indentation crack growth in $BaTiO_3$, *Journal of the European Ceramic Society*, vol. 19, pp. 1299-1306, 1999.

[105] Deluca M., "Microscopic Texture Characterization in Piezoceramics", *Advances in Applied Ceramics*, vol.115, no.2, pp.112-122, 2016.

[106] Li J. Y., Rogan R. C., Ustundag E., Bhattacharya K., "Domain Switching in Polycrystalline Ferroelectric Ceramics", Nature Materials, vol.4, pp.776-781, 2005

[107] Saylor D. M., Morawiec A., Rohrer G. S., "Distribution of Grain Boundaries in Magnesia as a Function of Five Macroscopic Parameters", *Acta Materialia*, vol. 51, no. 13, pp. 3663-3674, 2003.

[108] Park J., Kim S., Shin H., Jung H. S., Hong K. S., "Residual Stress Evolution in Multilayer Ceramic Capacitors Corresponding to Layer Increase and its Correlation to the Dielectric Constant", *Journal of Applied Physics*, vol. 97, no. 9, 2005.

[109] Gao Y., Uchino K., Viehland D., "Time Dependence of the Mechanical Quality Factor in "Hard" Lead Zirconate Titanate Ceramics", *Japanese Journal of Applied Physics*, vol. 45, no. 12R, pp. 9119, 2006.

[110] Stoakovic D., "Electron backscatter diffraction in materials characterization", *Processing and Application of Ceramic*, vol.6, no.1, pp.1-13, 2012.

[111] Winkelmann A., Britton T. B., Nolze G., "Constraints on the Effective Electron Energy Spectrum in Backscatter Kikuchi Diffraction", *Physical Review B*, vol. 99, no.6, pp.64-115, 2019.

[112] A. B. Kounga, T. Granzow, E. Aulbach, M. Hinterstein, and J. Rodel, "High-temperature poling of ferroelectrics," *Journal of Applied Physics*, vol. 104, no. 2, p. 24116–24116, 2008.

[113] Plessner K.W., “Ageing of the Dielectric Properties of Barium Titanate Ceramics”, *Proceedings of Physics Society*, vol. 69, pp.1261-1268, 1956

[114] Delaunay J., Smith P.L., “Aging of Barium Titanate and Lead Zirconate-Titanate Ferroelectric Ceramics”, NRL Report by Crystal Physics Branch, Solid State Division, 1970.

[115] Laugier M.T., “New Formula for Indentation Toughness in Ceramics”, *Journal of Materials Science Letters*, vol. 6, no. 3, pp.355-356, 1987

[116] Keimasi, M., “Flex Cracking and Temperature-Humidity-Bias Effects on Reliability of Multilayer Ceramic Capacitors” PhD Thesis, University of Maryland – College Park, Mechanical Engineering Department, Maryland, USA, 2007.

[117] Li J. Y., “The Effective Electroelastic Moduli of Textured Piezoelectric Polycrystalline Aggregates”, *Journal of Mechanics and Solids*, vol. 48, pp.529-552, 2000.

[118] Tan Y. et al., “Unfolding Grain Size Effects in Barium Titanate Ferroelectric Ceramics”, *Scientific Reports*, vol. 5, no. 9953, 2015.

[119] AEC-Q200-003 Rev B, “Passive Component Surface Mounted Ceramic Capacitors Beam Load (Break Strength) Test”, Automotive Electronics Council, 2010

[120] Boslaugh, Sarah. *Statistics in a nutshell: A desktop quick reference*. O'Reilly Media, Inc., 2012.

[121] Armitage P, Berry G. Statistical Methods in Medical Research (3rd edition). Blackwell, 1994.